University of Padova

Department of Industrial Engineering

PhD School in Industrial Engineering – XXVIII ciclo

Curriculum: Chemical, Materials and Mechanical Engineering

Centre for Mechanics of Biological Materials

A PROCEDURE FOR THE AUTONOMIC DIAGNOSIS OF ESOPHAGEAL MOTOR DISORDERS FROM HRM DATA PROCESSING

School Director: Ch.mo Prof. Paolo Colombo

Coordinator: Prof. Enrico Savio

Supervisor: Prof. Emanuele Luigi Carniel

Co-supervisor: Ch.mo Prof. Arturo N. Natali

PhD candidate: Alessandro Frigo

ABSTRACT

A proper understanding of physiological mechanisms for the propulsion of ingested food within the gastrointestinal canal is mandatory for the diagnosis of pathologies affecting its motility. One of the most discussed regions within the digestive system is the esophagus, as a tubular structure whose function pertains to bring food from mouth to stomach by means of a precise sequence of longitudinal and circumferential muscular contractions, called peristalsis. Pathologies and degenerative phenomena may influence this mechanism, leading to chest pain, acid reflux, cancer development and/or inability to swallow. As a growing number of subjects suffer from esophageal motility disorders, it represent a relevant social-health problem.

The diagnosis of esophageal motility disorders is actually performed by analyzing results from High Resolution Manometry (HRM), the gold standard in esophageal diagnostics. HRM consists in a clinical test designed to measure the pressure evolution over time at different positions within a duct by means of a special probe. A number of models have been proposed in literature to interpret data from HRM, but results are often inadequate because of an improper evaluation of the complex esophageal conformation and the corresponding heterogeneous distribution of physio-mechanical properties. Furthermore, an inadequate effort was made to identify relationships between model parameters and esophageal properties, and their identification was usually performed accounting for limited sets of experimental data. The guidelines in diagnosis of esophageal motility disorders are currently defined by the Chicago Classification: a hierarchical algorithm that accounts for specific parameters evaluated by analyzing HRM results. The main drawback in this procedure pertains to the requirement of specialized experts for the evaluation of such parameters, inducing intra- and inter-operator variabilities with regard to the final diagnosis.

The esophageal motility was investigated with the goal of providing a physiological model able to interpret results from HRM, accounting for parameters related to specific physio-mechanical properties of the esophagus and their heterogeneous distribution. Activities were focused on the implementation of a procedure for the autonomic detection of esophageal motility dysfunctions based on HRM measurements processing. As a result, objective criteria were defined to support the medical staff during the traditional diagnostic activity of esophageal motility disorders.

The physiological model was developed to this purpose to evaluate the pressure distribution due to the transit of a generic pressure wave. The corresponding optimal sets of model parameters were identified accounting for the HRM results of each subject of a training set composed by 229 patients and 35 healthy volunteers. Patients and volunteers were classified into groups according to their specific healthy or pathological conditions, as non-pathological (73 patients and 35 volunteers), Achalasia pattern I (34 subjects), Achalasia pattern II (44 subjects), Achalasia pattern III (7 subjects), Esophago-Gastric Junction (EGJ) outflow obstruction (39 subjects), hypertensive LES (9 subjects), Nutcracker esophagus (14 subjects) and Diffuse Esophageal Spasm (9 subjects). The identified model parameters were analyzed, and their distributions were assessed for each group of subjects, as basis for the implementation of the autonomic diagnosis procedure. Thus, the condition of a generic patient could be determined through the evaluation of a similarity index designed to correlate the model parameters of the patient to the parameters distributions of the training set.

As a result, a preliminary set of HRMs of healthy and pathological subjects was collected for a proper design and testing of the autonomic diagnosis software. The suitability of the developed physiological model was assessed by evaluating the coefficient of determination R^2 between clinical data and model results, ranging from 83% to 96% among the different groups of subjects. The application of the model to each subject of the dataset allowed to assess the distribution of model parameters with regard to different healthy or pathological conditions, as the basis for the development of the autonomic diagnosis procedure. Furthermore, the main differences between the parameters distributions of pathological groups and the parameters distribution of the healthy group were observed in specific regions where the different symptoms are manifested, endorsing the suitability of the model to interpret the variation of physiological properties in pathological situations. Finally, the reliability of the autonomic diagnosis procedure was assessed by analyzing the performance of the algorithm, which was able to match the correct diagnosis in the 86% of the considered cases. Results suggest that the computational tools provided may represent a reliable support to the medical staff during the traditional diagnostic activity.

As model parameters distributions represent the basis for the autonomic diagnosis procedure, there is room for improvement of the algorithm by considering a larger training set, which must be extended and continuously updated involving different research groups, as a future development of the research activity. Furthermore, the autonomic diagnosis procedure should be extended, in order to make it capable to diagnose pathologies accounting for additional clinical tests providing information about conductivity, morphometry and mechanical behavior of the involved biological

tissues. Such information should be collected in a single clinical test in order to reduce costs and invasiveness for the patient, and can be performed by means of an innovative esophageal endoscope that is already under development.

SOMMARIO

La procedura per la diagnosi di patologie della motilità intestinale non può prescindere da una conoscenza appropriata dei meccanismi fisiologici che regolano il trasporto del cibo ingerito all'interno dell'intestino. Una delle regioni più studiate del tratto gastrointestinale, infatti, è l'esofago: una struttura tubolare in grado di trasportare il cibo dalla bocca allo stomaco mediante una precisa sequenza di contrazioni delle fibre muscolari longitudinali e circonferenziali chiamata peristalsi. Sfortunatamente, alcune patologie e processi degenerativi sono in grado di alterare questo meccanismo, generando dolore toracico, reflusso gastro-esofageo, difficoltà nella deglutizione e/o carcinoma dell'esofago in un numero crescente di soggetti, costituendo un grave problema socio-sanitario.

Attualmente, la diagnosi di disturbi della motilità esofagea si svolge analizzando i risultati di un particolare esame clinico chiamato Manometria ad Alta Risoluzione (High Resolution Manometry – HRM), che consente di misurare l'evoluzione temporale della pressione intra-esofagea in diverse posizioni lungo esofago mediante un catetere trans-nasale appositamente progettato. In letteratura sono stati proposti diversi modelli per l'interpretazione di dati da manometria, ma con risultati spesso insoddisfacenti a causa di una valutazione impropria della distribuzione eterogenea delle proprietà fisio-meccaniche dell'esofago e di una inadeguata definizione della loro relazione con i parametri di modello utilizzati. Inoltre, l'identificazione di tali parametri è stata fatta sulla base di dataset ridotti. Oggi, le linee guida per la diagnosi di disordini motori dell'esofago sono definite dalla Classificazione di Chicago (Chicago Classification – CC): un algoritmo gerarchico che individua la patologia sulla base di parametri specifici estratti dall'analisi di dati da HRM. Il punto debole della CC consiste nella necessità di personale specializzato per il calcolo dei parametri, introducendo inevitabilmente variabilità intra- e inter-operatore nei confronti della diagnosi effettuata.

In questa ricerca è stata analizzata la motilità esofagea, con l'obiettivo di sviluppare un modello fisiologico in grado di interpretare risultati da esami di HRM. Tale modello è stato definito mediante parametri collegati direttamente a proprietà fisio-meccaniche specifiche dell'esofago, considerando la loro distribuzione eterogenea. Le attività hanno previsto l'implementazione di una procedura per l'individuazione automatica di disfunzioni motorie dell'esofago, basata sull'analisi di dati da HRM.

Sono stati quindi definiti alcuni criteri oggettivi per supportare la figura del clinico durante l'attività diagnostica tradizionale di disordini motori dell'esofago.

Il modello fisiologico è stato sviluppato per valutare la mappa pressoria generata dal passaggio di una generica onda di pressione. Con riferimento a tale modello, sono stati individuati i set di parametri ottimali per interpretare al meglio gli esami HRM di ciascuno dei soggetti di un training set composto da 229 pazienti e 35 volontari sani. Tutti i soggetti sono stati raggruppati in diverse categorie sulla base del corrispondente stato di salute: normali (73+35 soggetti), Acalasia I (34), Acalasia II (44), Acalasia III (7), ostruzione della giunzione gastro-esofagea (39), sfintere inferiore ipertensivo (9), esofago schiaccianoci (14) e Spasmo Esofageo Diffuso (9). I parametri così identificati sono stati analizzati statisticamente per valutare la loro distribuzione in ciascuna categoria. Le distribuzioni di tali parametri costituiscono la base per lo sviluppo della procedura di diagnosi automatica. Infatti, la condizione di salute di un generico paziente può essere determinata calcolando un "indice di similarità" definito appositamente per rappresentare numericamente l'affinità tra i parametri specifici del paziente e le distribuzioni dei parametri delle diverse categorie del training set.

E' stato così costituito un set preliminare di dati da manometria ad alta risoluzione, corrispondente a soggetti sani e patologici per sviluppare e testare il software sviluppato. L'adeguatezza del modello fisiologico per quanto riguarda l'interpretazione di dati da HRM è stata accertata valutando il coefficiente di determinazione R^2 tra i dati sperimentali e i risultati di modello, il quale variava tra 83% e 96% nelle diverse categorie. L'applicazione del modello a ogni soggetto del training set ha permesso inoltre di valutare la distribuzione dei parametri in diverse condizioni di salute. A ulteriore sostegno dell'adeguatezza del modello, è stato osservato che le differenze nelle distribuzioni di parametri tra soggetti sani e patologici sono state riscontrate in corrispondenza delle regioni dell'esofago colpite dalle diverse patologie. Infine, l'affidabilità della procedura di diagnosi automatica è stata valutata analizzando la performance dell'algoritmo, il quale si è dimostrato in grado di individuare la diagnosi corretta nell'86% dei casi considerati. I risultati ottenuti indicano che gli strumenti computazionali sviluppati possono rappresentare un valido sostegno per il personale medico durante l'attività diagnostica tradizionale.

Per quanto riguarda gli sviluppi futuri della ricerca, dal momento che le distribuzioni dei parametri costituiscono il fondamento della procedura di diagnosi automatica, le prestazioni del software possono essere migliorate considerando un training set più grande, condividendolo con altri centri di ricerca ed aggiornandolo continuamente. Inoltre, la procedura di diagnosi automatica può essere

estesa e resa capace di effettuare diagnosi sulla base di ulteriori esami clinici in grado di fornire informazioni sulla conducibilità, morfometria e comportamento meccanico delle strutture biologiche coinvolte. Queste informazioni potrebbero quindi essere raccolte mediante un unico test clinico per ridurre costi di indagine e invasività per il paziente, e potrebbero essere svolti in contemporanea mediante una sonda endoscopica innovativa già in fase di sviluppo.

ACKNOWLEDGEMENTS

I would like to thank Prof. Arturo N. Natali, head of the Centre for Mechanics of Biological Materials – University of Padova, who gave me the opportunity to operate in such a challenging environment. His valuable expertise greatly contributed to enrich the overall PhD program, providing meaningful advice for my research and fostering an effective communication of results within the scientific community.

I would like to express my gratitude to my supervisor, Prof. Emanuele Luigi Carniel, for the continuous support during my PhD study and related research. His patience, brightness and multidisciplinary competence guided me not only in all the experimental and computational activities, but also in writing this thesis and numerous papers.

Besides my advisors, I would like to thank all of the team of Biomechanics of the Centre for Mechanics of Biological Materials, and in particular Prof. Piero Pavan, Chiara Giulia Fontanella, Antonella Forestiero, Paola Pachera, Silvia Todros and Chiara Venturato, and Prof. Alessandro Rubini from the Department of Biomedical Sciences – University of Padova, for their close cooperation and constant support.

I must also acknowledge Mario Costantini, MD, Renato Salvador, MD, Tommaso Giuliani, MD and Loredana Nicoletti from the Department of Surgery, Oncology and Gastroenterology – University of Padova, directed by Prof. Stefano Merigliano, MD, for giving their fundamental contribution to this research.

Finally, I would like to thank my family for the support they provided me through the PhD studies. I would like to thank my parents for their unconditional approval in my life choices, Giulia for being far and close at the same time, Annalisa and Niccolò for their fundamental contribution in proof-reading this thesis and Serena for being so patient.

Se vuoi fare un passo avanti, devi perdere l'equilibrio per un attimo.

Massimo Gramellini, L'ultima riga delle favole, 2010

TABLE OF CONTENTS

INTRODUCTION

The esophagus is a tubular organ whose function pertains to bring food from mouth to stomach by means of a precise sequence of muscular contractions called peristalsis, which is able to propel the bolus downwards and to clear acid reflux from below. Motor disorders are pathologies characterized by neuromuscular deficiencies causing non-physiological movements. With regard to tubular structures, as the esophagus or the colon, such pathologies can be diagnosed by analyzing the intraluminal pressure evolution over time. Such measurement can be performed in different ways. One of them pertains to the High Resolution Manometry (HRM), which represents the state of the art in this field, since it allows to collect data at more than 36 positions along a duct at the same time.

Computational models, such as physiological models, can be developed to interpret results from HRM and, hence, to evaluate the overall functionality of entire organs. They consist in functions designed to interpret the mathematical relationship between the measured pressure, position along the duct and time, and can be applied in different ways. As a matter of example, they can be accounted to define criteria for the characterization of pathologies and to implement procedures able to perform the autonomic diagnosis of diseases in order to support the medical staff and to reduce the inter- and intra-observer variabilities that currently affect the traditional diagnostic process. Computational models are usually defined accounting for specific parameters that are identified by minimizing the discrepancy between experimental data, as HRM results, and model results. The identified model parameters can be processed and compared to a training sets in order to autonomously diagnose pathologies.

In Chapter 1 general notes are given about the histology, morphometry and physiology of the main components of the gastrointestinal canal, in order to understand their conformation from a biomechanical point of view. Particular attention will be paid to the functionality of the esophagus and to the deglutition mechanism. Esophageal pathologies are described in Chapter 2, together with the diagnostic techniques that are mainly adopted for the detection of motor disorders of the gastrointestinal tract, with particular regard to the manometry test. Different mathematical models were proposed in literature to interpret the pressure map due to the transit of the peristaltic wave: they are compared within Chapter 3, along with the description of an innovative physiological model, which was defined in order to overcome the main limitations of the existing models. A

possible application of the developed physiological model is described within Chapter 4, as the implementation of an automatic diagnosis procedure, which is defined to support the medical staff during the traditional diagnostic activities.

The study of the peristaltic movement cannot leave aside a proper understanding of the mechanical behavior of the involved tissues and structures. To this purpose, a procedure for the characterization of hollow organs was defined. It is summarized within Appendix A. In Appendix B, future developments of the present work are presented, with particular regard to the production of an innovative biomedical device for the functional, morphometrical and mechanical characterization of the esophagus. Contextually, a brief discussion about the possible advantages of a shared database of physio-mechanical data is reported.

CHAPTER 1

MORPHOLOGY AND FUNCTIONALITY OF GASTROINTESTINAL STRUCTURES

A basic knowledge of the anatomy and histology of the gastrointestinal tract, with particular regard to the pharynx and the esophagus, is mandatory for a proper description and characterization of its functionality. To this purpose, a general scheme of its structure is firstly reported in this chapter, in comparison with the morphometry and functionality of other regions of the gastrointestinal (GI) district.

The digestive system consists of a multilayered tube of about 9 meters in length [1], five sphincters, a number of glands and different organs (Figure 1.1). Each component of the GI tract is characterized by one or more specific tasks, aiming at processing ingested food, absorbing substances that are required by the human body and eliminating unnecessary residuals [2].

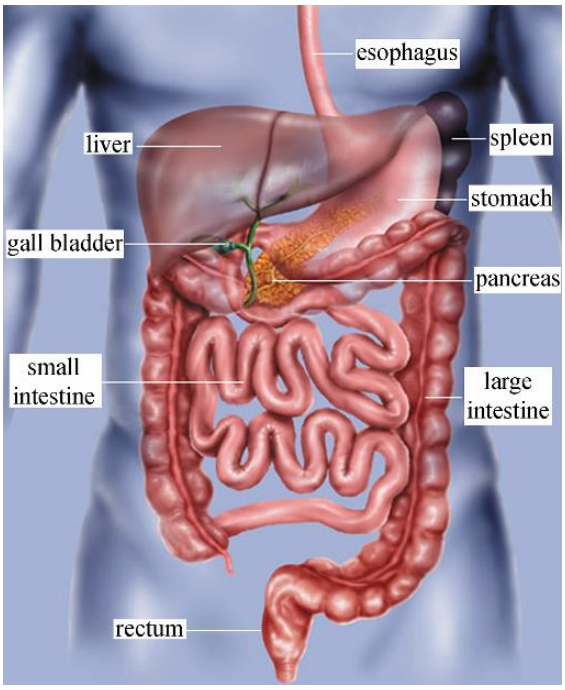

Figure 1.1 Representation of the main components digestive system.

1.1 Cross-section of the gastrointestinal canal

From a biomechanical point of view, the gastrointestinal canal is a fascinating mechanical device designed by nature to move the fluids taken in. Food at different stages of digestion is propelled forward and mixed in various complex ways to optimize the fermentation, to provide specific flow patterns required for the absorption of the nutrients and to remove indigestible residue. The overall length of the GI tube is characterized by a multilayered section (Figure 1.2) which may vary its operation to adjust to the different physical and chemical properties of the materials presented to it [3]. In detail, starting from the most inner layer, four main components can be observed within the GI wall:

1) The mucosa is composed of an epithelial lining, a lamina propria of loose soft connective tissue rich in blood and lymph vessels and smooth muscle cells, sometimes containing also glands and lymphoid tissue. The inner surface of mucosa is lined by intestinal villi in specific regions of the GI tract: 0.5-1.5 mm long outgrowths projecting into the lumen, considerably increasing the area of contact between the intestinal surface and food.
2) The submucosa is composed of connective tissue containing numerous blood and lymph vessels, glands and lymphoid tissue in a dense network of collagen fibers. Collagen fibers play a fundamental mechanical role in the overall structural response of the GI canal, offering a strong resistance to an excessive distension of the wall [4]. From a histological point of view, the main role of mucosa and submucosa pertains to the secretion of digestives enzymes and absorption of nutrients. The muscularis mucosae is a thin muscular layer placed between mucosa and submucosa, and is responsible of the movement of the mucosa independently of other movements of the digestive tract, to increase the contact with food.
3) The muscularis externa can be divided in two distinct layers of smooth muscular fibers, an inner circumferential and an outer longitudinal one, separated by the myenteric nerve plexus and a thin layer of soft connective tissue. The contraction of the two muscular layers is coordinated by the nerve plexus and allows propelling and mixing food within the digestive tract.
4) The serosa is a thin layer composed of loose soft connective tissue rich in blood and lymph vessels and adipose tissue, and a simple squamous covering epithelium (mesothelium). It secretes the serous fluid with the goal of lubricating the outer surface of the tubular structure, preventing organs from sticking to the abdominal wall and to each other.

Protrusions of the serosa gradually become mesenteries, biological structures that connect small and large intestines to the abdominal wall.

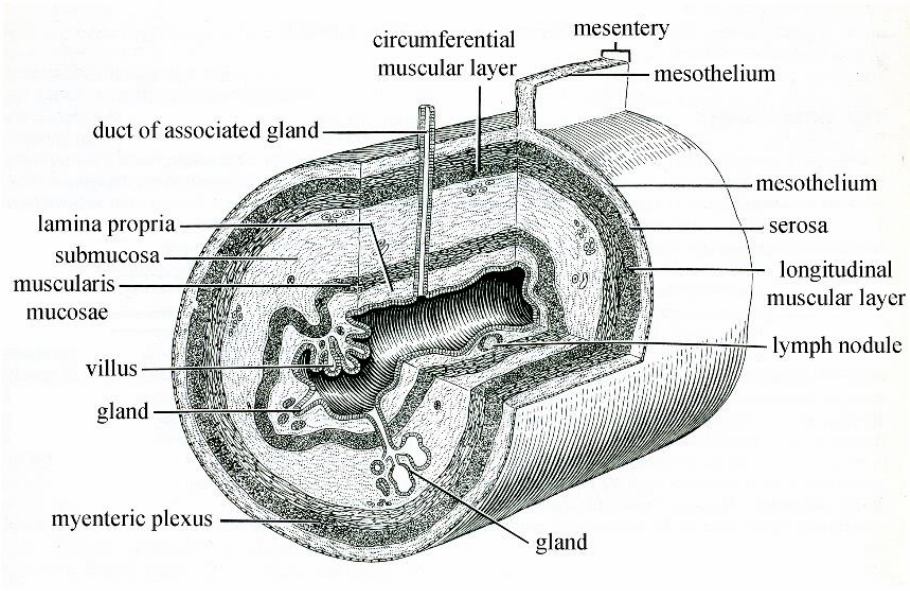

Figure 1.2 Detail of the multilayered section of the GI tube [5].

1.2 Oral cavity

The oral cavity is responsible of different tasks. Ingested food is firstly analyzed and processed by the mechanical action of teeth and tongue before being swallowed. Saliva is secreted during this phase for a better lubrication of the bolus and for a first chemical treatment of the food which transform complex carbohydrates into simpler sugars.

1.3 Pharynx

Pharynx represents a common way for the transit of air, liquids and solids, and present specific voluntary muscles involved in triggering the deglutition reflex (Figure 1.3). In detail, constrictor muscles contract to propel the bolus downwards, palatopharyngeus and stylopharyngeus muscles are able to shorten and widen the pharynx itself, while the palatal muscle is able to raisen the soft palate and the surrounding tissues.

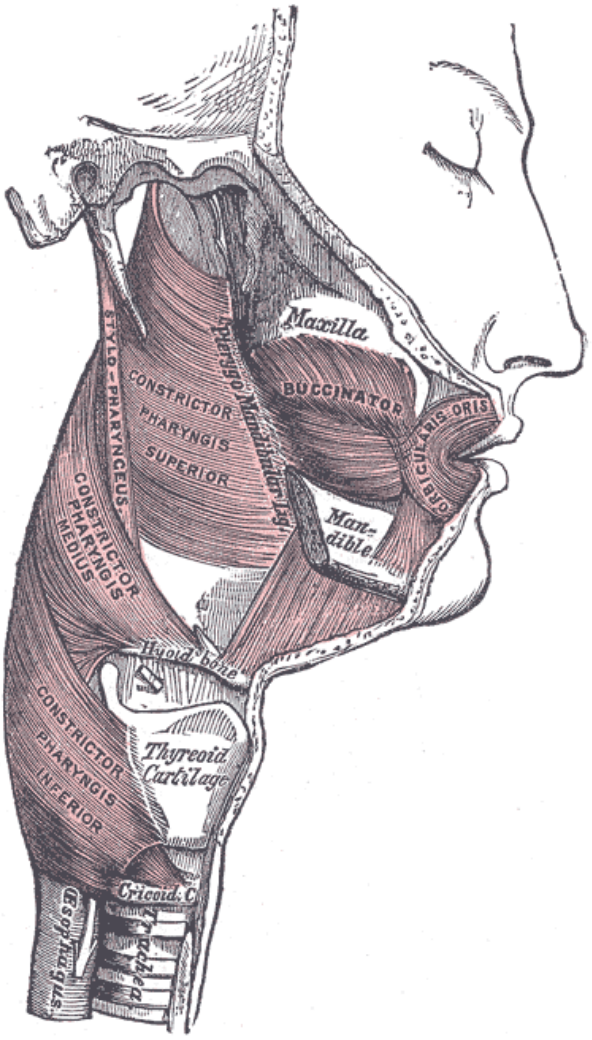

Figure 1.3 Muscles of the pharynx and cheek [6].

1.4 Esophagus

1.4.1 Histological and morphometrical configuration

The esophagus is a tubular organ of about 25 cm in length and 2 cm in diameter, whose function pertains to bring food from mouth to stomach. It is located behind the trachea and extends from the pharynx, where the upper esophageal sphincter (UES) prevents the ingestion of air, to the stomach, where the lower esophageal sphincter (LES, hiatus or Esophago-Gastric Junction (EGJ)) prevents gastric acid reflux. It can be longitudinally divided in two main regions, the upper esophagus and the lower esophagus, characterized by striated and smooth muscle fibers, respectively. Such regions are connected by a transition zone characterized by mixed features.

Within the wall of the esophagus, four layers can be identified: mucosa, submucosa, muscularis propria and adventitia (Figure 1.4). Unlike other areas of the GI canal, the esophagus does not present a serosal covering, allowing esophageal tumors to spread more easily and making their surgical removal very difficult perform [7]. Because of the specific interest in esophageal functionality, further notes about tissues conformation are reported:

1) The mucosa is arranged in longitudinal folds that disappear during the tissues distention, and consists in three sublayers:
    a. The mucous membrane is a non-keratinized squamous epithelium, which covers the entire inner surface of the esophagus, except for the lower sphincteric region. It is composed of three sublayers: a basal layer with boasophilic cells for the regeneration of the epithelium, an intermediate layer and a superficial layer.
    b. The lamina propria consists in a thin layer of soft connective tissue.
    c. The muscularis mucosa is a layer of longitudinally arranged smooth muscular fibers, thinner in the proximal part than in the distal part [8].
2) The submucosa is made of dense connective tissues, containing mucous glands able to secrete substances that are fundamental in esophageal clearance and tissues resistance to acid [9]. Within this layer, collagen fibrils are organized according to a loose and random network, offering strong resistance to the deformation of the overall tubular structure [10].
3) The muscularis propria contains two distinct families of fibers: an inner circumferential and an outer longitudinal one. They are responsible for the actual esophageal motor function, as they are capable to perform the overall structure narrowing and shortening, respectively.
4) The most external layer is the adventitia: a fibrous layer consisting of loose connective tissue that covers the esophagus, facing the neighboring structures.

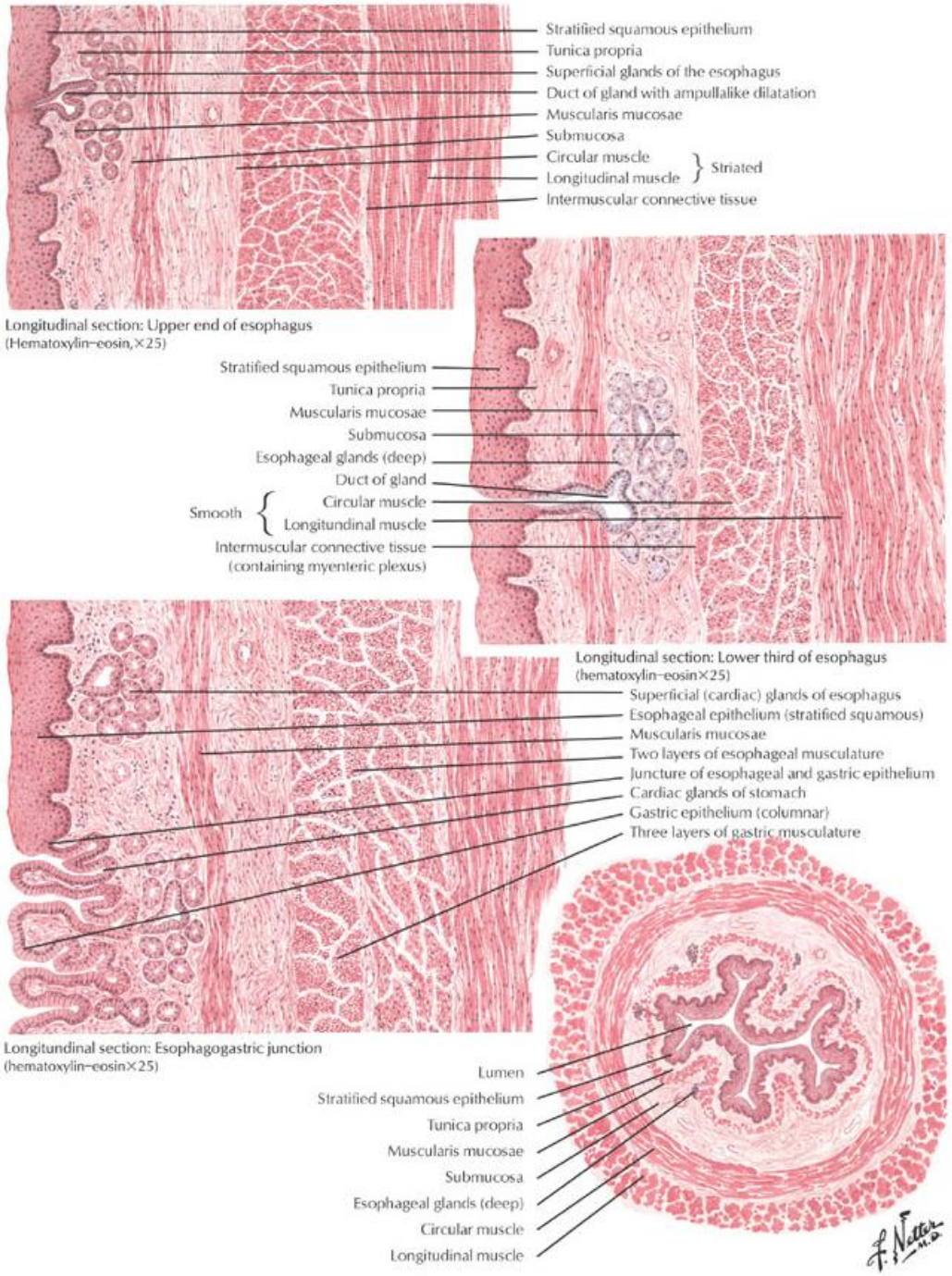

Figure 1.4 Histological sections of the esophagus [11].

Esophageal tissues are vascularized by esophageal arteries and vessels derived from the thyrocervical trunk and the external carotid artery at the neck level, from the bronchial arteries at the mediastinum, and from the celiac trunk and the inferior phrenic arteries in the abdominal tract.

Venous blood is collected by the inferior thyroid, azigos and gastric veins and is finally drained into the superior vena cava or into the portal vein. A proper understanding of the innervation of the esophagus is essential for a proper characterization of the esophageal motility, as part of the deglutition reflex is not voluntary. As a matter of fact, the esophageal tissues are innervated by the vagus nerve, which plays a fundamental role in initiating the deglutition process, and the sympathetic system by means of the esophageal plexus, for the involuntary reflex [2] (Figure 1.5).

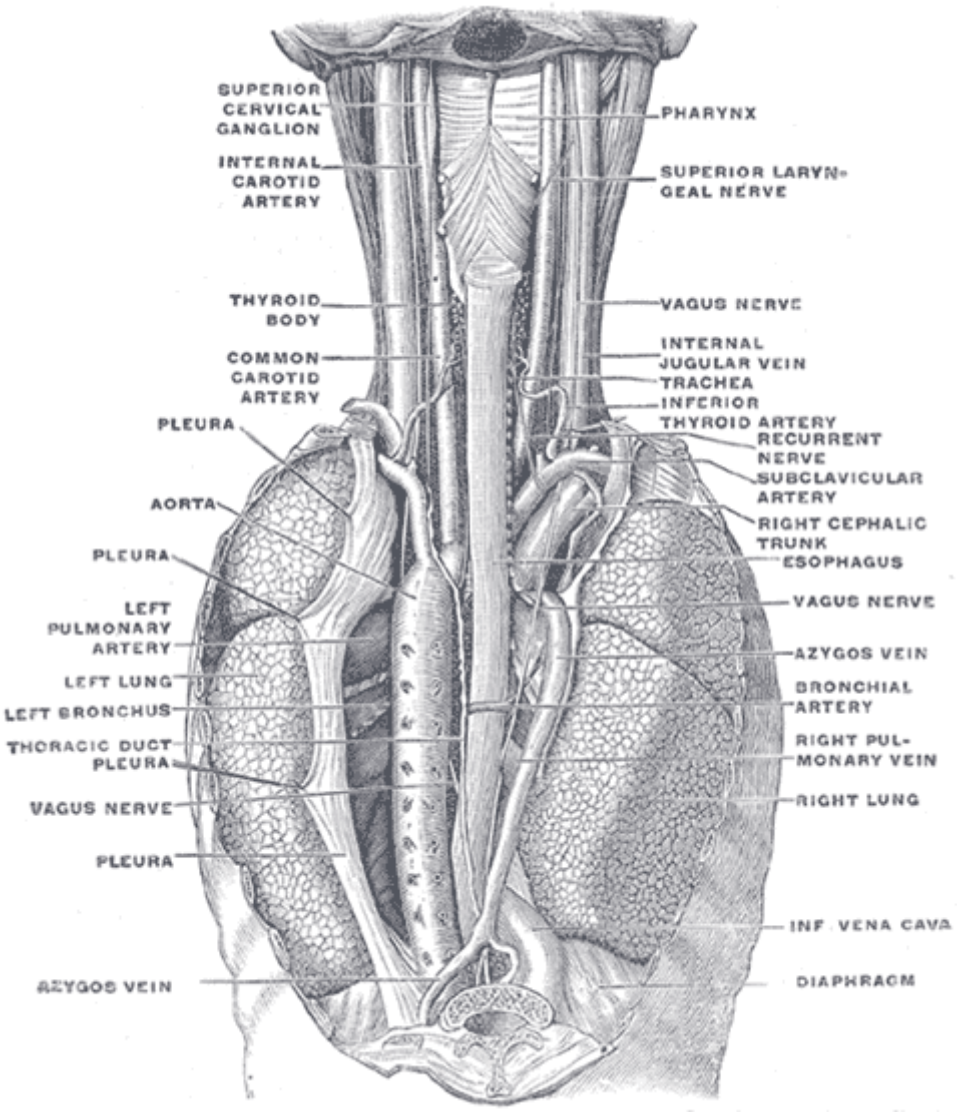

Figure 1.5 Position and relation of the esophagus in the cervical region and in the posterior mediastinum. Seen from behind. [6]

1.4.2 Deglutition

Deglutition is a complex process that initiates voluntarily and continues spontaneously. It can be divided in three phases (Figure 1.6):

1) During the oral phase, after the bolus formation by mastication and moistening, a trough is formed at the frontal part of the tongue by the intrinsic muscles. The obliteration of the trough against the hard palate from front to back forces the bolus to the back of the tongue. The same mechanism operates at the back of the tongue, which is finally elevated to the soft palate such that the tongue slopes downwards posteriorly. Finally, the superior longitudinal muscle elevates the apex of the tongue to make contact with the hard palate and the bolus is propelled to the back of the mouth, towards the pharynx, triggering the pharyngeal involuntary reflex.
2) The pharyngeal phase is initiated by proprioceptive receptors, which are scattered over the base of the tongue. During this phase, the nasopharynx and the larynx are closed, chewing, breathing, coughing and vomiting reflexes are inhibited, and the pharynx is pulled upwards and forwards to receive the bolus. The palate-pharyngeal folds are brought close together to allow the transit of small boluses only. At the same time, the nasopharynx is closed and the auditory tube is opened by the elevation of the pharynx, causing the pressure equalization between the nasopharynx and the middle ear. Since the true vocal folds adduct during swallowing, a short period of apnea must necessarily take place with each swallow. Subsequently, the adduction of false vocal fold and of the aryepiglottic folds, and the retroversion of the epiglottis take place closing the aditus to prevent ingestion of air. Then, the hyoud is elevated by the digastric and sylohyoid, lifting further the pharynx and larynx. Finally, the bolus moves down through the esophagus, propelled by the pharyngeal peristalsis. The action is performed by means of the superior, middle and inferior pharyngeal constrictor muscles, since the inferior constrictor is closed in resting conditions, and opens to allow the bolus transit, which happens at approximately 35 cm/s [12].
3) As the pharyngeal phase, the esophageal phase is under involuntary neuromuscular control, but the propagation of the bolus is significantly slower of 3 to 5 cm/s. It consists in a sequence of narrowing and shortening of segments of the esophagus, like a peristaltic wave, obtained by means of a precise coordination of the families of muscular fibers within the tonaca muscularis. In detail, the LES, which is tonically contracted in resting conditions, relaxes at the end of the pharyngeal phase, in order to allow the bolus transit. Subsequently,

the esophageal peristalsis takes place within the proximal esophagus and continues in the distal esophagus after a brief interruption at the transition zone. The peristaltic wave takes about 10 s to reach the LES, which performs a hypertonic contraction of about 5 s in duration after the end of the peristaltic wave, in order to prevent gastric acid reflux.

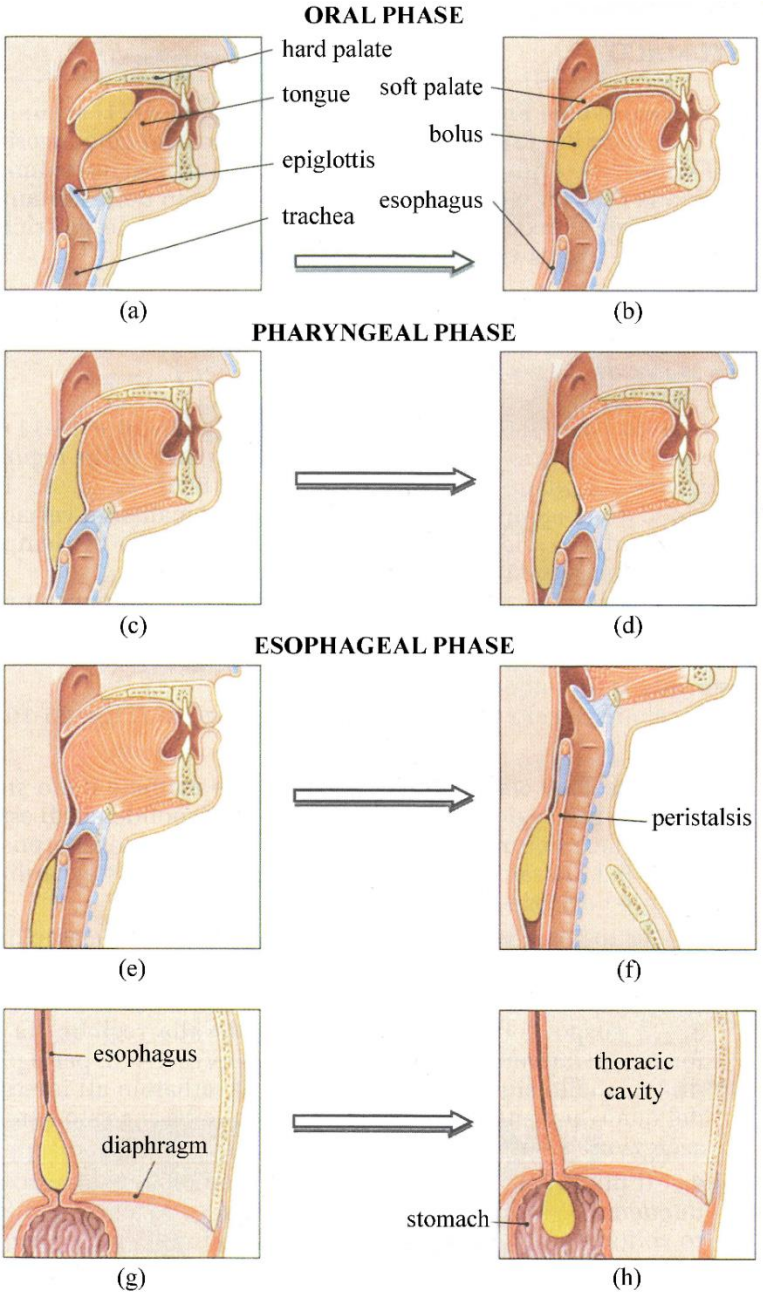

Figure 1.6 Deglutition mechanism. The sequence is obtained from a sequence of radiograms, showing the different phases of the deglutition reflex [2].

1.5 Stomach

The stomach is a muscular hollow, dilated part of the GI canal lying below the diaphragm. It can expand from 45 ml to more than 1 l of volume, and is responsible of three main functions, such as storage, mechanical processing and chemical digestion of ingested food. The stomach is also responsible for the absorption of small molecules, including water, medication, amino acids, 10 to 20% of ingested ethanol and caffeine. In this tract, ingested food is mixed with gastric acid secreted by the gastric glands within the surrounding tissues and digesting enzymes, and becomes "chime". Two sphincters keep the contents of the stomach: the LES and the pyloric sphincter, i.e. the junction with the duodenum. The stomach is surrounded by parasympathetic and orthosympathetic plexi, which regulate both the secretion activities and the motor function of the muscles within its wall. It can be divided in four sections: the cardia, the fundus, the body, and the pylorus (Figure 1.7).

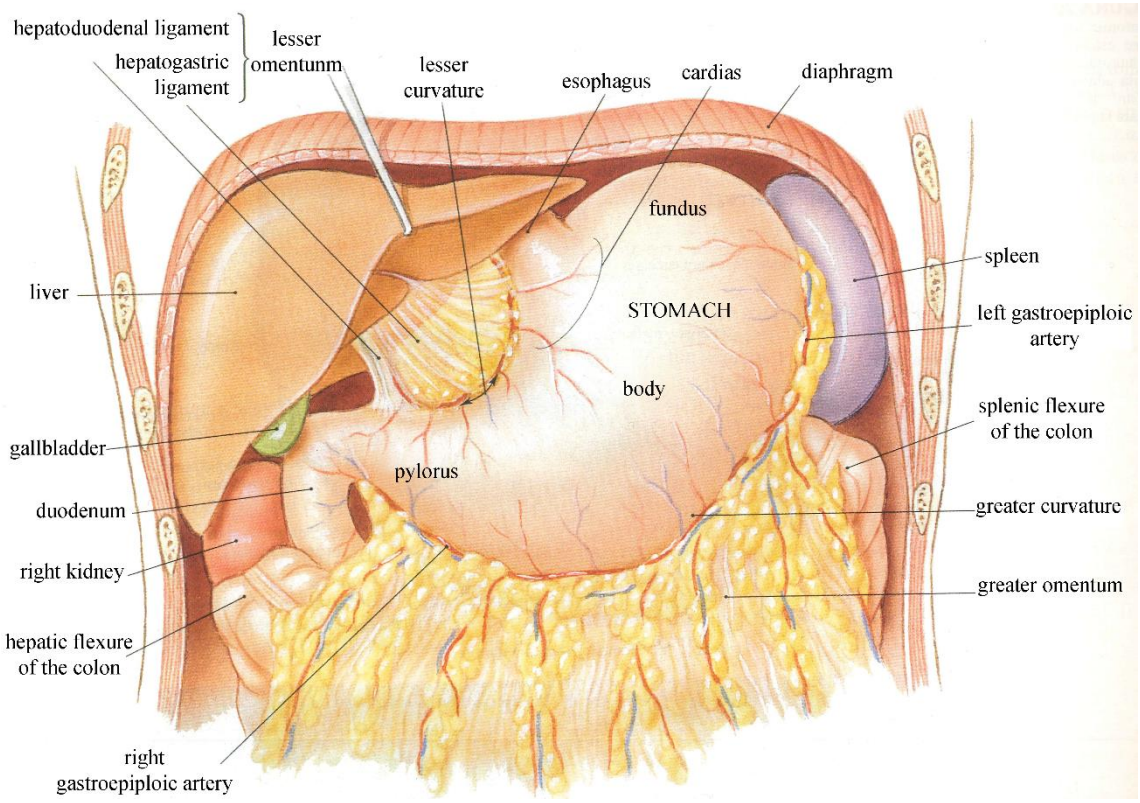

Figure 1.7 Stomach: anterior view [2].

The stomach is constituted by the four layers typical of gastrointestinal structures, as mucosa, submucosa, muscularis externa and serosa. Unlike other parts of the GI canal, the muscularis

externa of the stomach is organized in three layers: an inner oblique layer, a middle circular layer and an outer longitudinal layer, considering the different functionality of the stomach. Food is churned by the stomach through peristalsis, reducing the volume of the fundus before looping around it [13] and the body of the stomach. Here, boluses become chime, which passes through the pylorus and into the duodenum and subsequently in the small intestine, where the extraction of nutrients begins.

1.6 Small intestine

The small intestine can be divided in three main sections, as shown in Figure 1.8:

1) The duodenum is the shortest and widest tract of the small intestine, measuring about 25 cm in length. It receives chime from the stomach and digestive secretions from the liver and pancreas.
2) The jejunum is responsible for the most of the digestive processes and absorption of nutrients.
3) The ileus is the last and longest tract of the small intestine and measures about 3.5 m in length. Its end coincides with the ileocecal valve (ICV), which marks the beginning of the large intestine.

The overall length of the small intestine is characterized by folds and microvilli to increase the interacting surface for a better exchange of substances. In fact, the surface of the equivalent smooth-walled tube is about 0.22 m^2, while the actual inner surface measures more than 200 m^2 [2]. The cross section of the different parts of the small intestine is similar to the typical conformation of the structures of the GI canal (with mucosa, submucosa, muscularis externa and serosa) and only differs in the number and type of secreting glands and in the size of folds and microvilli. Its mechanical functions pertain to fragmentation and mixing the chime, and propulsion of the content forward, by means of a peristaltic mechanism similar to the one observed within the esophagus.

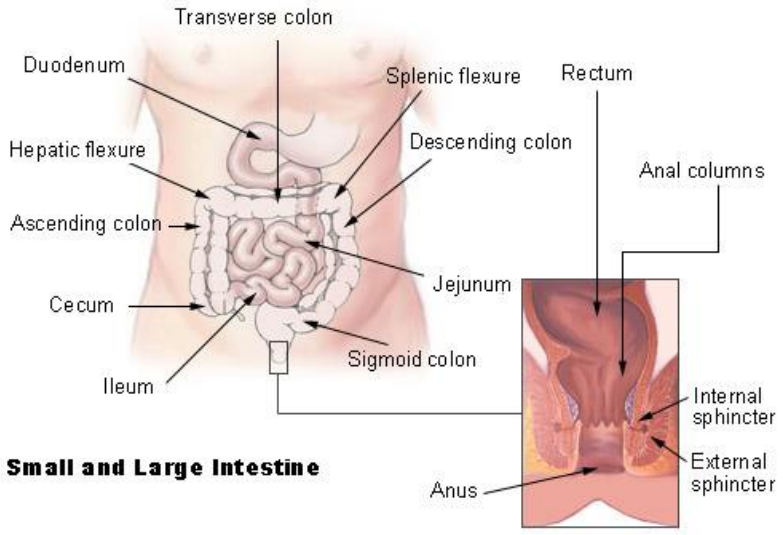

Figure 1.8 Sections of the small and large intestine.

1.7 Large intestine

The large intestine is the last portion of the GI canal, measures about 1.5 m in length and about 7.5 cm in diameter. It can be divided in three sections, as cecum, colon and rectum (Figure 1.8). The vermiform appendix is a blind-ended tube of about 9 cm in length and 8 mm in diameter, connected to the cecum at 2 cm beneath the ICV. It serves as a haven for useful bacteria when illness flushes them from the rest of the intestine [14]. The large intestine is responsible of three main functions, as:

1) water and electrolytes absorption to compact chime into feces,
2) absorption of vitamins
3) storage of feces prior to defecation.

The wall of this tubular structure can vary in width, but is generally thinner and stiffer than in the small intestine, because of the more demanding mechanical action that is required to move and compact feces.

CHAPTER 2

DIAGNOSTIC TECHNIQUES AND ESOPHAGEAL PATHOLOGIES

Esophageal motility disorders represent a relevant social-health problem, and understanding the functionality of the biomedical devices involved in the detection of such diseases is essential for a proper definition of new tools and devices. To this purpose, a review of the principal diagnostic techniques is reported in this chapter, together with different methods proposed in literature for the classification of diseases affecting the esophageal motor function.

2.1 History of Esophageal manometry

Manometry is the most widespread clinical test for the evaluation of the functionality of the esophagus and for the detection of esophageal motor disorders; it is performed by measuring pressure within the esophagus during swallowing. It is designed to evaluate the action of the esophageal muscles, with particular regard to the tonic contraction of sphincteric regions and the peristaltic features of the esophageal body.

2.1.1 "Open tipped" and "balloon tipped" catheters

The first experimental tests about esophageal functionality were conducted in 1883 by Samuel James Meltzer and Hugo Kronecker [15] (Figure 2.1).

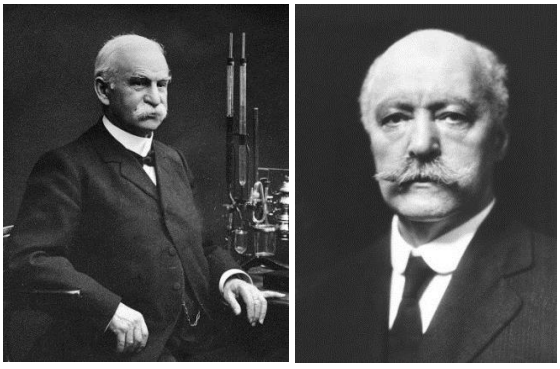

Figure 2.1 Hugo Kronecker (left) and Samuel James Meltzer (right)

They have been the first researchers who described the peristaltic mechanism by running manometric tests on the esophagus using "open tipped" and "balloon tipped" systems. Such methods have been adopted to describe the peristaltic contractions of the esophagus, but their precision was limited and a stable measurement of the upper tract and of the LES was impossible, especially during the deglutition process, when the physiological esophageal shortening causes a relative movement between sphincter and catheter. Such studies allowed to understand the physiological mechanism that prevents gastric reflux, since no true sphincter had been anatomically demonstrated yet [16].

2.1.2 Station pull-through

In the 20th century, the technical progress allowed to build a special probe consisting of a tiny balloon-covered pressure transducer and open tipped pipes, which were connected to other pressure transducers (Figure 2.2). The overall system was inserted into the stomach from the nasal cavity, and pulled through the LES by 0.5 cm stages, in order to monitor the physiological sphincteric pressure [17][18]. This is the reason for naming this procedure "station pull-through".

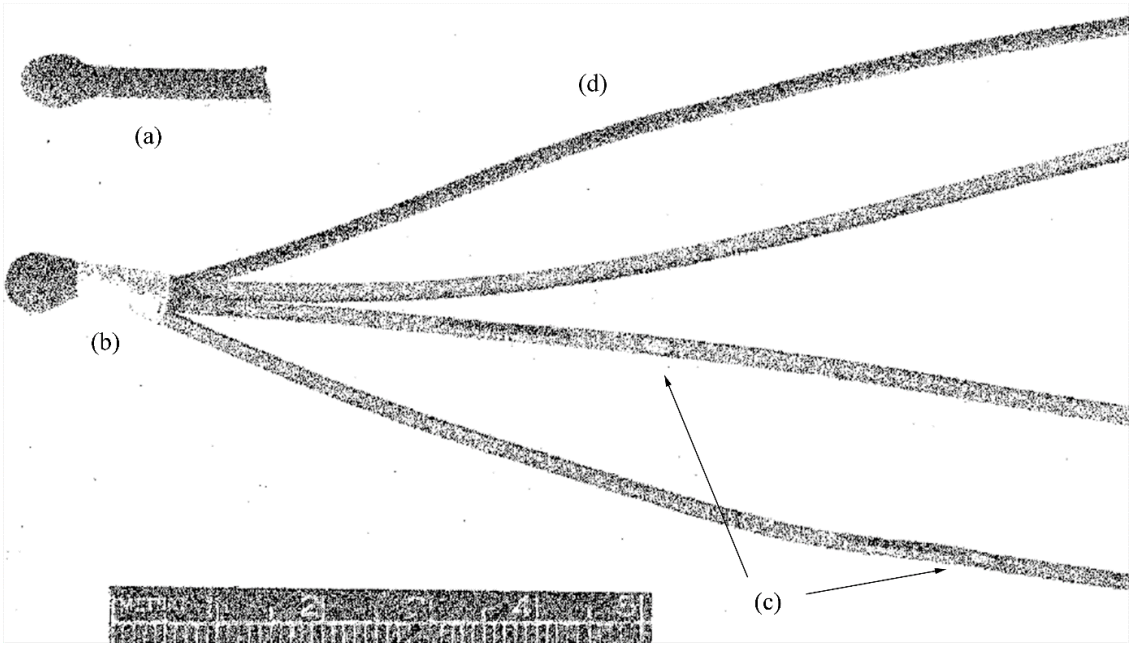

Figure 2.2 System used to detect pressures in the gastroesophageal sphincter and esophagus. Balloon (a) is tied over a narrow polyethylene tube (b), while tubes are notched laterally at 5 and 10 cm from the balloon (c). Each system is water-filled, and the uppermost tube contains wire to stiffen the entire structure and facilitate passage (d).

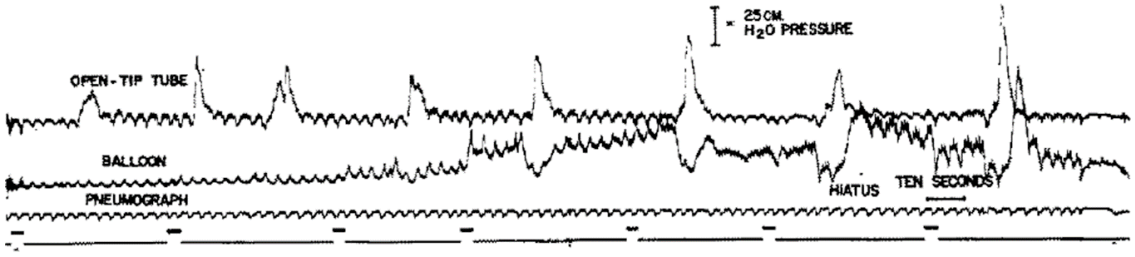

Figure 2.3 Clinical results with regard to the LES of a 28-year-old man with small sliding hiatal hernia and intermittent dysphagia. Each break in the base line corresponds to 0.5 cm oral withdraw. Swallows re indicated by the contraction registered by the open-tip tube 5 cm above the balloon.

2.1.3 Non-compliant pneumohydraulic infusion pump

In 1976 R. C. Arndorfer et al. introduced the "non-compliant pneumohydraulic infusion pump", which was designed to transfer a specified volume of water inside a capillary system by applying a constant pressure [19] (Figure 2.4). This device, together with the first multilumen catheters with side holes, allowed to perform a more reliable pull-through test, laying the foundations for the modern manometry. During the following decades, several improvements in catheters production led to the introduction of the modern manometry into the clinical practice.

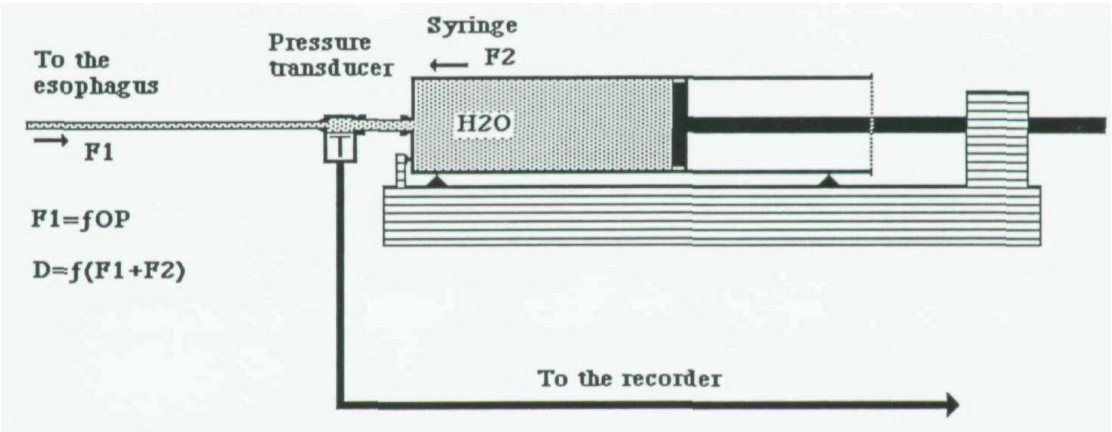

Figure 2.4 Arndorfer syringe perfusion system. F1 represents the force related to the intraesophageal counterpressure, which is due to the motility, F2 represents the perfusion pressure generated by the plunger syringe, while D is the outflow, represented as a function of the differential pressure.

2.1.4 Sleeve sensor

Even though the pull-through approach brought several advantages in the study of the LES, it became soon obsolete, since it could not address the challenge for recording LES relaxations. In fact, it is quite invasive and may influence the LES pressure. Furthermore, it can only provide a limited number of samples of LES pressure, which can be highly variable over short time periods [20][21]. In 1976, John Dent was able to overcome to these limitations, by introducing the "sleeve sensor" – a 5 cm pressure sensor able to measure the maximum LES pressure in all of its length [22] (Figure 2.5). The latter catheter was developed simultaneously with the corresponding analysis software by Medical Measurements Systems (MMS, Enschede, Holland) [23][24].

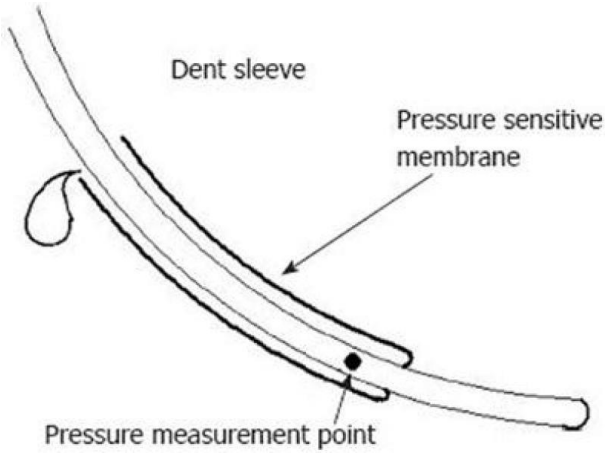

Figure 2.5 DentSleeve [25]

Different researchers endorsed this approach during the 80s and 90s, thanks to its abilty to provide a continuous monitoring of the LES during swallow and to measure the corresponding relaxations (Transient Lower Oesophageal Sphincter Relaxations – TLOSRs), which were considered as the main cause of the Gastro-Esophageal Reflux Disease (GERD) [26][27].

2.1.5 Water-perfused and solid-state catheters

Catheters have been improved through years and evolved in two main categories: "water-perfused catheters" and "solid-state catheters". Multi-lumen water-perfused catheters show three to eight tubes with side-holes along their body, and a balloon at the end (Figure 2.6 b). Concerning the cross section of the catheters, tubes are radially oriented and perfused by a low-compliance infusion pump (Figure 2.6 a). Differently, solid-state catheters show an array of tiny strain gauges, which are

equally spaced along a flexible tube (Figure 2.6 c) and guarantee higher temporal resolution. Each sensor records information on the intraluminal pressure at its specific position along the longitudinal axis of the esophagus [28].

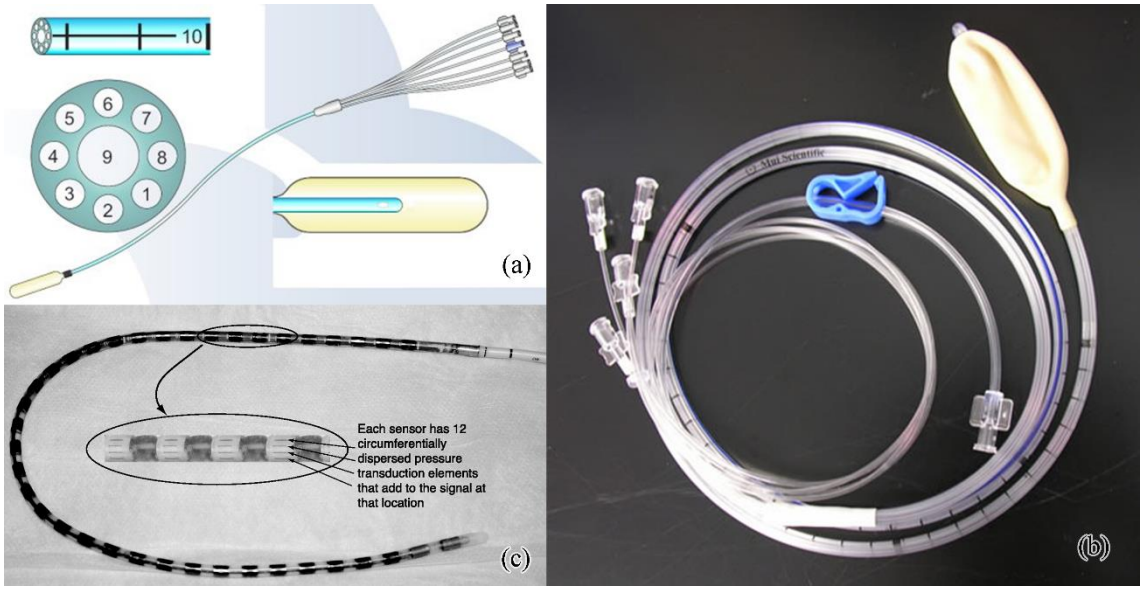

Figure 2.6 Scheme, section (a) and picture (b) of a water-perfused catheter; solid-state catheter (c).

2.1.6 Topographic analysis

The current guidelines for the conventional manometry suggest the adoption of systems with three to eight pressure sensors. This approach requires a sizeable approximation: since no information is given about the pressure distribution between consecutive sensors, it must be interpolated numerically. Unfortunately, during the 80s, the actual benefit of a higher spatial resolution did not gain widespread consensus among the researchers in the field [29]. The disagreement was resolved by Clouse and Staiano between 1991 and 1993. In fact, they used a traditional three-point catheter, which was statically re-positioned after each deglutition series, in order to characterize the overall esophagus. The traditional manometric data were then converted in the corresponding planar representation by means of a topographic analysis software, so that the height of the curves corresponded to the wave amplitude for each sensor position [30] (Figure 2.7).

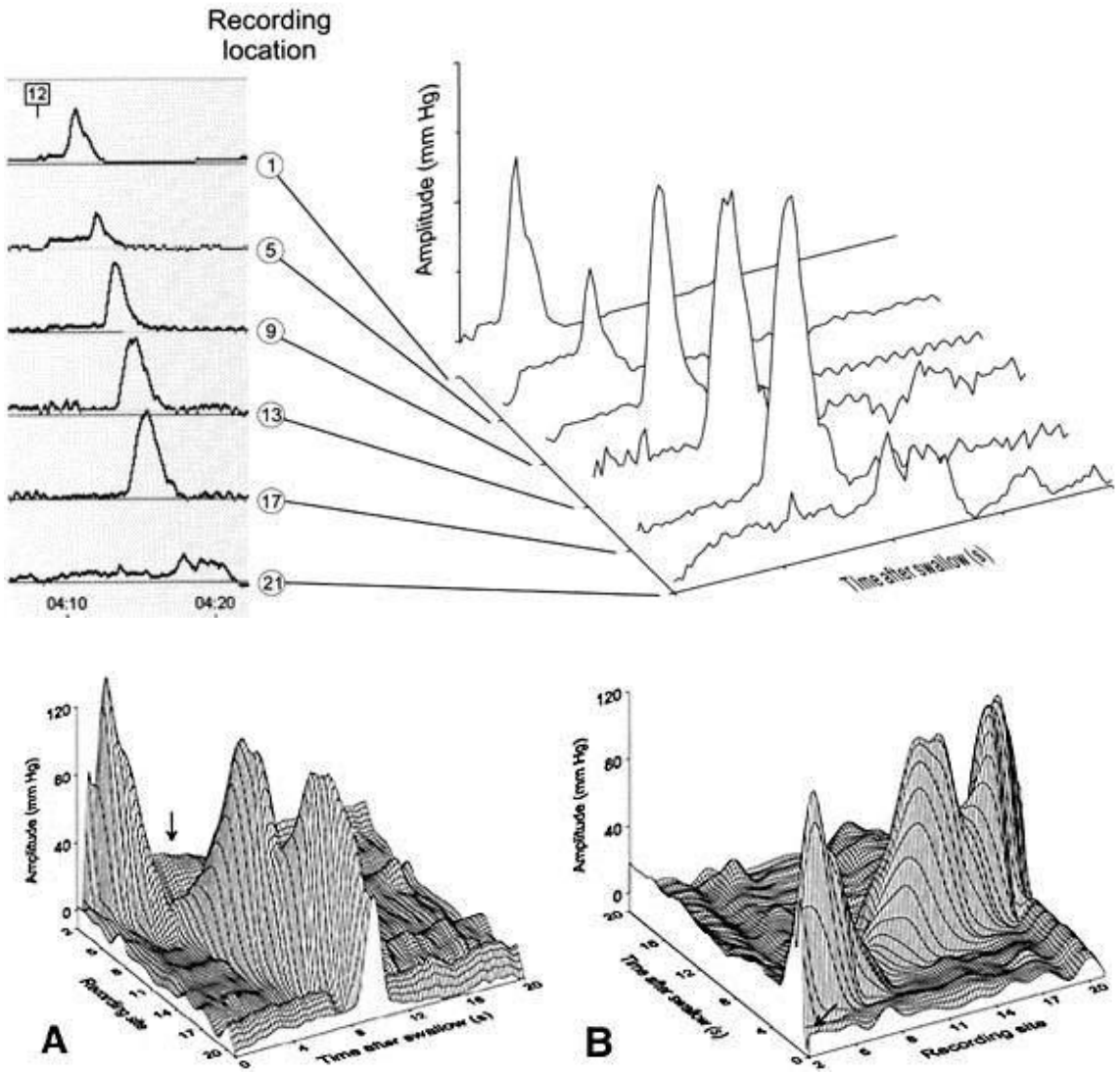

Figure 2.7 First step of the topographic analysis: synchronization of the pressure evolutions recorded by each one of the equally spaced sensors after each re-positioning of the catheter (top). Final result of the digitalization process of the synchronized data, represented as a 3D topographic map from two different points of view (bottom).

It was immediately clear that the new approach could collect a larger amount of information about the functional anatomy of the esophagus, which was not perceptible by conventional manometry. Despite their high degree of innovativeness, these methods demanded a lot of mathematical post-processing, introducing artefacts and, more importantly, giving only static information about the esophageal motility, which was obtained by processing measurements corresponding to different deglutitions. Such procedure prevented to achieve information about a specific deglutition, which

is a fundamental step in the diagnostic process [31]. In conclusion, a tool able to continuously record the esophageal motility with high spatial resolution was not available.

2.1.7 Contour plot

In 1998, Clouse and Staiano developed a 3D analysis tool to represent the distribution of pressure with time and position. The topographic representation was obtained from a digital system able to interpolate data from consecutive sensors, in order to display each swallow as a surface plot without disrupting the signal between the sensors. A more intuitive way to display manometric data was obtained from the surface plot: the so called "contour plot" ("Clouse plot"). The contour plot consisted in a vertical perspective of the corresponding surface plot, where pressure was represented by means of a color grid instead of a third coordinate. Such representation showed concentric rings corresponding to different pressure levels, just like the level curves used in topography [23]. The procedure was similar to the pull through maneuver, with 1 cm-steps between consecutive recordings [32].

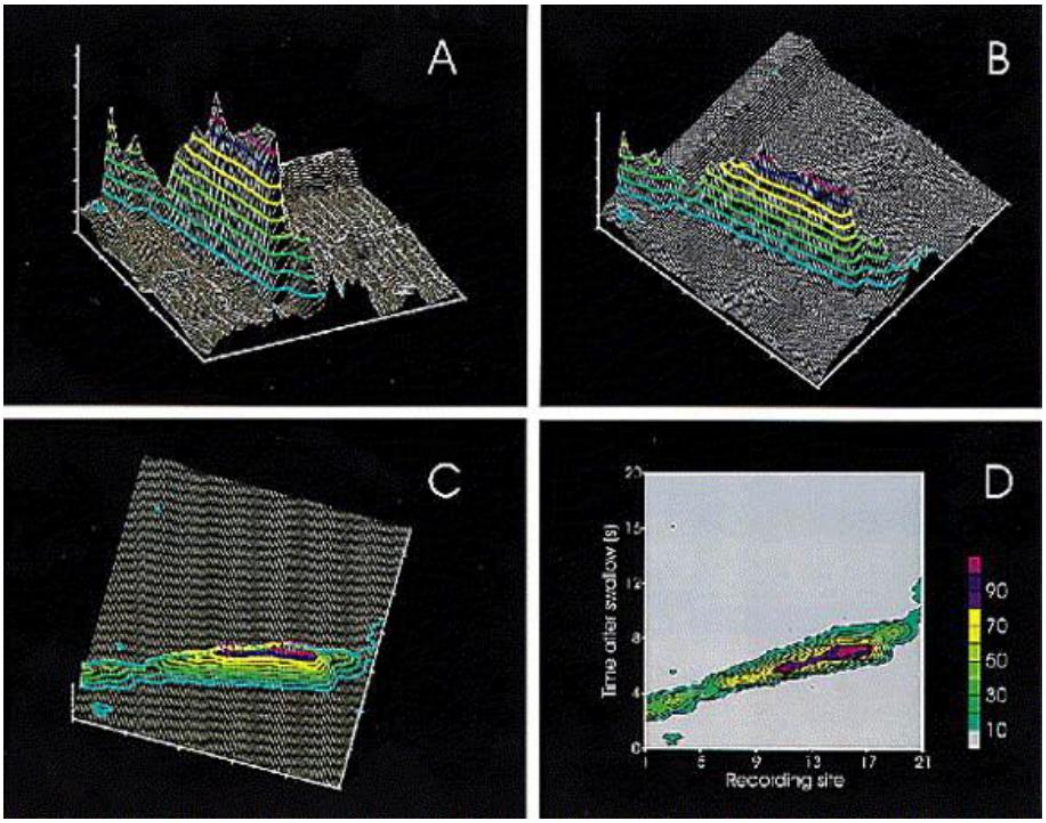

Figure 2.8 From surface plot (A) to contour plot (D)

2.1.8 High Resolution Manometry

In 2003 the American company Sierra Scientific Instruments (LA, USA) developed the 4.2 mm-thick catheter that later became the standard for the diagnosis of esophageal motor disorders: Manoscan™. Such catheter was developed in parallel with the corresponding analysis software, Mano View™ and eSleeve™. It was characterized by 36 equally spaced circumferential solid state sensors 1 cm apart, allowing to acquire manometric data with the highest spatial resolution ever seen on an esophageal catheter. For this reason, the clinical test was called "High Resolution Manometry" (HRM). The presence of solid state sensors allowed to display and process manometric data in real-time from all of the sensors simultaneously, without requiring any re-positioning of the catheter [32].

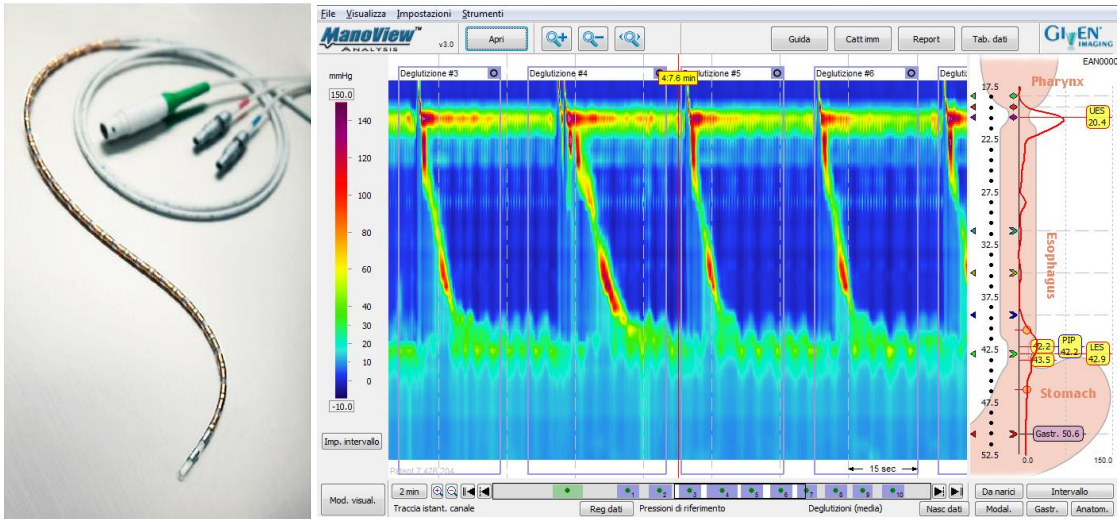

Figure 2.9 Mano Scan catheter (left) and Mano View processing software (right) [33]

HRM brought several advantages to the traditional diagnostic techniques, since it was more easily understandable, the test duration decreased from 30 to 8 minutes [34], the esophageal functional anatomy was more clearly detectable, and the simultaneous real-time monitoring of the relaxation of both sphincters became finally possible [35]. In detail, a high spatial resolution made it possible to represent the exact correlation among the actions of the different muscular components during deglutition, which represent fundamental elements for a proper description of the biomechanics of the bolus transportation [16]. In conclusion, manometry is a clinical test specifically focused on esophageal motility, which is evaluated on the basis of the distribution of the intraluminal pressure

of the esophagus over position and time. It is typically executed on patients with symptoms potentially related to esophageal motor disorders. In detail, manometry is recommended to:

- establish the origin of dysphagia (in case mechanical obstruction are excluded) or other symptoms potentially related to Achalasia (see below) or other primary motor-disorders;
- diagnose minor motility issues that may derive from systemic syndromes (for example systemic sclerosis);
- position intraluminal biomedical devices, such as probes for pH monitoring;
- perform pre-surgery evaluation of anti-reflux surgery candidates, in order to exclude other diagnoses and to define surgery details;
- perform the follow-up of patients who have undergone Achalasia or GERD surgery.

Notwithstanding, since manometry cannot substitute other more specific types of investigation, HRM is not recommended as first level of investigation for the diagnosis of gastro esophageal reflux disease (GERD), as it requires a 24 hours pH monitoring, and in case of chest pain [36].

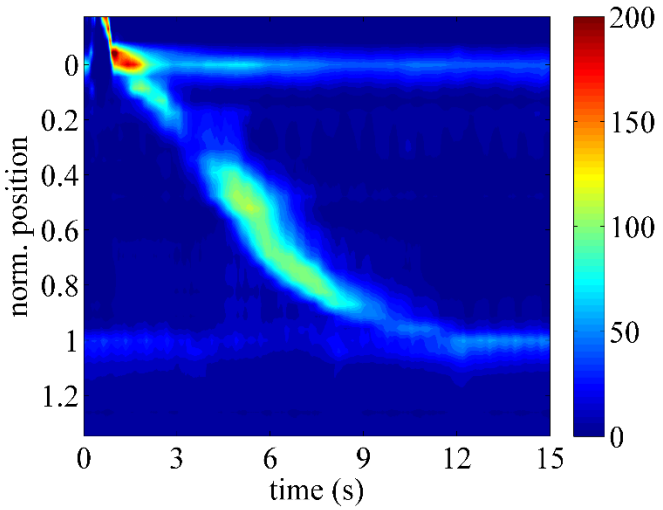

Figure 2.10 Esophageal pressure topography of the HRM test of a healthy subject. Moving from the upper to the lower edge, the main features of the muscular actions are clearly visible. Time is represented on the "x" direction, position along the esophageal axis (0=LES, 1=UES) is represented on the "y" direction, while local pressure is represented by the color of each pixel of the image, according to the pressure/color grid on the right. The swallowing process starts at the pharynx level where a pressure peak propels food from mouth to the upper esophagus, across the LES. LES is clearly visible at the top of the image, as a constant pressure band, which decreases only for less than a second at the beginning of the swallowing process to allow the bolus transit. The first part of the esophageal peristalsis, a sequence of muscular contractions aimed at propelling food forward to the stomach, is due to the action of the striated muscular component, and can be located as an oblique cloud, in the upper esophagus. A pressure gap divides voluntary and involuntary peristalsis. Involuntary peristalsis is due to the action of the smooth muscular component of the lower esophagus, and occur in the lower half of the esophagus. The LES can be located as a horizontal band in the lower part of the image, as it shows a basal pressure during rest. Such pressure decreases at the beginning of the deglutition to allow the bolus transit and contracts to a hypertonic value after the end of the deglutition to avoid gastric reflux.

2.2 Classification of motor disorders according to Spechler and Castell

The deglutition process requires a fine neuro-muscular coordination between the esophageal sphincters and the muscular components of the esophageal body. Motor disorders are characterized by an alteration of such coordination, causing abnormal peristalsis, abnormal sphincter(s) relaxation, ineffective bolus propulsion and/or gastric reflux. Common symptoms are dysphagia, chest pain and gastric reflux-related symptoms [37].

The primary manometric abnormalities of the esophageal motility can be divided in four main patterns [38]: inadequate LES relaxation, uncoordinated contraction, hypercontraction and

hypocontraction. Details about pathologies connected to each pattern are reported in the following paragraphs.

2.2.1 Inadequate LES relaxation

Pathologies connected to the inadequate LES relaxation pattern are related to the inhibition of the innervation of the lower esophageal sphincter, which causes an abnormal relaxation of the sphincter. An abnormal relaxation can be either incomplete in amplitude or too short in duration [39][40], and has important physiological implications, because it delays the esophageal clearance exposing the esophagus to the action of gastric acid.

2.2.1.1 Esophageal Achalasia

The term "Achalasia" comes from the Greek "α-χάλασις" ("a-chálasis") that means "non-relaxation". It is the best understood and best characterized esophageal motility disorder, but its cause is unknown. It has been proved that it is related to the degeneration of inhibitory neurons in the wall of the esophagus [41][42], which produce nitric oxide (NO), affecting the relaxation of the esophageal smooth muscle tissue [43][44]. In fact, the LES is normally contracted at rest and relaxes when intraluminal neurons release their inhibitory neurotransmitters [45]. Loss of inhibitory innervation induces increased basal sphincteric pressures and can interfere with normal relaxation, but does not induce resting tone in esophageal body. Even when Achalasia does not directly affect the muscular components of the esophagus, the functionality of the esophageal body is not immune to the loss of inhibitory innervation, as it can result in aperistalsis [46]. In classic Achalasia, deglutition is often followed either by no activity in the esophageal body or by simultaneous esophageal contractions of low amplitude (<40 mmHg) [47]. The term "classic Achalasia" was introduced to distinguish the "classic" pattern of Achalasia to the pattern of "variant Achalasia" (or "vigorous Achalasia"), which displays simultaneous esophageal contractions with amplitude >40 mmHg. Chest pain is usually more prominent in patients with a variant form of Achalasia. Despite the several abnormalities that often characterize the functionality of the esophagus body of a patient with Achalasia, symptoms are primarily due to the inadequate relaxation of the LES, which is either incomplete or too short in duration [48].

The two manometric features proposed for classic Achalasia by Spechler and Castell [38] are incomplete relaxation of the LES (LES pressure during deglutition >8 mmHg above gastric

pressure) and aperistalsis in the body of the esophagus (no apparent contractions or simultaneous contractions with amplitudes <40 mmHg). Other features are commonly detected in classic Achalasia, but are not required for the diagnosis:

1) elevated resting LES pressure (>45 mmHg),
2) resting pressure in the esophageal body exceeding the pressure in the stomach,
3) high UES residual pressure [49],
4) short UES relaxation [45],
5) repetitive UES contractions [50],
6) abnormal belch reflex [51].

Typical symptoms presented by patients with Achalasia are dysphagia, vomit, hypersalivation and chest pain.

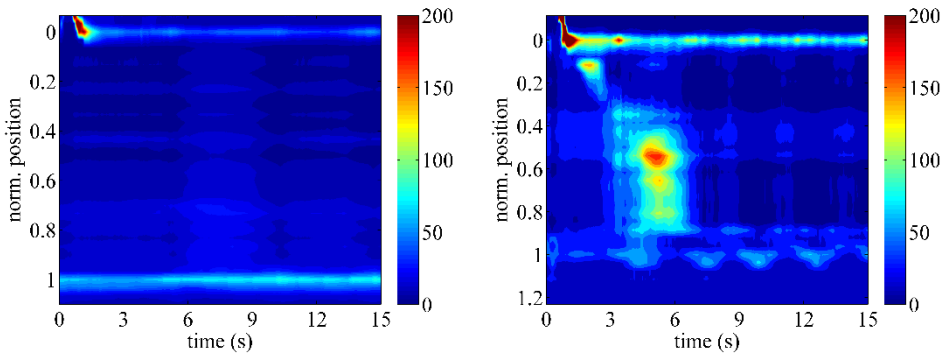

Figure 2.11 HRM results regarding patients with classic Achalasia (left) and variant Achalasia (right)

2.2.1.2 Atypical disorders of LES relaxation

The diagnosis of Achalasia can be excluded if one or more of the following manometric features are noticed:

1) one or more preserved peristalsis,
2) esophageal contractions with high amplitudes (>40 mmHg),
3) complete LES relaxation of inadequate duration [47][52]–[54].

The typical symptoms of the atypical disorders of LES relaxation are dysphagia and chest pain, but they cannot be explained by fixed neoplasms, eosinophilic esophagitis, constrictions, varices,

paraesophageal hernia or stenosis. The barium swallow often shows features that may be related to classic Achalasia with a dilated esophagus and a "rat's tail" (or "bird beak") dysfunctional LES. These disorders can be suspected on the basis of symptoms and manometric tests, but the diagnosis can be confirmed only by the positive response to treatments that aim to reduce the LES pressure, such as calcium channel blockers, pneumatic dilation, Heller myotomy or botulin injection.

Figure 2.12 Typical results of an esophagogram (barium swallow) of a patient with bird's beak esophagus.

2.2.2 Uncoordinated esophageal contraction

2.2.2.1 Diffuse Esophageal Spasm (DES)

The most common presenting symptoms of DES are dysphagia and a recurrent chest pain that is almost indistinguishable from that of cardiac angina [40]. Such symptoms probably come from abnormal esophageal contraction in the distal tract of the esophageal body, which is due to a low swallowing inhibition. It has been proved that no histologic alterations of the myenteric plexus are connected to this disorder [55], but, in spite of this, functional studies and the good response to myorelaxing treatments seems to support this hypothesis. Radiographies of patients with DES show tertiary contractions of the esophagus, while the corresponding manometric tests reveal spastic activity in the lower esophagus.

The manometric features proposed by Spechler and Castell [38] for the diagnosis of DES are simultaneous contractions in more than 10% of wet swallows and the mean amplitude of simultaneous contractions >30 mmHg. As for atypical disorders of the LES relaxation, some

features are commonly found in the manometry test of patients with DES, even if they are not required for the diagnosis. Such features include spontaneous esophageal contractions, repetitive contractions, multiple peaked contractions and intermittent normal peristalsis.

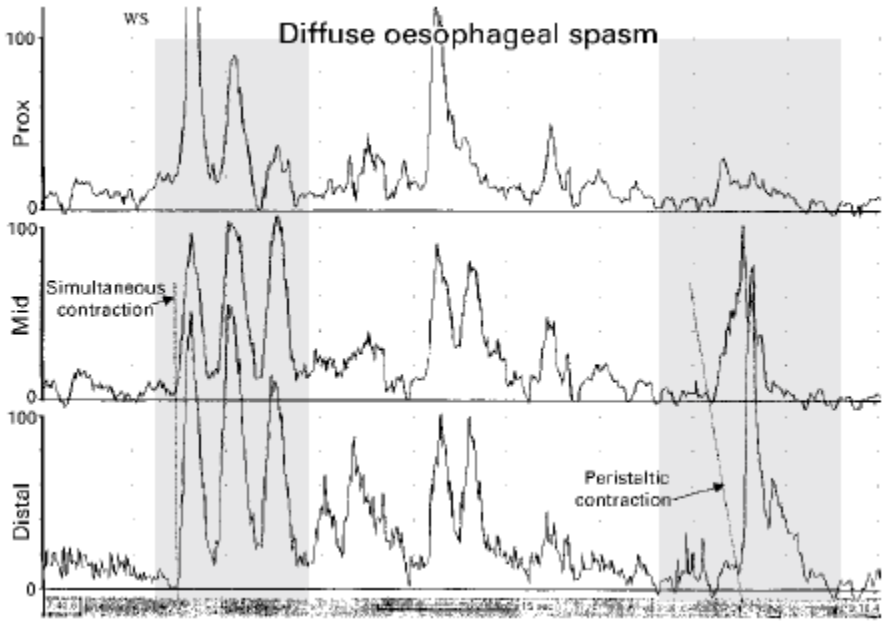

Figure 2.13 Esophageal manometry of a patient with DES at 3, 8 and 13 cm above the LES. Note that, after the simultaneous spastic contractions (left), some peristaltic activity can be preserved (right).

2.2.3 Esophageal hypercontraction

2.2.3.1 Nutcracker Esophagus

The term "Nutcracker esophagus" has been coined for patients accusing non-cardiac chest pain and/or dysphagia, and exhibiting peristaltic activities in the lower esophagus with mean amplitudes exceeding normal values by more than twice the standard deviation (SD) [56]. Consequently, the threshold can vary depending on the experimental data at disposal, in fact different values are reported in literature. Benjamin et al. in 1979 advanced a cutoff value of 120 mmHg [31], while subsequent studies reported 180 mmHg as diagnostic criterion [57][58]. Further variability is introduced by the positioning of the pressure sensors within the esophagus, with particular regard to their distance from the LES [31][59]. The most frequently adopted solutions are 3 and 8 cm [57][60] and 2 and 7 cm above the LES [61].

The manometric feature proposed by Spechler and Castell [38] for the diagnosis of Nutcracker esophagus is a mean distal esophageal peristaltic wave amplitude >180 mmHg, which must be measured at 3 and 8 cm above the LES. Common features of the Nutcracker esophagus are prolonged peristaltic contractions (>6 s) and high resting pressures [58], but they are not required for the diagnosis.

Patients with nutcracker esophagus often present two key symptoms, as non-cardiac chest pain, which is the most common, and/or dysphagia. Such symptoms can be intermittent, and may occur even in resting conditions [62].

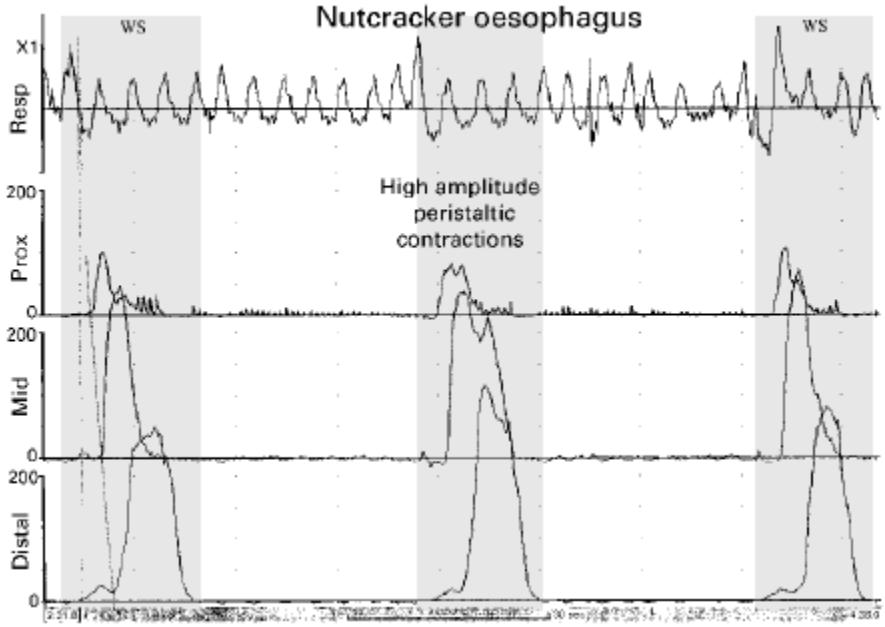

Figure 2.14 Manometry of a patient with nutcracker esophagus, with recording sites at 3, 8 and 13 cm above the LES.

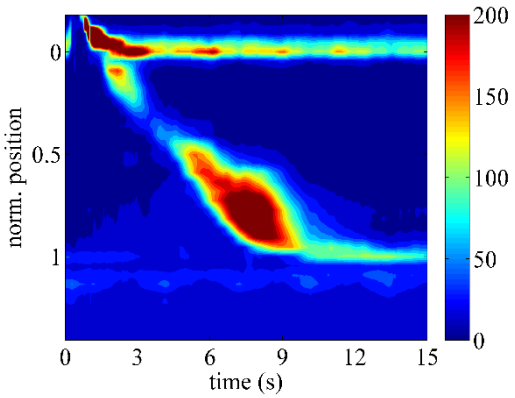

Figure 2.15 High Resolution Manometry of a patient with nutcracker esophagus.

2.2.3.2 Hypertensive LES

The Hypertensive LES disorder was described almost 40 years ago [63], but its physiological consequences are still unclear. Several studies agreed in classifying as hypertensive LES disorders showing elevated resting LES pressure (>2SD [64], >26.5 mmHg [65] or >45 mmHg [66]), abnormal pressure of the LES after relaxation (>2SD=45 mmHg, when measured using the station pull-through technique [58][66][67]) and incomplete LES relaxation [68]. The last feature seems to be the condition that mostly affects the esophageal clearance, but Spechler and Castell [38] agreed to consider only the second one as required for the diagnosis of hypertensive LES.

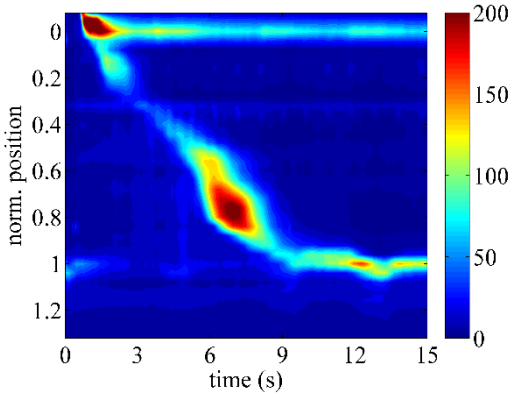

Figure 2.16 High Resolution Manometry of a patient with hypertensive LES.

2.2.4 Esophageal hypocontraction

The manometric pattern of esophageal hypocontraction can be found in the 80% of patients with scleroderma [69]. The word "scleroderma" derives from the ancient Greek and literally means "hard skin". It affects esophageal muscles and nerves, like fibrosis and vascular obliteration [70], with particular regard to the distal part of the esophagus [71], weakening the muscle component decreasing the amplitude of peristaltic waves (<30 mmHg [72][73]) and compromising the normal esophageal clearance [74][75], exposing the lower esophagus to gastrointestinal reflux. The LES can also be compromised by scleroderma, as different research groups reported different resting pressures at this level (<10 mmHg [71][72], 15.8+-1.2 mmHg [73]).

The peristaltic abnormalities commonly observed in patients with esophageal hypocontraction are:failed peristalsis in the distal esophagus, simultaneous distal esophageal contractions of low amplitude and no discernible contractions at all [71]–[76], but the required manometric feature proposed by Spechler and Castell [38] pertains to the evidence of hypocontraction in the distal esophagus in at least 30% of wet swallows. Such criterion consider as evidence of hypocontraction any combination of the following features:

1) peristaltic or non-peristaltic contractions in the distal esophagus with amplitudes <30 mmHg,
2) failed (ineffective) peristalsis
3) absent peristalsis.

2.2.4.1 Ineffective Esophageal Motility (IEM)

IEM is the most representative disorder of a number of functional abnormalities defined as Non-specific Esophageal Motor Disorders (NEMD). It was introduced during the 90's as a standalone clinical entity, and it is characterized by an increased esophageal exposition to the gastric juices and by a strict relation with the Gastro-Esophageal Reflux Disease (GERD) [77].

2.2.5 Non-specific esophageal motility abnormalities

The features required for the diagnosis of the cited esophageal motility abnormalities are summarized in Table 2.1, but some manometric tests may present features that do not meet the

requisite criteria for any of the recognized conditions. Such patients are better to be classified as affected by a form of non-specific esophageal motility abnormality [38].

Table 2.1 Manometric features of named esophageal motility abnormalities

Esophageal motor disorder	**Basal LES pressure**	**LES relaxation**	**Wave propagation**	**Distal wave amplitude**
Achalasia	Usually high, may be normal, rarely low	Incomplete	Simultaneous or absent, no peristalsis	Low or normal
Atypical disorders of the LES relaxation	Low, normal or high	Inadequate (incomplete or short duration)	Some normal peristalsis, may have simultaneous or absent sequences	Low, normal or high
Hypertensive LES	High	Complete	Normal	Normal
DES	Low, normal or high	Complete	Simultaneous in >10% of swallows	Normal or high
Nutcracker esophagus	Low, normal or high	Complete	Normal	High
IEM	Low or normal	Complete	Normal, simultaneous or absent	Low in ≥30% of wet swallows

2.3 Traditional classification of esophageal motor disorders

The traditional classification of esophageal motor disorders considers an additional disease characterized by the incompetence of the LES. To this category pertain the manometric measurements characterized by a so called "defective LES", and are frequently related to the GERD [78]. Two parameters must be evaluated to diagnose a defective LES disorder: a decreased length of the LES, and the LES pressure, which has to be lower than normal values. Classic diagnostic techniques, such as the barium swallow and manometry (Figure 2.17), are able to identify the precise value of such parameters and represent reliable tools for the clinical practice. On the other

hand, some symptoms, as non-obstructive dysphagia and chest pain, are not always related to manometric or radiographic alterations [37].

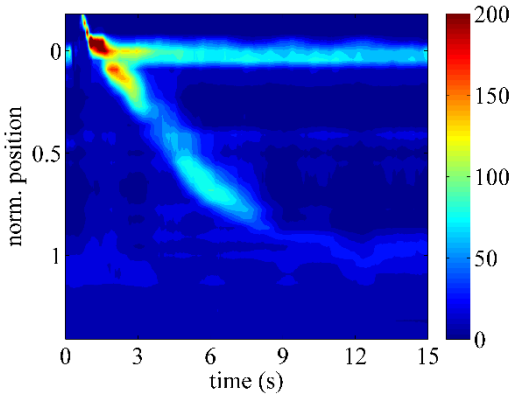

Figure 2.17 High Resolution Manometry of a patient with defective LES.

The traditional diagnostic process consists in a complicated evaluation of symptoms and tests, but the evaluation of a manometric test are summarized in Table 2.2.

Table 2.2 Criteria for the evaluation of the manometric tracing according to the traditional diagnostic process

Esophageal motor disorder	**Diagnostic criteria**
Achalasia	- absent or simultaneous contractions in 100% of swallowings - abnormal LES relaxation
Atypical disorders of the LES relaxation	- abnormal relaxation of the LES, and absent peristalsis - absent or simultaneous contractions may occur
Hypertensive LES	- basal LES pressure >45 mmHg - normal LES relaxation - normal peristalsis
DES	- contraction speed >8cm/s, recorded by sensors at 3 and 8 cm above the LES, in ≥10% of the deglutitions - mean wave amplitude >30 mmHg
Nutcracker esophagus	- mean peristaltic wave amplitude >180 mmHg recorded by sensors at 3 and 8 cm above the LES
Defective LES	- basal LES pressure <2.5th percentile - abdominal LES length <5th percentile - entire LES length <2.5th percentile
Normal	- normal bolus speed - normal wave amplitude - intact wave propagation in >70% of the deglutitions

2.4 The Chicago Classification

Recent technological and computational advances, such as the introduction of HRM and the development of algorithms for the representation of pressure topography plots, have revolutionized the performance of clinical esophageal manometry, permitting the visualization of esophageal motility as a spatial continuum along the length of the esophagus. Such advancements essentially excluded the influence of movement-related artifacts, which represented a huge limitation of the conventional manometry, and made it possible to define the contractile characteristics of the esophagus and its sphincters much more precisely. At first, the majority of the clinicians was suspicious about the innovation, and did not take advantage of it. Some of them decided to dumb such technologies down and transform the pressure topography back to the conventional line tracing, inevitably losing the information gained with the new tools at disposal.

With new devices, new algorithms and way more data, the classification of the esophageal motility had to be redefined because it was developed on the basis of old techniques, as conventional manometric systems. In order to diagnose abnormalities esophageal motility on the basis of the newer and richer datasets, new and more specific parameters were defined to characterize different features of a HRM test: Integrated Relaxation Pressure (IRP), Pressurization Front Velocity (PFV), Distal Latency (DL), Distal Contractile Integral (DCI) and the analysis of the 20 mmHg contour. Further details about the computation of such parameters are given in the following paragraphs [79]. The Chicago Classification (CC) consists in a diagnostic scheme developed to identify pathologies on the basis of the value of such parameters. The definition of the parameters and the algorithm itself have seen major revisions in the last years [24][80] and a further major revision is now in progress, confirming that the widely used current classification is still far from a final configuration. The definitions of the minor disorders of peristalsis and the hierarchical scheme of the diagnostic procedure are detailed in Table 2.3 and Figure 2.18, respectively [80].

Table 2.3 Definitions of the minor esophageal motility disorders accounting for CC 3.0

Achalasia and EGJ outflow obstruction	**Criteria**
Type I Achalasia (classic Achalasia)	Elevated median IRP (>15 mmHg), 100% failed peristalsis (DCI <100 mmHg s cm). Premature contractions with DCI values less than 450 mmHg s cm satisfy criteria for failed peristalsis.
Type II Achalasia (with esophageal compression)	Elevated median IRP (>15 mmHg), 100% failed peristalsis, panesophageal pressurization with ≥20% of swallows. Contractions may be masked by esophageal pressurization and DCI should not be calculated.
Type III Achalasia (spastic Achalasia)	Elevated median IRP (>15 mmHg), no normal peristalsis, premature (spastic) contractions with DCI >450 mmHg s cm with ≥20% of swallows. May be mixed with panesophageal pressurization.
EGJ outflow obstruction	Elevated median IRP (>15 mmHg), sufficient evidence of peristalsis such that criteria for types I-III Achalasia are not met.
Absent contractility	Normal median IRP, 100% failed peristalsis. Achalasia should be considered when IRP values are borderline and when there is evidence of esophageal pressurization. Premature contractions with DCI values less than 450 mmHg s cm meet criteria for failed peristalsis.
Diffuse esophageal spasm	Normal median IRP, ≥20% premature contractions with DCI >450 mmHg s cm. Some normal peristalsis may be present.
Jackhammer esophagus	At least two swallows with DCI >8000 mmHg s cm. Hypercontractility may involve, or even be localized to, the LES.
Ineffective esophageal motility (IEM)	≥50% ineffective swallows. Ineffective swallows can be failed or weak (DCI<450 mmHg s cm). Multiple repetitive swallow assessment may be helpful in determining peristaltic reserve.
Fragmented peristalsis	≥50% fragmented contractions with DCI > 450 mmHg s cm.
Normal esophageal motility	Not fulfilling any of the above classifications.

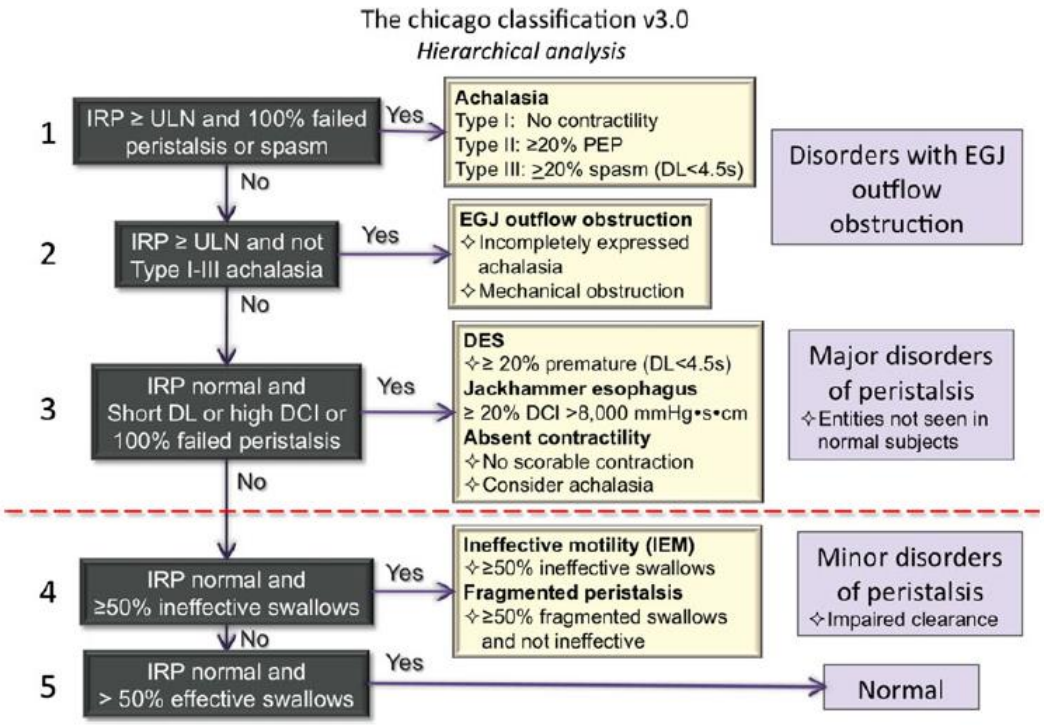

Figure 2.18 Hierarchical algorithm for the interpretation of HRM studies with CC 3.0.

2.4.1 Integrated Relaxation Pressure (IRP)

IRP is a parameter describing the relaxation capacity of the LES. It is defined as the minimal average pressure during a 3- or 4-second relaxation period within the deglutitive LES relaxation window (Figure 2.19).

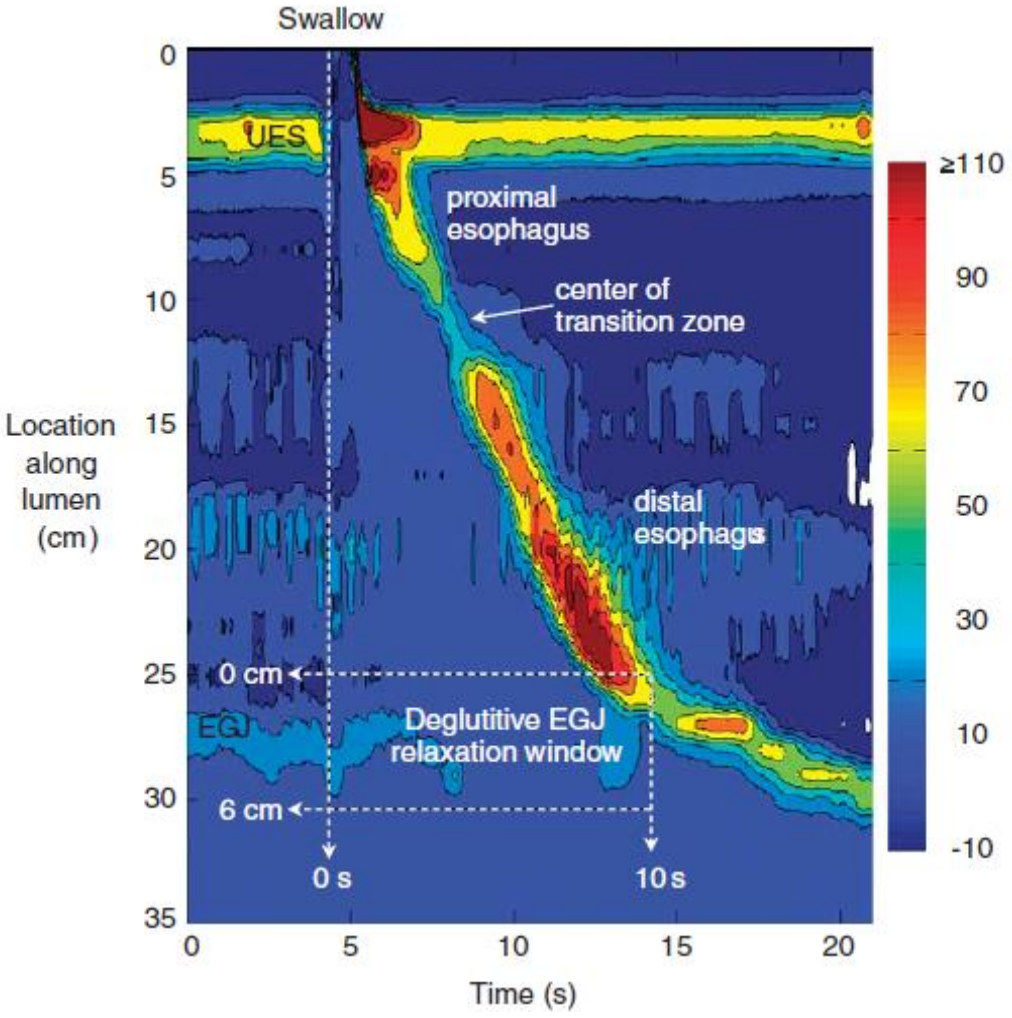

Figure 2.19 Pressure topography of a swallow of a healthy subject. The y axis spans from pharynx (0-2 cm) to stomach (32-35 cm). The transition zone spans from the end of the proximal esophageal segment (striated muscle) to the beginning of the distal esophageal segment (smooth muscle). The deglutitive relaxation window is defined by the 10 seconds following the upper sphincter relaxation. The spatial domain of the EGJ is user defined.

In other words it is defined as the integral of the curve in Figure 2.20, divided by 3 or 4 seconds, respectively. The relaxation period do not need to be contiguous, in order to make this index less vulnerable to crural diaphragm artifact.

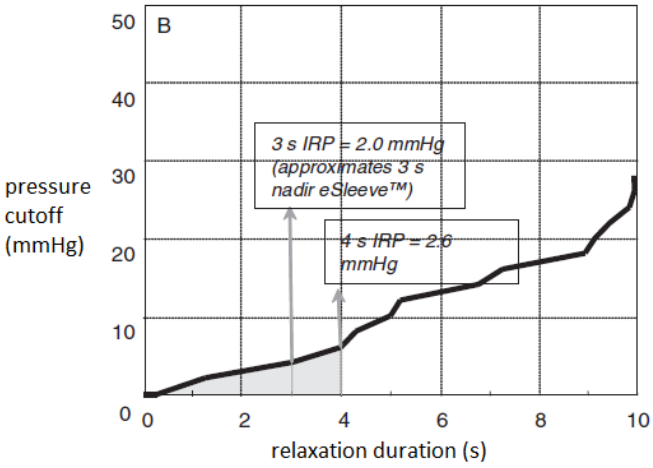

Figure 2.20 Methodology for calculating the LES relaxation. Each point of the curve represents the duration of the relaxation when the corresponding average pressure cutoff was considered. The duration of the relaxation is defined as the amount of time in which LES pressure is lower than the cutoff value.

2.4.2 Pressurization Front Velocity (PFV)

The PFV is an important feature that was used in the CC 1.0 to evaluate the peristaltic capabilities of the esophageal body. The identification of such parameter is facilitated by the generation of the isobaric 30 mmHg contour plots at the lower half of the esophagus, which provide a reliable means of differentiating intrabolus pressure from closure pressure and the timing of the onset of the peristaltic contraction. The PFV is calculated by marking the distal temporal margin of the transition zone and the superior margin of the EGJ on the isobaric contour, and then calculating the corresponding slope, as represented in Figure 2.21.

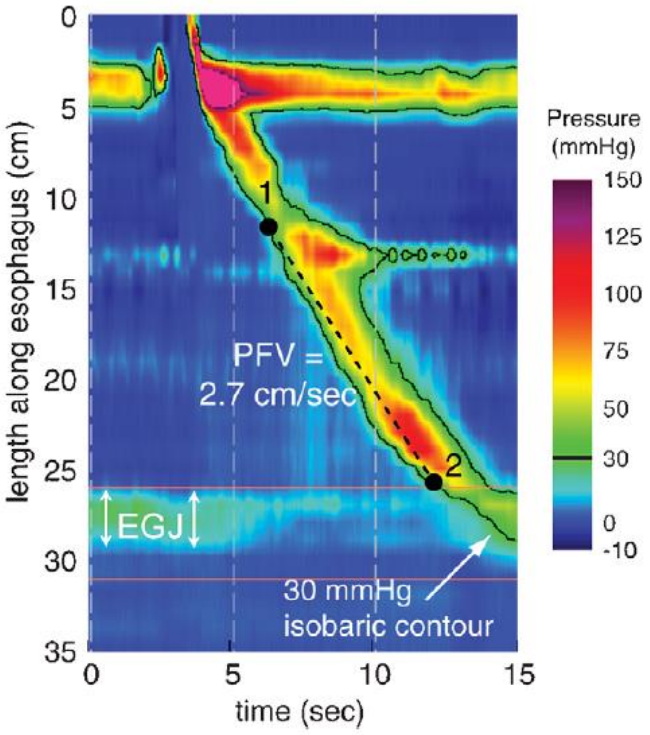

Figure 2.21 Calculation of the pressurization front velocity (PFV) from 30-mm Hg isobaric contour plots (black line). Distal temporal margin of the transition zone (point 1) and proximal margin of the EGJ on the 30-mm Hg isobaric contour (point 2) were localized by hand.

2.4.3 Distal Latency (DL)

The definition of DES in the CC depends on identifying premature contractions, which consist in muscular activities that occur prematurely within the distal esophagus. The early occurrence of such contractions can be detected by means of the DL, and physiologically represents the attenuation of deglutitive inhibition.

The DL is measured as the time interval from UES relaxation to the Contractile Deceleration Point (CDP). In pressure topography plots, the CDP represents the inflexion point in the Contractile Front propagation Velocity (CFV) in the distal esophagus [81]. It must be localized within 3 cm from the LES [36] and along an isobaric contour line of greater magnitude in case of compartmentalized pressurization. However, it was clearly demonstrated that a rapid CFV lacks of specificity for spasm, often instead identifying fragmented peristaltic contractions with atypical pattern [82], leading the International High Resolution Manometry Working Group to conclude that the CFV should not be used as a defining metric in the 3.0 version of the CC.

2.4.4 Distal Contractile Integral (DCI)

The DCI summarizes the distal esophageal contractile length, vigor and persistence, quantifying the contractile pressure exceeding 20 mmHg for the region spanning from the transition zone to the proximal aspect of the LES. Imaging a 3D representation of a Clouse plot (Figure 2.22), it is computed as the volume of the domain above the 20 mmHg isobaric contour within the distal esophagus [79], thus, it is measured in mmHg*s*cm [35].

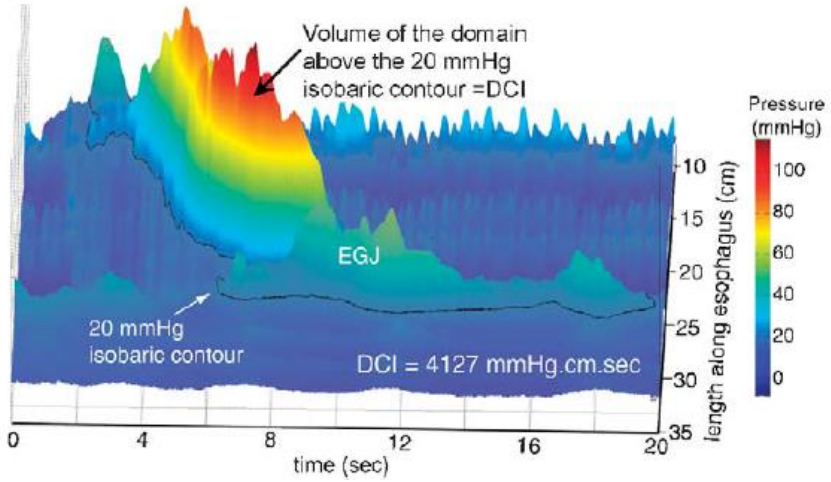

Figure 2.22 Derivation of the DCI.

2.4.5 Analysis of the 20 mmHg contour plot

The contour of the area exceeding a pressure value of 20 mmHg (Figure 2.23) is usually plot in order to assess the presence of fragmented peristalsis. An esophageal contraction is classified as "fragmented" if the 20 mmHg contour present a break larger than 5 cm at the transition zone of the esophagus.

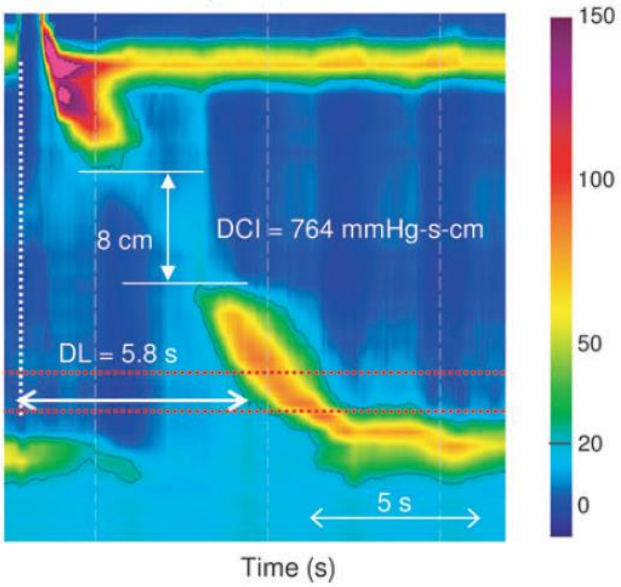

Figure 2.23 HRM of a fragmented peristaltic contraction and corresponding 20 mmHg contour plot (black line)

CHAPTER 3

MODELS TO INTERPRET THE ESOPHAGEAL MOTILITY

Mathematical models are often developed in research to interpret data collected from experimental activities or observed phenomena. Such models consist in mathematical formulations that are defined to explain the mathematical relation between one or more quantities as functions of one or more variables, accounting for specific values of one or more parameters introduced to affect model results. The parameter(s) identification process aims at finding the best value(s) of the model parameter(s), according to a specified criterion, that usually aims at minimizing the discrepancy between experimental data and model results. Reliable mathematical models must be formulated on the basis of a theory that is able to explain the observed phenomenon.

3.1 Existing models

As regards the esophageal motility, there exists extensive literature on the mathematical models to interpret different physiological phenomena, such as the peristaltic transport of the bolus, the variation of the geometrical conformation of the duct over time, the mechanical behavior of the biological tissues and structures involved, the distribution of the inner esophageal pressure and so on.

This section provides an overview of the existing models to interpret the evolution over time of the distribution of the pressure within the esophageal duct. Pressure is always explained as a function of time and position along the esophagus itself, and different parameters are defined depending on the specific formulation developed.

3.1.1 Li and Brasseur

Different researchers carried out several investigations on the peristaltic transport of Newtonian [83]–[88] and non-Newtonian [89]–[91] fluids through tubes within tubes of circular [92] and non-circular [93] cross sections. Some of them considered infinite length tubes, while Li and Brasseur [94] pointed out that a finite length tube was more appropriate mimic the esophagus, and improved the conventional sinusoidal wave equation by considering the position of the wall as a function of

the minimum radius of the tube, which can only contract inwardly. Consequently, they suggested that the wall shape should be a function of the radius of the stationary tube rather than the contracted one, and when the wall relaxes, the dilation should be restrained within the stationary boundary. They proposed the following formulation to evaluate the mathematical relationship between the intraluminal pressure $p(x,t)$, the wall geometry $H(x,t)$ and velocity, as represented in Figure 3.1:

$$p(x,t) = p_0(t) + \int_0^x \frac{\partial p}{\partial x}(s,t)\,\mathrm{d}s$$

where x represents the position along the esophagus, t is time and

$$\frac{\partial p}{\partial x} = \frac{1}{H^4(x,t)}\left(G_0(t) + 16\int_0^x H(s,t)\frac{\partial H(s,t)}{\partial t}\,\mathrm{d}s \right)$$

with

$$G_0(t) = \frac{p_L(t) - p_0(t) - 16\int_0^L H^{-4}(s_1,t)\left(\int_0^{s_1} H(s_2,t)\frac{\partial H(s_2,t)}{\partial t}\,\mathrm{d}s_2 \right)\mathrm{d}s_1}{\int_0^L H^{-4}(s,t)\,\mathrm{d}s}.$$

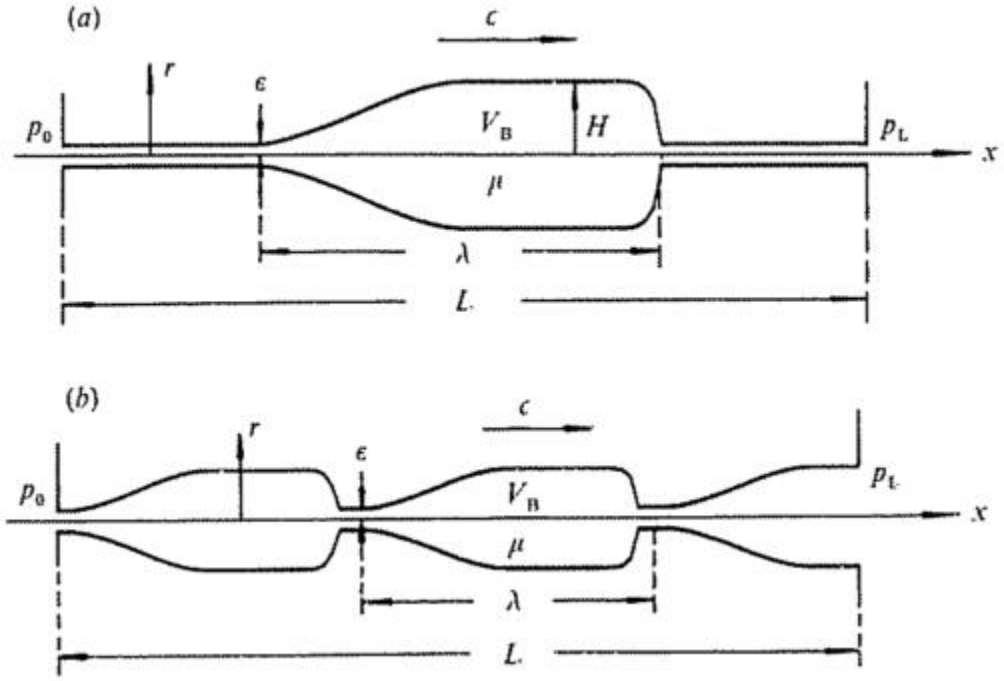

Figure 3.1 Peristaltic transport according to Li and Brasseur: single contraction wave (a), continual production of "train waves" (b). In both cases, the fluid bolus is transported from left to right against a pressure difference p_1-p_0 by peristaltic contraction waves along the tube. The contraction wave speed, wavelength, tube length and tube occlusion are defined as c, λ, L and ε, respectively. The fluid viscosity and the fluid volume within one wavelength are μ and V_B.

3.1.2 Misra and Pandey

Misra and Pandey in 2001 [95] presented a mathematical model for the transport of foot through the esophagus, by considering the transport of a power-law fluid, representing the food inside a finite length tube with a circular section, representing the esophagus itself. They implemented the concept of inward contraction, considering the peristaltic tube as vibrating only in one direction according to a sinusoidal wave propagation, restricted within the stationary wall of the esophagus, along its length. This model simulates the stimulation of the wall of the esophagus by means of a periodic transverse contraction wave, and its path is subsequently retracted so that its original position is attained. The motion $\hat{h}$ of the wall, as the evolution of its displacement from the centerline (Figure 3.2), is represented by

$$\hat{h}\left(\hat{z},\hat{t}\right) = a - 0.5\hat{\phi}\left\{1+\cos\frac{2\pi}{\lambda}\left(\hat{z}-c\hat{t}\right)\right\},$$

where $\hat{z}$ is the axial distance, $\hat{t}$ the time, a the radius of the stationary tube, $\hat{\phi}$ the amplitude of the wave, λ the wave length and c the speed of the wave.

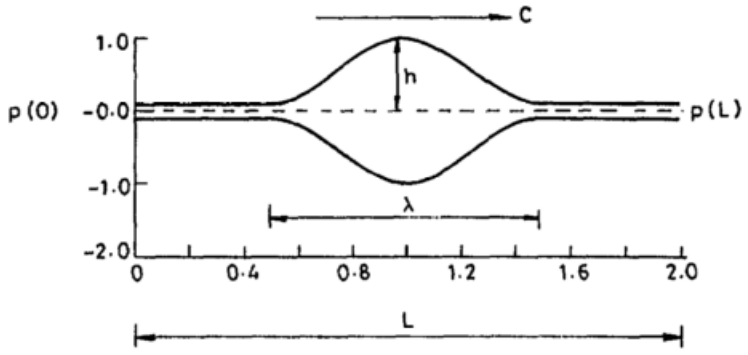

(a) Propagation of single wave of contraction.

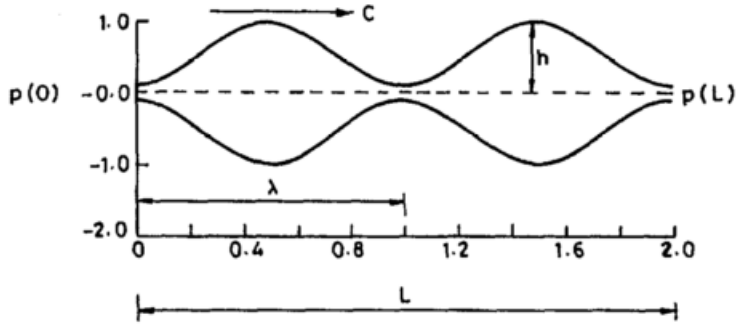

(b) Propagation of train-waves of contraction against a pressure difference of $p(L) - p(0)$ along the length of the oesophagus.

Figure 3.2 Peristaltic transport through the esophagus according to Misra and Pandey.

After the transformation of some parameters and the removal of negligible effects, the equations governing the motion of the bolus reduce to

$$\frac{\partial p}{\partial z} = \left(\operatorname{sign} \frac{\partial u}{\partial r} \right) \left[\frac{1}{r} \frac{\partial}{\partial r} \left\{ r \left| \frac{\partial u}{\partial r} \right|^n \right\} \right], \quad \frac{\partial p}{\partial r} = 0 \text{ and } \frac{1}{r} \frac{\partial (rv)}{\partial r} + \frac{\partial u}{\partial z} = 0$$

where r is the normalized radial distance. The application of different constraints and boundary conditions and integrating the pressure gradient $\frac{\partial p}{\partial z}$, the pressure along the length of the tube can be determined as

$$p(z,t)-p(0,t)=\frac{1}{h^{1+3n}}\int_0^z\left[\frac{3n+1}{n}\int_0^z h\frac{\partial h}{\partial t}\mathrm{d}\bar{z}+G_0(t)\right]\times\left|\frac{3n+1}{n}\int_0^z h\frac{\partial h}{\partial t}\mathrm{d}\bar{z}+G_0(t)\right|^{n-1}\mathrm{d}\bar{z}$$

where $G_0(t)$ is an arbitrary function of t alone. This quantity can be also expressed as a function of the normalized flow rate $Q(z,t)$, as

$$p(z,t)-p(0,t)=-2\int_0^z\left[\frac{3n+1}{n}\frac{Q(\bar{z},t)}{\eta h^{(1+3n)/n}}\right]\left|-\frac{3n+1}{n}\frac{Q(\bar{z},t)}{\eta h^{(1+3n)/n}}\right|^{n-1}\mathrm{d}\bar{z}$$

where $\eta=1$ for train-waves and $\eta=L/\lambda$ when the condition of single wave transport is analyzed. The local shear stress can be determined as well:

$$\tau_{\omega(z,t)}=\left(\operatorname{sign}\frac{\partial p}{\partial z}\right)h^{1/n}\left|\frac{1}{2}\frac{\partial p}{\partial z}\right|^{1/n}.$$

3.1.3 Toklu model

Differently from Li and Brasseur, Ethem Toklu described the mechanism of inward contraction by considering the position of the wall as a function of the radius of the stationary tube, rather than a function of the radius of the contracted tube. According to Toklu, the dilation should be restrained within the stationary boundary when the wall relaxes from contraction [96]. This modification makes the adjustment of the wave amplitude unnecessary, even if the minimus radius varies. Toklu treated the esophagus as a circular tube of finite length, and assumed the flow as a single-phase Newtonian incompressible fluid of uniform viscosity. His modeling activities were based on an experimental result of Ren et al. [97], who observed that, even if calculations have always been done accordingly to the hypothesis of sinusoidal pressure distributions along the esophagus, it should rather be described by means of a polynomial form.

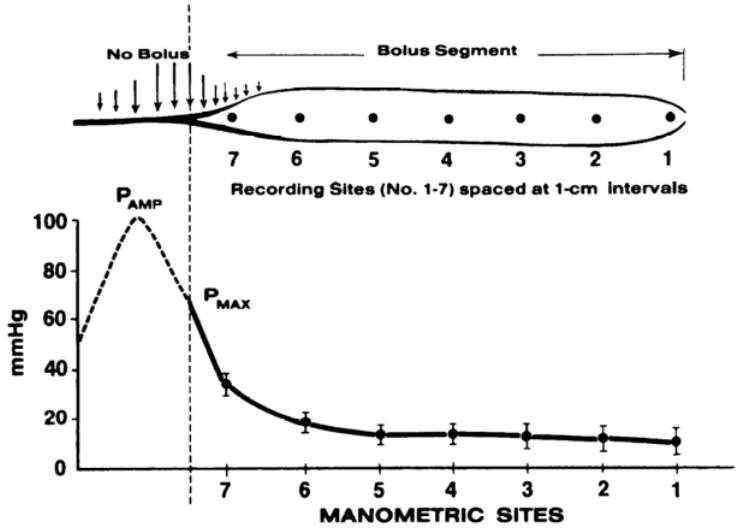

Figure 3.3 Axial distribution of intrabolus pressure during effective peristaltic transport of 5 ml low viscosity barium bolus. Pressures were measured during different swallows in 6 subjects at istant when proximal manometric site (number 7) was determined on fluoroscopy to be 0.5 cm from tip of bolus tail. The seven manometric sites were spaced 1 cm apart. [97]

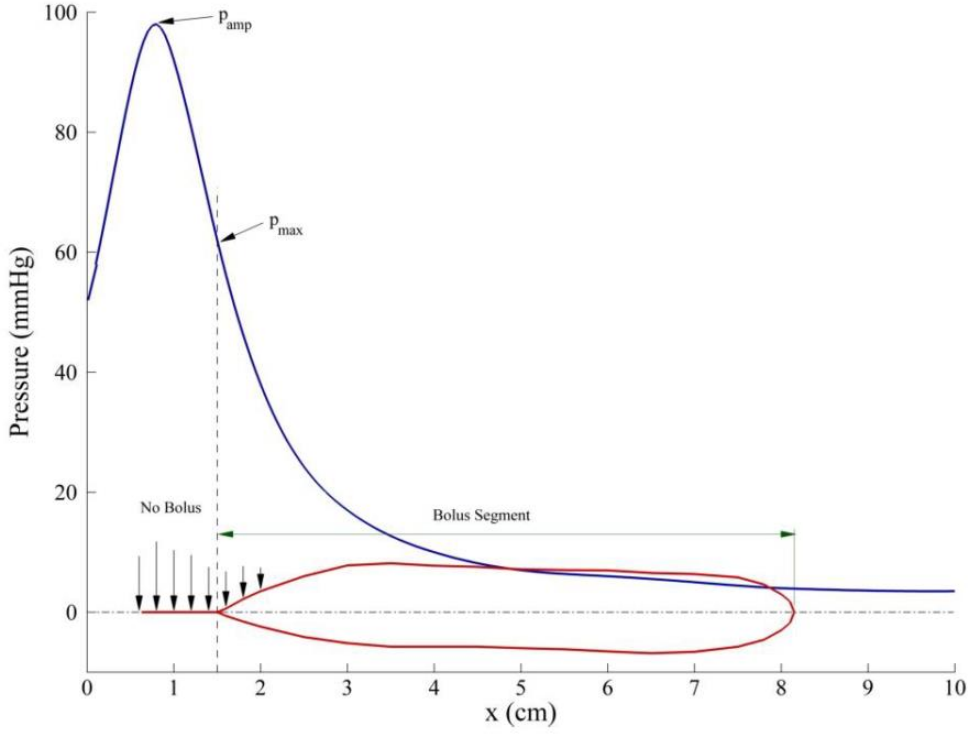

Figure 3.4 Axial distribution of intrabolus pressure during esophageal peristaltic transport of low viscosity barium bolus [96].

According to the Toklu model, the shape of the bolus tail and head can be described using sinusoidal functions, and the main body of the bolus can be approximated with a constant radius:

$$H\left(x,t\right)=\varepsilon+0.5\alpha\left(1-\cos\left(2\pi\left(\frac{x-ct}{\lambda}\right)\right)\right),$$

where x is the position along the axial direction of the duct, t is time, ε is the minimum radius of the tube, $\alpha=2a-\varepsilon$, a is the average radius of the bolus, c is the characteristic velocity of the peristaltic wave and λ is the bolus wavelength, as depicted in Figure 3.5.

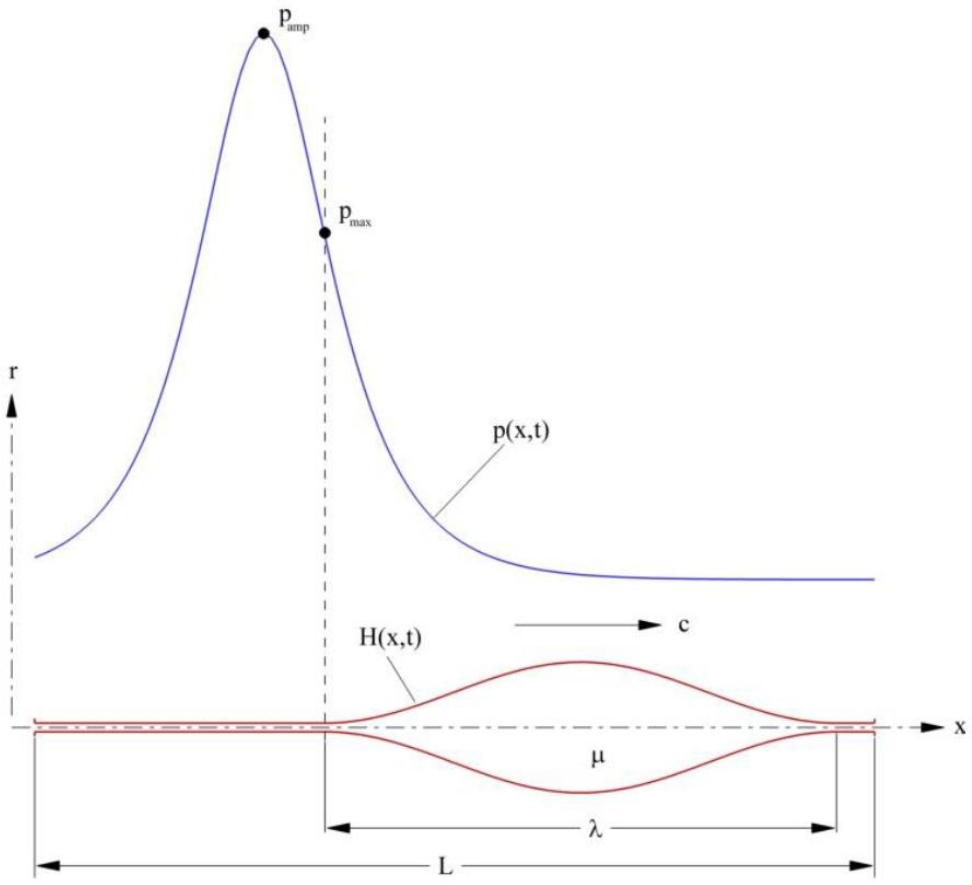

Figure 3.5 Bolus geometry and pressure distribution, according to Ethem Toklu [96].

Toklu identified three different regions in Figure 3.5, since pressure distribution along the esophagus can be defined as:

a) no bolus region: high pressure zone (p_0+p_1),

b) bolus segment: pressure gradient decrease gradually, while p_{max} is effected at the bolus tail (p_0+p_1),
c) after bolus segment: low pressure zone (p_0),

where p_0 represents the resting pressure, p_1 the pressure difference between peak and resting conditions and $p_{max}=p_0+p_1$.
Such distribution was interpreted by a mathematical model designed to explain the relationship between pressure, position and time along the esophagus length by means of a hyperbolic formulation:

$$p(x,t) = p_0 + p_1 \operatorname{sech}\left(\frac{b_1(x-ct)-b_2}{L}\right).$$

Here, b_1 and b_2 are constants referred to the contraction speed and delay. Such formulations, together with the equations of conservation of momentum in an axisymmetric coordinate system moving with the wave shape [94], were processed numerically in order to achieve the analytical bolus shape and pressure distribution. As represented in Figure 3.6, these results were compared to the experimental results and a qualitative agreement was assessed, to show that polynomial form of pressure distribution along the esophagus can be calculated successfully. In conclusion, Toklu proved that his model was qualified to interpret some biological situations where a single pressure wave travels down the length of an organ of finite dimension like the esophagus or the urethra.

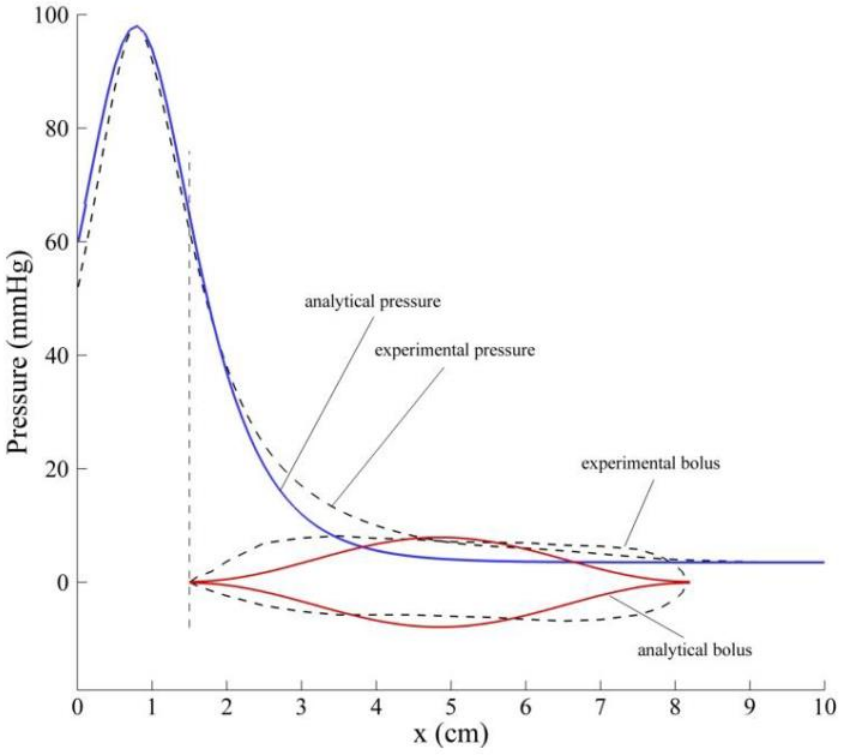

Figure 3.6 Analytical and experimental pressure distribution and wall shape.

3.1.4 Limitations of existing models

As described in detail in Chapter 1, the esophagus is a complex biological structure from both functional and morphometrical view-point at micro- and macroscopical level. In detail, esophagus is able to play its physiological role by means a number of active and passive biological components which are organized in a multilayered configuration. Such components are coordinated in a complex and synchronized action to propel the food towards the stomach. The heterogeneous distribution of the physiological properties of the esophagus can be observed not only from the analysis of its cross-section, but also from the study of the structural conformation along its length. In detail, different tracts, such as the sphincters, the transition zone and the upper and lower tracts of the esophagus, play distinctive roles in propelling the food downwards, preventing the ingestion of air, or preventing gastric reflux.

A mathematical model designed to interpret the manometric results of the esophageal peristalsis must be able to account for all of these differences in order to be suitable for its purpose. In detail, the involved parameters should be expressed as functions of the position along the esophageal

length in order to account for its complex conformation and the heterogeneous distribution of its mechanical and physiological properties. Furthermore, relationships between model parameters and physio-mechanical properties of esophageal structures must be identified in order to properly understand their role within the mathematical model.

None of the models found in literature meet the criteria reported above, and model parameters identification has usually been performed accounting for limited sets of experimental data.

3.2 Development of a physiological model

3.2.1 Formulation

Part of the investigation reported in this work pertained to the development of a new physiological model proposed to overcome the limitations of the existing ones. The model was designed to interpret the pressure map due to the transit of a generic wave, with particular regard to the peristaltic wave measured during esophageal High Resolution Manometry. The physiological model described here consists in a formulation designed to interpret the mathematical relationship between pressure *p*, time *t* and normalized position along the esophagus *x*. Position *x* is normalized in order to allow the comparison of results between subjects with different esophageal lengths. In detail, *x* ranges from 0, as the position of the UES to 1, as the position of the LES. As already suggested in literature, pressure is expressed by means of hyperbolic formulations [96]. In detail, it is formulated as the sum of two components: a "bell-shaped" function, *s* and an "s-shaped" function, δ. The former was introduced to interpret the actual wave propagation, while the latter was introduced to interpret the hypertonic contraction that occurs after the bolus transit to prevent acid reflux or air ingestion (Figure 3.9 a):

$$p(x,t) = s(x,t) + \delta(x,t)$$

where

$$s(x,t) = p_0(x) + \left[p_{max}(x) - p_0(x)\right] sech\left\{\frac{\beta(x)}{L}\left[x - \eta(x)t\right]\right\}$$

$$\delta(x,t) = \frac{5}{4}\Delta(x)\left\{tanh\left[\frac{2}{\phi(x)}\left(t - \frac{x}{\eta(x)}\right)\right] - \frac{1}{5}tanh\left[\frac{2}{5\phi(x)}\left(t - \frac{x}{\eta(x)}\right)\right]\right\}.$$

The second hyperbolic tangent was introduced to force $\frac{\partial \delta(x,t)}{\partial t}$ to 0 at its middle point $t = \frac{x}{\eta(x)}$ and, thus, to ensure that the maximum of $p(x,t)$ coincides with the maximum of $s(x,t)$.

3.2.2 Model parameters

The proposed formulation accounts for a set of parameters, as $p_0(x)$, $p_{max}(x)$, $\beta(x)$, $\eta(x)$, $\Delta(x)$ and $\phi(x)$ which are expressed as functions of the position *x* in order to make the model capable to interpret the heterogeneous distribution of the physiological properties along the esophageal length. Each parameter is related to a specific physiological property of the esophagus and can be associated to a specific feature of the esophageal motility, as represented in Figure 3.9 a. In detail, for each specific position *x* along the esophagus, the physiological meaning of each parameter can be described as follows:

- $p_0(x)$ represents to the esophageal basal pressure, as the pressure measured when the deglutition is not in action;
- $p_{max}(x)$ represents to the pressure difference between the basal pressure and the peak pressure measured during the swallowing process;
- $\beta(x)$ is directly related to $\phi(x)$, the duration of the contraction, by $\beta(x) = \frac{2L \cdot arsech(1/2)}{\phi(x)\eta(x)}$;
- $\eta(x)$ is related to the average propagation speed of the pressure wave, as the pressure peak at position *x* is measured at time $t_{max}(x) = x/\eta(x)$;
- $\Delta(x)$ represents the pressure difference between the pressure measured after the bolus transit and the pressure measured before the bolus transit.

3.2.3 Model parameters identification

The identification of the optimal set of model parameters used to evaluate model results that better interpret a given pressure map entailed the application of a non-linear optimization procedure, as a

consequence of the strong non-linearity of the model formulation. In detail, the lsqnonlin function was applied in Matlab™ (The MathWorks Inc., Natick, MA) in order to minimize the discrepancy between experimental data and model results (Figure 3.9 c) by means of a trust-region reflective algorithm (details in Appendix C). Regarding the pressure evolution over time at a specific position (as the data recorded by one single sensor), such discrepancy was represented by means of the following cost function:

$$\Omega\left(p_0(x), p_{max}(x), \beta(x), \eta(x), \Delta(x)\right) = \sum_{i=1}^{n}\left[\left(p(x,t_i) - p_{exp}(x,t_i)\right)^2\right].$$

The minimization procedure requires to specify initial values of parameters as the starting point for the algorithm. The selection of the starting point represents a fundamental issue, since the strong non linearity of the problem may lead to convergence in local minimum points of the cost functions, as represented in Figure 3.7 with regard to a one-dimensional problem.

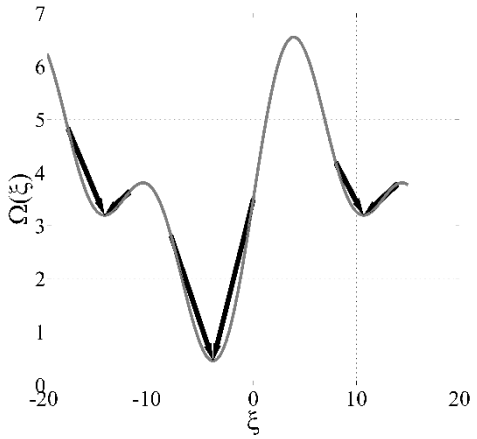

Figure 3.7 Generic cost function (gray line) of a generic parameter ξ; initial values of the parameter (starting points of black arrows) and corresponding convergence points of the trust-region-reflective algorithm (ending points of black arrows).

As far as the analysis of HRM data is concerned, initial values of the parameters were evaluated by processing the so called "median deglutition". The mean deglutition is defined as the pressure map obtained by overlapping the ten deglutitions acquired during HRM exam, and considering the median value of the corresponding pixels (Figure 3.8). It was autonomously evaluated in order to reduce the influence of artifacts due to breathing movements and heartbeat.

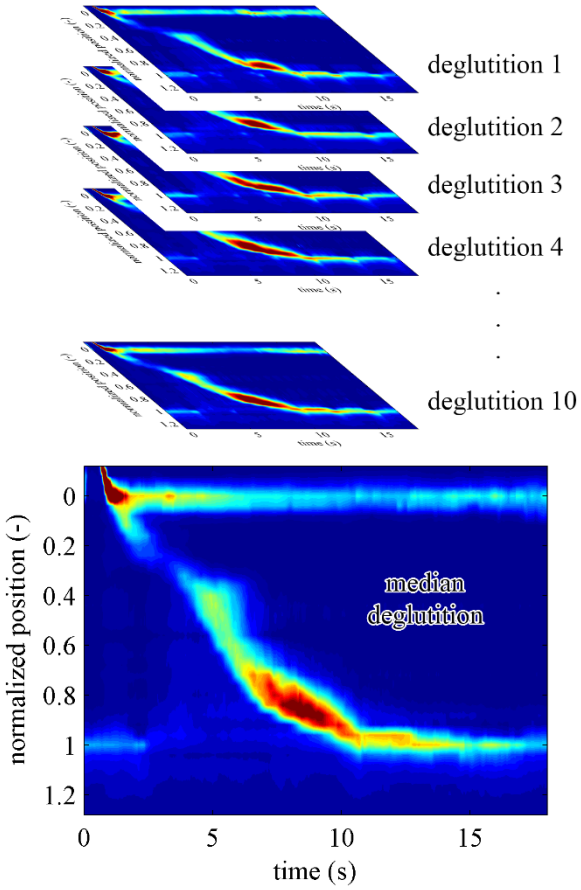

Figure 3.8 Computation of the median deglutition on the basis of the ten deglutitions acquired during the HRM test.

With regard to the data collected by each sensor, the initial values of the parameters were evaluated as follows:

- basal pressure values were averaged, leading to p_0^{init};
- $p_{max}^{\text{init}} = p_{peak} - p_0^{\text{init}}$ and $\eta^{\text{init}} = x/t_{peak}$ were initialized by considering pressure, as p_{peak}, and time, as t_{peak} at the wave peak;
- $\beta^{\text{init}} = \dfrac{2L \cdot arsech(1/2)}{\phi^{\text{init}} \eta^{\text{init}}}$, where ϕ^{init} is the full width of the pressure wave at its half maximum;
- the computation of the difference between the average basal pressure after the wave peak and the average basal pressure before the wave peak led to Δ^{init}.

A graphical representation of the computation of the initial values is given in Figure 3.9 b.

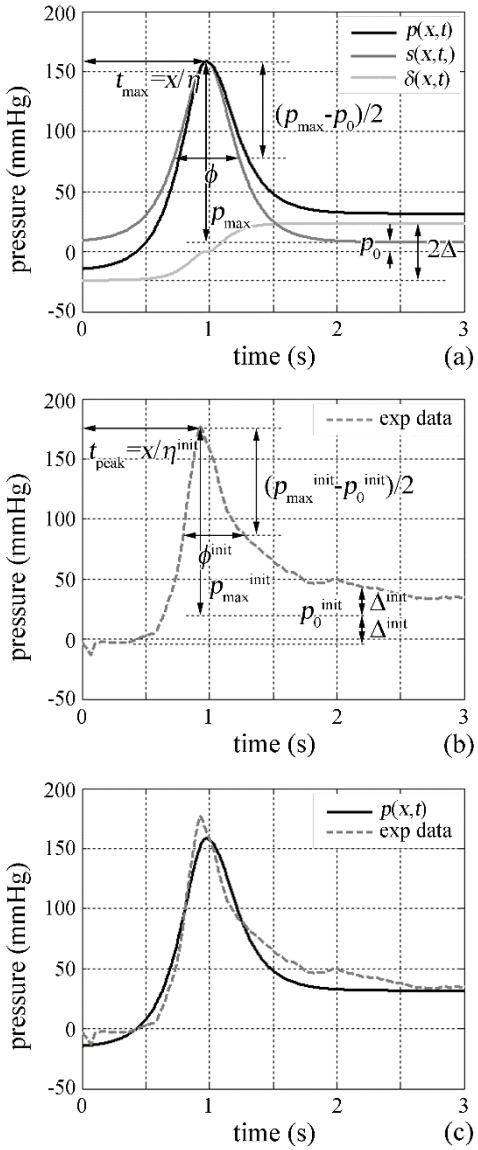

Figure 3.9 Physical meaning of model parameters (a); identification of initial values of parameters by processing experimental data (b); comparison of model results and experimental data after discrepancy minimization (c).

The identification procedure is run on the median data from each sensor. The corresponding results consist in a set of curves representing the values of the different parameters at each position along the esophagus length, as represented in Figure 3.10. The actual wave propagation speed $v(x)$ was also computed accounting for $t_{max}(x)$ and numerical differentiation techniques [98].

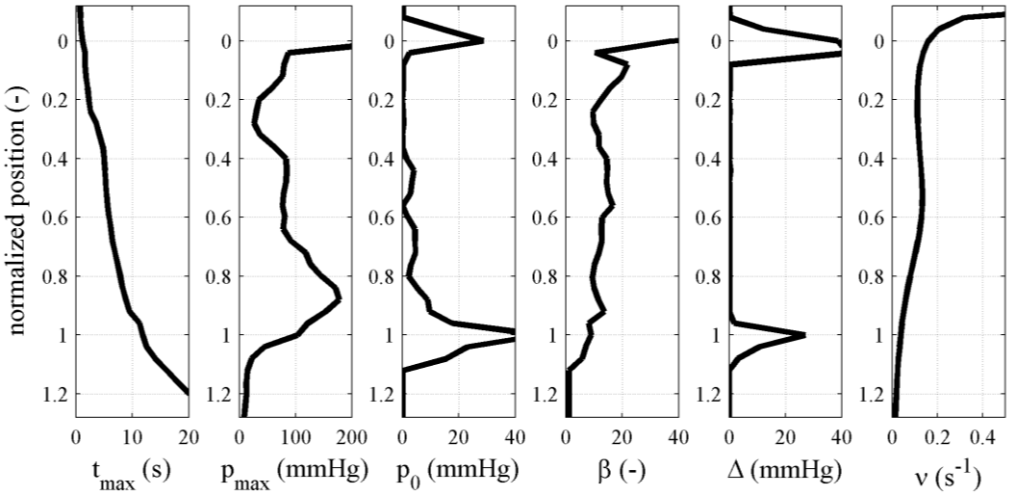

Figure 3.10 Results of the model parameters identification procedure: a set of curves representing the evolution of the identified model parameters as a function of the position along the esophagus.

3.2.4 Reliability assessment

The evaluation of the model results was performed accounting for the identified optimal set of model parameters. Two representations of the same data are given below, in order to emphasize the evolution of the median data from each sensor and the corresponding model results (Figure 3.11 a and b, respectively), and the corresponding pressure maps (Figure 3.11 c and d).

A first empirical proof of the suitability of the model to interpret data from HRM can be given by the high similarity of the two pressure maps (Figure 3.11c and d). The similarity can be also assessed from a clinical point of view, since the two images bring the same amount of clinically relevant information.

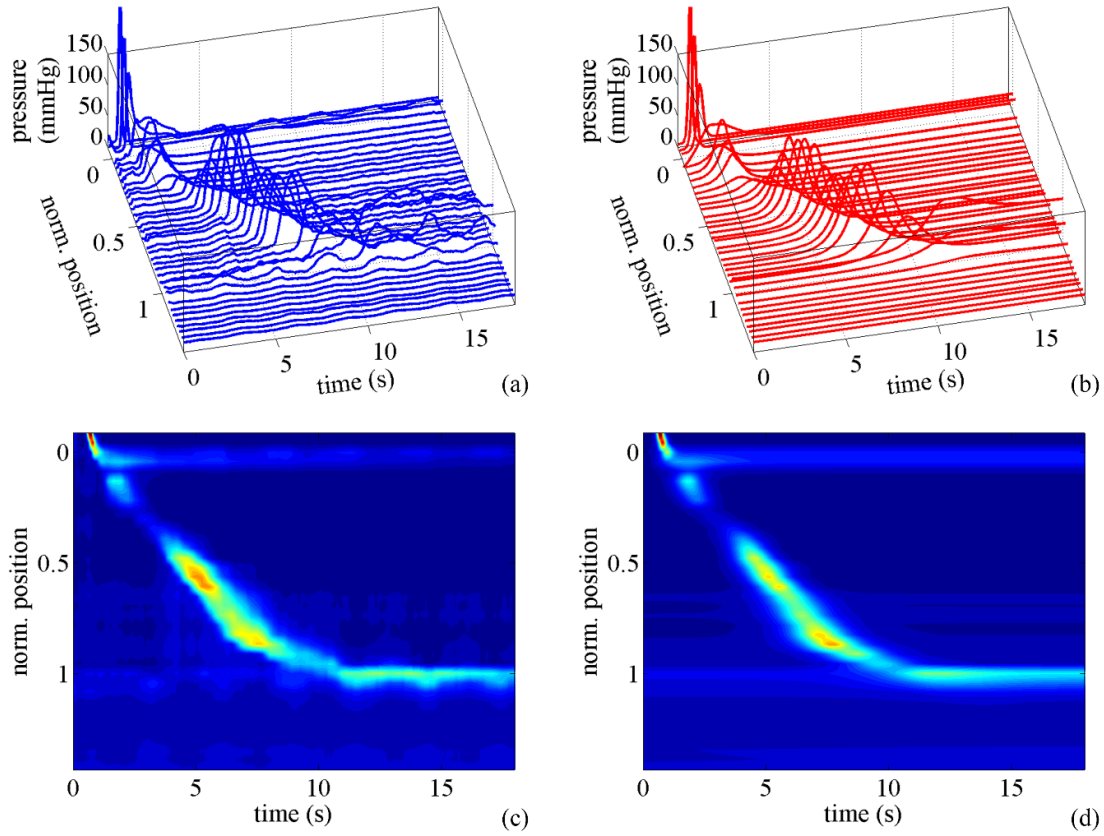

Figure 3.11 Two representations of the same data: pressure evolution of each sensor (a, b) and corresponding pressure maps (c, d). Data are referred to the median deglutition of a healthy subject (a, c) while the corresponding model results (b, d) are computed on the basis of the identified optimal set of model parameters.

The comparison between clinical data and model results is reported in Figure 3.12 with regard to the different pathological conditions in order to assess the suitability of the developed model to explain data from HRM in healthy and pathological conditions.

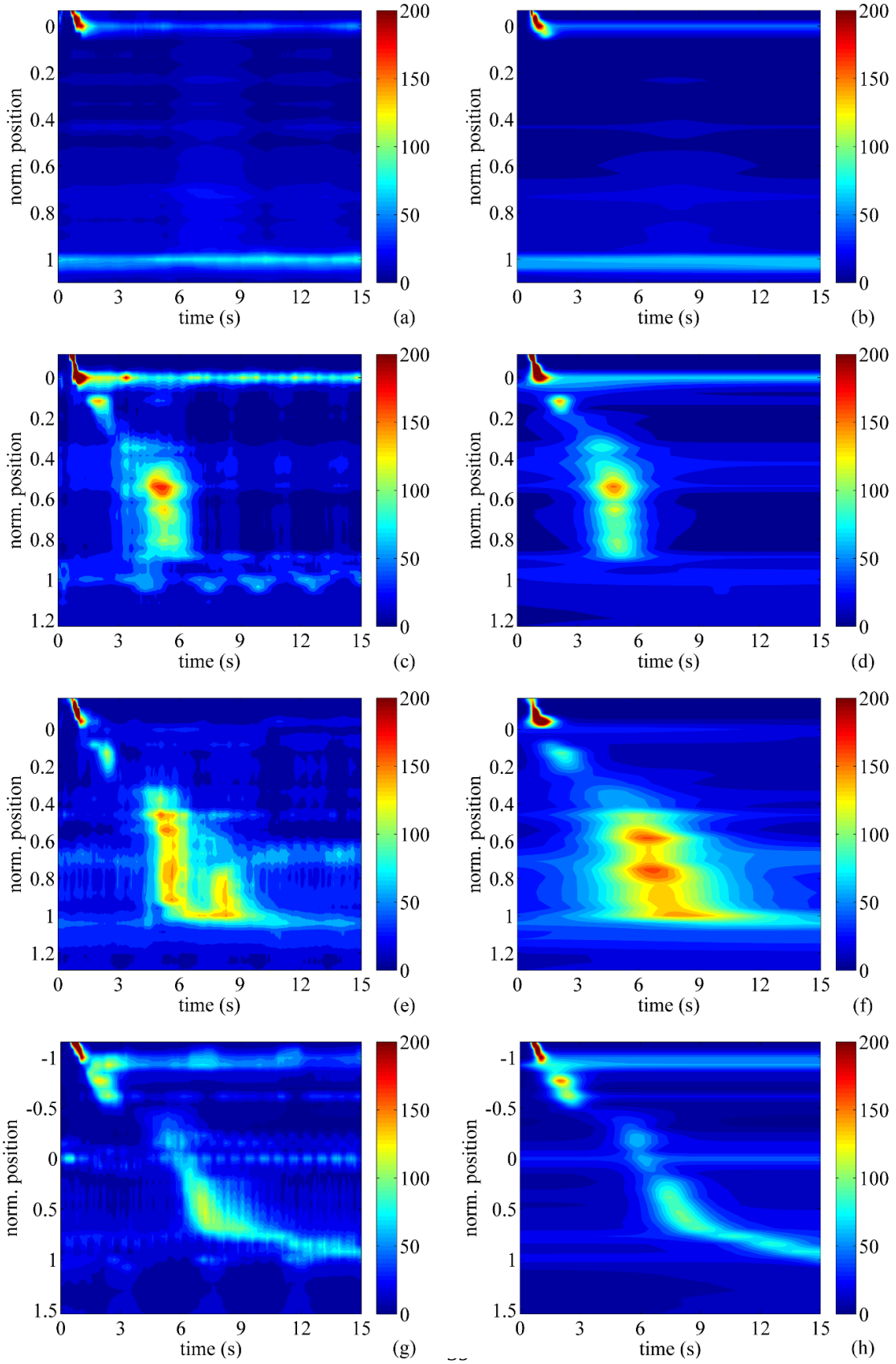
norm. position
time (s)
(a)
(b)
(c)
(d)
(e)
(f)
(g)
(h)

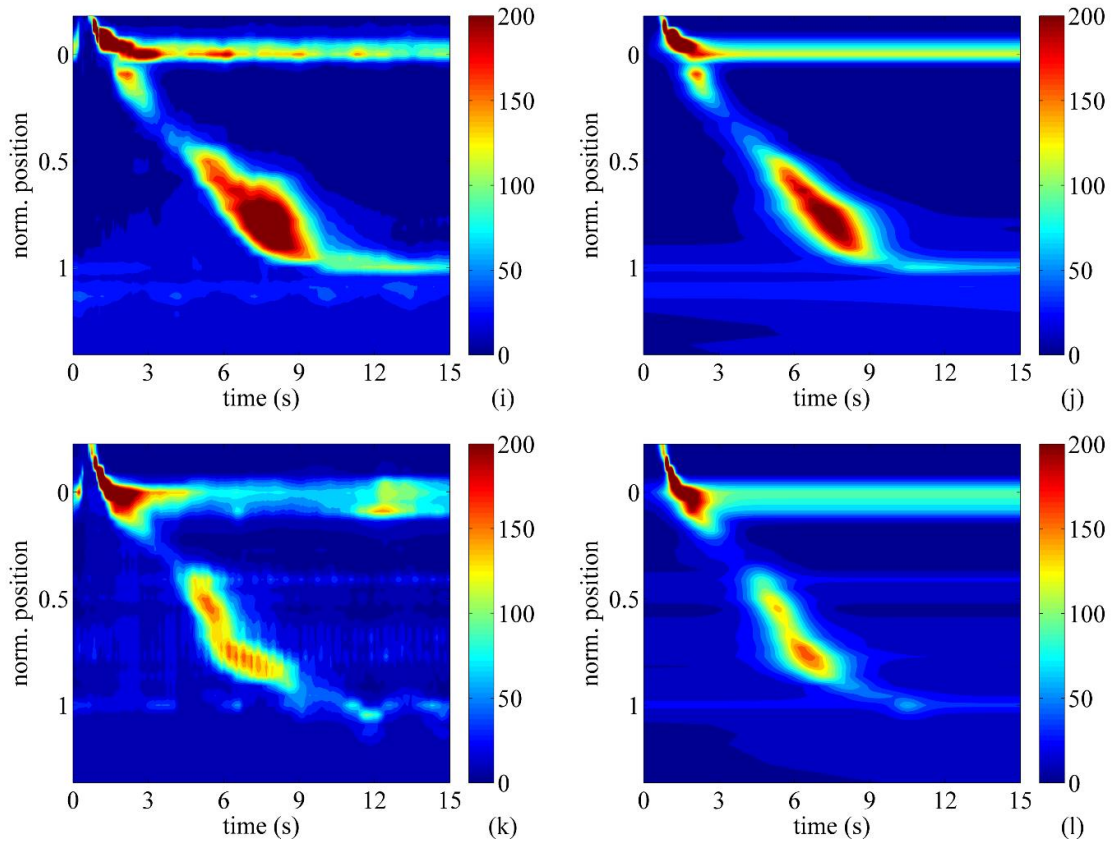

Figure 3.12 Median deglutitions of patients with different pathologies, as Achalasia pattern I (a), 2 (c) and 3 (e), EGJ Outflow Obstruction (g), Nutcracker Esophagus (i) and Diffuse Esophageal Spasm (k), and corresponding model results ((b), (d), (f), (h), (j) and (l), respectively).

A more rational approach to the assessment of the suitability of the model consists in the computation of the coefficient of determination R^2 [99], indicating how well the model can fit experimental data. In detail, with regard to each sensor, the coefficient of determination is computed as

$$R^2(x) \equiv 1 - \frac{\sum_i \left(p_{exp}(x,t_i) - \bar{p}_{exp}(x) \right)^2}{\sum_i \left(p_{exp}(x,t_i) - p_{mod}(x,t_i) \right)^2},$$

where $\bar{p}_{exp}(x)$ is the mean value of the pressure measured by the sensor during the considered timespan, $\bar{p}_{exp}(x) = \frac{\sum_{i=1}^{n} p_{exp}(x,t_i)}{n}$, and x is the position along the esophagus of the sensor itself.

$R^2 = 1$ corresponds to a perfect fit of the experimental data, while $R^2 = 0$ indicates that the model does not fit the data at all. Accordingly, the goodness of the fit of an entire pressure map can be expressed as the mean of the coefficients of determination computed for the 36 sensors:

$$R^2 = \frac{\sum_{j=1}^{36} R^2(x_j)}{36}.$$

The coefficient of determination was evaluated for each subject of a collection of healthy volunteers and patients referred to the Department of Surgery, Oncology and Gastroenterology – University of Padova. The collection included healthy and pathological subjects, as reported in Table 2.1. Such analysis provided median values of the obtained coefficients of determination ranging from 0.83 to 0.96 among the different categories, proving the developed model to be a reliable tool to interpret HRM data.

Table 3.1 Age and weight distribution of volunteers and patients, along with the corresponding coefficient of determination R^2.

		healthy	**Achalasia pattern I**	**Achalasia pattern II**	**Achalasia pattern III**	**EGJ outflow obstruction**	**Hypertensive LES**	**Nutcracker esophagus**	**Diffuse Esophageal Spasm**
males	**subjects no.**	53	20	25	4	15	3	6	3
	age (years)	45.6 ± 15.6	56.2 ± 16.9	54.0 ± 16.7	70.0 ± 5.8	52.5 ± 23.6	53.0 ± 8.3	51.6 ± 12.9	55.5 ± 17.7
	body weight (kg)	76.6 ± 12.7	75.8 ± 14.4	73.8 ± 14.2	78.0 ± 7.1	77.6 ± 9.5	80.4 ± 10.5	73.6 ± 7.9	78.2 ± 20.9
females	**subjects no.**	55	14	19	3	24	6	8	6
	age (years)	46.4 ± 17.5	60.4 ± 13.6	55.4 ± 18.3	71.5 ± 2.1	52.5 ± 14.2	44.2 ± 20.8	50.5 ± 12.9	56.3 ± 22.7
	body weight (kg)	64.2 ± 15.5	59.9 ± 13.5	62.6 ± 16.8	55.9 ± 11.5	60.6 ± 9.1	56.0 ± 6.9	56.2 ± 7.4	64.8 ± 14.1
males & females	**subjects no.**	108	34	44	7	39	9	14	9
	age (years)	46.0 ± 16.5	57.6 ± 15.8	54.5 ± 17.1	70.5 ± 4.7	52.5 ± 16.7	46.0 ± 18.4	51.0 ± 12.2	56.1 ± 20.6
	body weight (kg)	70.3 ± 15.4	70.5 ± 15.8	70.3 ± 15.7	70.6 ± 13.7	65.5 ± 12.0	60.9 ± 11.6	64.9 ± 11.7	68.2 ± 15.6
	R^2	0.959 ±0.026	0.883 ±0.210	0.828 ±0.180	0.886 ±0.038	0.956 ±0.027	0.891 ±0.021	0.958 ±0.014	0.919 ±0.040

CHAPTER 4

AUTONOMIC DIAGNOSIS OF PATHOLOGIES

As described in paragraphs 2.3 and 2.4, esophageal motor disorders are currently diagnosed by analyzing data from HRM. Unfortunately, human intervention is always required in such procedures, introducing inter- and intra-observer variabilities to the final diagnosis. An autonomic and completely unbiased procedure, which is designed to support the medical staff during the traditional diagnostic activity, was implemented with the fundamental contribution of the Department of Surgery, Oncology and Gastroenterology – University of Padova, and is described in this chapter.

4.1 Parameters distributions

The model parameters identification procedure reported in paragraph 3.2.3 was applied to each subject of the dataset described in paragraph 3.2.4. The resulting parameters evolutions was subsequently summarized in bands for each group of subjects by considering the 25^{th} and 75^{th} percentiles and the median values corresponding to each value of a common normalized position grid. The resulting parameters distributions achieved are reported in Figure 4.1.

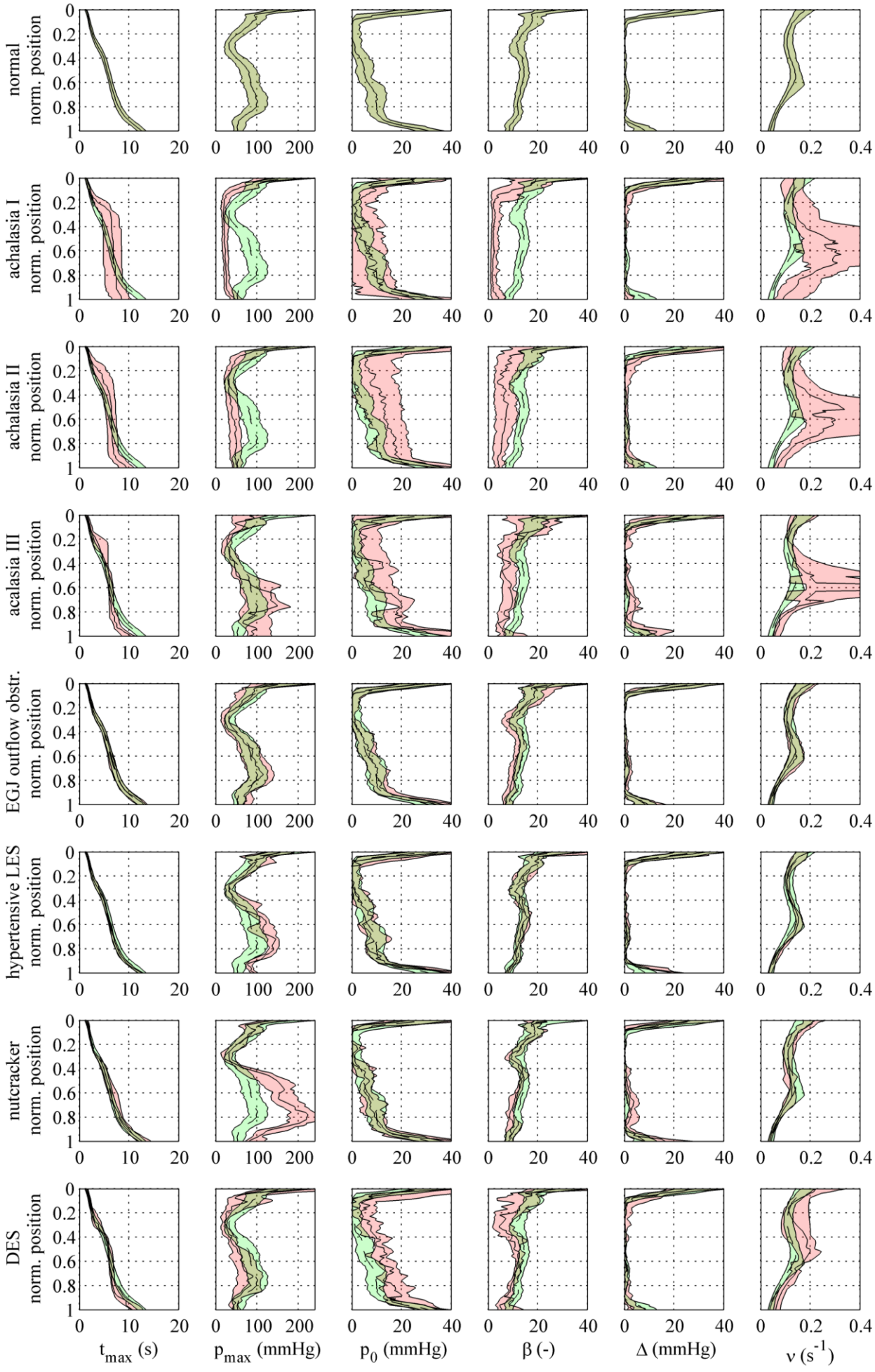

Figure 4.1 Parameters distribution of the different groups of subjects, as 50% scatter bands (colored areas) and median values (continuous or dashed lines). The parameters distributions of healthy subjects (green areas) are overlapped to the parameters distributions of other groups (red areas), in order to emphasize the differences.

With regard to the parameters distribution of healthy subjects, some of the main features can be highlighted and matched to the corresponding HRM pressure maps. In detail, peaks of p_0 can be identified at the sphincteric levels (x=0 and x=1). Such peaks can be explained by the higher resting pressures that are measured in the sphincteric regions, which are able to prevent ingestion of air and gastric reflux. In the same tracts, peaks of the parameter Δ can be noticed as well. They can be explained by the higher relaxation capacity of the sphincters, if compared to the relaxation capacity of the rest of the esophagus.

The comparison between the parameters distribution of healthy subjects and the parameters distributions of subjects belonging to different pathological groups is reported in the following. In order to show that significant differences in parameters distributions are found in specific regions, a direct correlation with the main physiological symptoms of the different pathologies is also reported. In detail,

- Achalasia pattern I subjects showed significantly lower p_{max} at $x \in [0.4,0.9]$, reflecting the absent peristalsis, and lower Δ at the lower sphincteric level, due to the LES dysfunction;
- Achalasia pattern II subjects showed similar abnormalities with respect to Achalasia pattern I distributions, because of the spastic contractions showing slightly higher amplitude;
- Achalasia pattern III subjects showed significantly higher ν along the overall esophagus, because of the simultaneous contraction of the overall distal part of the esophagus;
- no significant differences were found between EGJ outflow obstruction subjects and healthy situations;
- hypertensive LES subjects showed significantly higher p_{max} and Δ at the lower sphincteric region, due to the hypertonic contraction of the sphincter;
- nutcracker esophagus subjects showed significantly higher p_{max} at $x \in [0.5,0.9]$, because of the hypertonic peristaltic contractions;
- DES subjects showed significantly higher ν at $x \in [0.3,0.8]$, because of the simultaneous contraction of the overall proximal-central part of the esophagus.

4.2 Autonomic procedure

In order to autonomously identify the healthy or pathologic condition of a patient, the implemented procedure interprets the median deglutition of the patient by means of the physiological model reported in section 3.2.1. The application of the model to the clinical data of a specific patient allows the identification of the evolution of model parameters vs. normalized position along the esophagus, as shown in Figure 3.10. The comparison between the parameters of the patient and the parameter distribution of each group of subjects (Figure 4.2) leads to the classification of the patient to the "most probable" category, as represented in Figure 4.2.

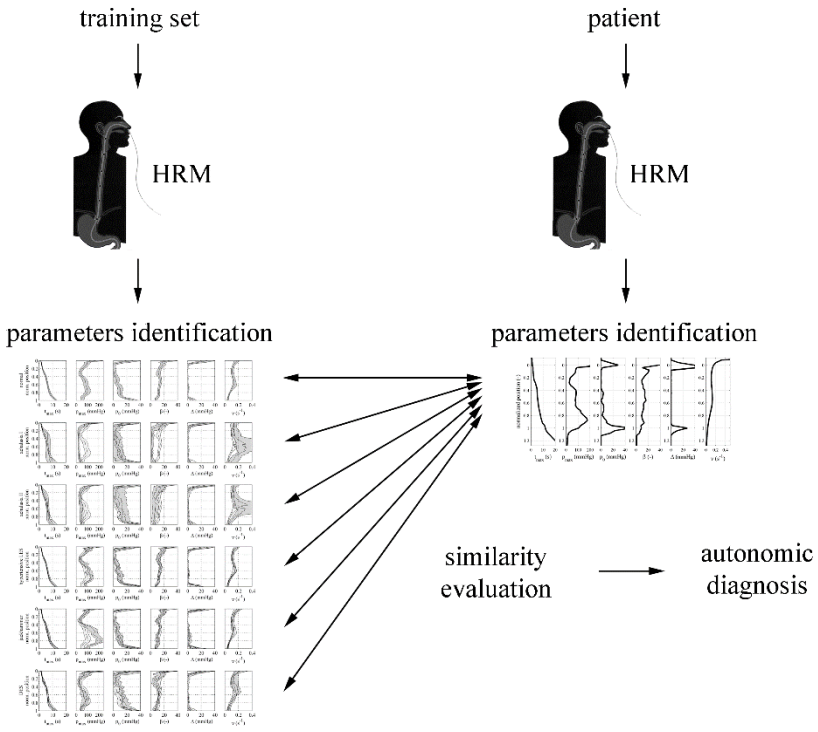

Figure 4.2 Flow chart of the autonomic diagnosis algorithm

4.3 Similarity index calculation

Once the parameters distribution of each group of subjects was assessed and the parameters of the patient were identified, a direct comparison could be performed, in order to autonomously select the "most similar" group. To this purpose, a similarity index Π^i, with

$i \in \{healthy; Achalasia\ I; Achalasia\ II; hypertensive\ LES; Nutcracker\ esophagus; DES\}$,

was defined to interpret the affinity between the parameters evolution of a subject and the parameters distribution of each specific group of subjects. The definition of Π^i represents the core of the entire autonomic procedure, since the diagnosis directly depends on the definition of Π^i. Before defining the similarity index between a specific patient and a group of subjects, different sub-definitions must be given.

$\pi_j^i\big|_{x=\bar{x}_k}$, where $j \in \{p_{max}; p_0; \beta; \Delta; \upsilon\}$ represents the similarity index between the value of a specific parameter $j^{subject}(\bar{x}_k)$ of the patient, evaluated at a specific position $\bar{x}_k$, and the corresponding parameter distribution $j^i(\bar{x}_k)$ at the same position $\bar{x}_k$ of the group i. $\pi_j^i\big|_{x=\bar{x}_k}$ is defined as a function of the cumulative relative frequency (crf) [100] of $j^{subject}(\bar{x}_k)$ with regard to the sample $j^i(\bar{x}_k)$:

$$\pi_j^i\big|_{x=\bar{x}_k} = 0.5 - \left| crf\left(j^{subject}(\bar{x}_k), j^i(\bar{x}_k)\right) - 0.5 \right|.$$

More intuitively, the value of $\pi_j^i\big|_{x=\bar{x}_k}$ is high if $j^{subject}(\bar{x}_k)$ is "close" to the median of the sample $j^i(\bar{x}_k)$, while it is low if $j^{subject}(\bar{x}_k)$ is "far" from the median of $j^i(\bar{x}_k)$.

The similarity index between a specific parameter and the corresponding parameter distribution of a specific category is denoted by π_j^i, and it is computed as the average of $\pi_j^i\big|_{x=\bar{x}_k}$ evaluated at the different positions $\bar{x}_k$ along the esophagus, which are defined within specific regions of interest:

$$\pi_j^i = \frac{\sum_{k=1}^{m} \pi_j^i\big|_{x=\bar{x}_k}}{m}.$$

Details about the definition of the regions of interest, as the specific *m* positions $\bar{x}_k$, are reported below.

Finally, Π^i is computed as the weighted mean of the similarity indexes between each parameter and the corresponding parameter distribution:

$$\Pi^i = \frac{\sum_{i=\{healthy;\, Achalasia\ I;\, ...\}} \omega_j^i \pi_j^i}{\sum_{i=\{healthy;\, Achalasia\ I;\, ...\}} \omega_j^i}$$

where ω_j^i are specific weights introduced accounting for the influence of the pathology on the specific parameters. The weights are identified by iteratively maximizing the success rate of the autonomic diagnosis procedure and are reported in Table 2.1.

Table 4.1 Weights identified for the computation of the similarity index between the parameters evolution of a patient and the parameters distribution of a group of subjects.

	$\omega_{p_{max}}^{...}$	$\omega_{p_0}^{...}$	$\omega_{\beta}^{...}$	$\omega_{\Delta}^{...}$	$\omega_{\upsilon}^{...}$
$\omega_{...}^{achalasia\ p.1}$	0.7936	0.0969	0.8272	0.8561	0.6309
$\omega_{...}^{achalasia\ p.2}$	0.6386	0.5809	0.6977	0.0464	0.6463
$\omega_{...}^{hypertensive\ LES}$	0.3599	0.4353	0.0964	0.6794	0.0964
$\omega_{...}^{normal}$	0.6474	0.6669	0.6465	0.6160	0.7676
$\omega_{...}^{nutcracker}$	0.8667	0.4007	0.3671	0.4012	0.0963
$\omega_{...}^{DES}$	0.2387	0.3945	0.4676	0.2734	0.0963

Parameters of different classes must be compared within different regions as specific pathologies may affect specific tracts (distal portion, lower sphincter, whole tract, etc.) and/or specific physiological properties (pressure wave duration, pressure wave peak, pre-post wave difference, etc.) of the esophagus. Regions of interest for the evaluation of the similarity indexes are defined accounting for the information given by Figure 4.1 and further clinical information. In detail, similarity indexes are defined accounting for the data of the non-overlapping regions of the colored bands, which often coincide with the zones affected by the corresponding pathologies.

4.4 Performance evaluation

The performance of the autonomic diagnosis procedure described within paragraph 4.2 can be evaluated by analyzing actual clinical cases and comparing the autonomic diagnoses with the corresponding real diagnoses, which were assessed case by case by experts in the field. The performance of the algorithm is connected to its success rate (SR), as the number of correct diagnoses with respect to the total number of clinical cases considered.

$$SR = \frac{n_{subjects\_with\_matching\_diagnosis}}{n_{total\_subjects\_considered}}$$

The algorithm has been tested running the autonomic diagnosis procedure on the data from the training set described in paragraph 3.2.4, showing *SR*=79.8%. The performance of the algorithm is even higher (*SR*=86.2%) when the difference between the different patterns of Achalasia is not considered. The success rate of the algorithm can also be represented by means of a grayscale map (Figure 4.3) in order to provide further details about the performance of the algorithm for each specific healthy or pathological condition.

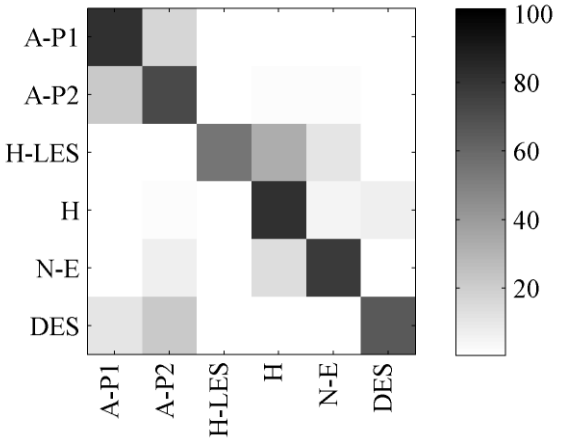

Figure 4.3 Results of the autonomic diagnosis algorithm with regard to the different healthy and pathological conditions, as Achalasia pattern I (A-P1), Achalasia pattern II (A-P2), hypertensive LES (H-LES), healthy (H), Nutcracker esophagus (N-E) and Diffuse Esophageal Spasm (DES). Rows correspond to the actual healthy or pathological conditions, while columns correspond to the results of the autonomic diagnoses. The color of each cell represents the percentage of subjects diagnosed correctly within each group of subjects.

CONCLUSIONS

In the past decades, diagnosis of esophageal motility disorders based on manometric data has been a challenging field with several methods being proposed for the definition of standard criteria and aiming to an objective classification of the different diseases. Due to the limitations imposed by available technologies (e.g. the perfused stationary manometry), the associated classification of pathologies was not adequate, since some of them were not well defined and often overlapping [101]. The development of HRM allowed the definition of the Chicago Classification (CC), accounting for parameters that were inaccessible just few years before. The CC [79][102] has seen major revisions in 2012 [24] and in 2015 [80], and a further major revision is now in progress, confirming that the widely used current classification is still far from a final configuration. Its principal problem pertains to the requirement of highly specialized interpreters of data. Furthermore, intra- and inter-observer variabilities and dependence of the diagnosis on the interpreter accuracy have been widely reported [103]–[105]. The lack of a reliable and unbiased classification system prevents the application of the best available treatment for a given disease. There is therefore a need for a more accurate classification tool for the motility disorders of the gullet, featuring a close interaction between clinicians and engineers.

A general framework for processing of clinical data from high resolution manometry has been developed in this work, aiming to provide an autonomic decision support system for the diagnosis of esophageal motility diseases. To this purpose, an accurate histo-morphometrical analysis of specific segments of the digestive system was firstly developed, in order to properly understand their micro and macro structural conformation and the corresponding physiological functionality. A review of the available technologies and methods was also reported for a better definition of the state of the art in esophageal diagnostics and to highlight the principal operational procedures in this field. A physiological model was then provided to interpret the trend of pressure with time along the esophagus during swallowing, as the typical condition investigated by high resolution manometry. The model accounts for parameters which are related to specific physiological properties of the esophageal structures, providing a description of the distribution of such properties along the esophagus itself. A procedure was contextually implemented for the fast and reliable identification of model parameters through iterative minimization of the discrepancy between HRM data and model results. Clinical data from both healthy volunteers and pathological subjects referring to the Department of Surgery, Oncology and Gastroenterology of the University of Padova

have been processed by the developed routines and model results were consistent with experimental data. The action allowed to evaluate the influence of pathologies on the parameters distributions, and significant variations of parameters distributions of pathological patients were observed. Such variations were noticed within the regions of the esophagus where the corresponding pathologies actually influence the physiological properties associated to the parameter itself. Subsequently, the capability of the physiological model to interpret HRM data was tested by assessing the mean coefficient of determination R^2. Results suggested that the developed physiological model represent a reliable computational tool for the diagnostic activity, as it could be applied for the implementation of an autonomic diagnosis procedure. In detail, the clinical data of the patient are processed to identify the patient-specific parameters and subsequently compared to a database, where model parameters pertaining to healthy and pathologic subjects are identified and the corresponding parameters distributions are assessed. The reliability of the procedure was assessed by analyzing its success rate, as the percentage of patients diagnosed correctly by the software. The obtained success rate of 86% suggested that the developed procedure may represent a reliable tool to support the medical staff during the traditional diagnostic activity by reducing the inter- and intra-observer variabilities with regard to the final diagnosis.

Presented results are promising and suggest that the developed procedure may represent a useful tool in diagnostics of esophageal motility disorders, but a lot of work is yet to be done in this field. Both the developed physiological model and the autonomic diagnosis procedure may be applied in order to develop new tools – or to improve existing ones – to provide better support to the medical staff during the diagnostic activity and to reduce invasiveness for the patient. Applications of the provided computational tools, possible improvements and future advancements of the presented research are reported within Appendix B.

BIBLIOGRAPHY

[1] Ambrosi G, Cantino D, Castano P, Correr S, D'Este L, Donato RF, … Zummo G. *Anatomia dell'Uomo*, 2001; (2nd ed.). Edi.Ermes.

[2] Martini, Timmons, & McKinley. *Anatomia Umana*, 2000; . Napoli: EdiSES.

[3] Gregersen H. *Biomechanics of the Gastrointestinal Tract*, 2003. Springer.

[4] Gabella G. The cross-ply arrangement of collagen fibres in the submucosa of the mammalian small intestine. *Cell and tissue research*, 1987; 248(3):491–7.

[5] Junqueira L, & Carneiro J. *Basic Histology: Text & Atlas*. *statrefcom*, 2005.

[6] Gray H. *Anatomy of the Human Body*. *The American Journal of the Medical Sciences*, 1919.

[7] Yamada T, Alpers DH, Kaplowitz N, Laine L, Owyang C, & Powell DW. *Textbook of Gastroenterology*, 2003; (4th ed.). Philadelphia: Lippincott Williams & Wilkins.

[8] Christensen J, Wingate DL, & Gregory RA. *A guide to gastrointestinal motility*, 1983. Oxford: Butterworth-Heinemann.

[9] Long JD, & Orlando RC. Esophageal submucosal glands: structure and function. *The American journal of gastroenterology*, 1999; 94(10):2818–24. doi:10.1111/j.1572-0241.1999.1422_b.x

[10] Natali AN, Carniel EL, & Gregersen H. Biomechanical behaviour of oesophageal tissues: Material and structural configuration, experimental data and constitutive analysis. *Medical Engineering and Physics*, 2009; 31(9):1056–1062. doi:10.1016/j.medengphy.2009.07.003

[11] Mashimo H, & Goyal RK. Physiology of esophageal motility. *GI Motility online*, 2006. doi:10.1038/gimo3

[12] Clavé P, De Kraa M, Arreola V, Girvent M, Farré R, Palomera E, & Serra-Prat M. The effect of bolus viscosity on swallowing function in neurogenic dysphagia. *Alimentary Pharmacology and Therapeutics*, 2006; 24(9):1385–1394. doi:10.1111/j.1365-2036.2006.03118.x

[13] Gore RM, & Levine MS. *Textbook of Gastrointestinal Radiology*, 2007. Philadelphia: Saunders.

[14] Randal Bollinger R, Barbas AS, Bush EL, Lin SS, & Parker W. Biofilms in the large bowel suggest an apparent function of the human vermiform appendix. *Journal of Theoretical Biology*, 2007; 249(4):826–831. doi:10.1016/j.jtbi.2007.08.032

[15] Meltzer A. Samuel James Meltzer, M.D. March 22, 1851 – November 7, 1920. *Proceedings*

of the Society for Experimental Biology and Medicine, 2000; 223(2):114–117.

[16] Fox MR, & Bredenoord a J. Oesophageal high-resolution manometry: moving from research into clinical practice. *Gut*, 2008; 57(3):405–423. doi:10.1136/gut.2007.127993

[17] Fyke Jr FE, Code CF, & Schlegel JF. The gastroesophageal sphincter in healthy human beings. *Gastroenterologia*, 1956; 86:135–150. doi:10.1159/000200544

[18] Kelley ML. Deglutitive pressure responses in the gastroesophageal sphineters of symptomatic hiatal hernia patients. *The American Journal of Digestive Diseases*, 1965; 10(7):582–595. doi:10.1007/BF02237632

[19] Arndorfer RC, Stef JJ, Dodds JW, & Hogan WJ. Improved infusion system for intraluminal esophageal manometry. *Gastroenterology*, 1977; 73(1):23–27.

[20] Dent J, Dodds WJ, Friedman RH, Sekiguchi T, Hogan WJ, Arndorfer RC, & Petrie DJ. Mechanism of gastroesophageal reflux in recumbent asymptomatic human subjects. *Journal of Clinical Investigation*, 1980; 65(2):256–267. doi:10.1172/JCI109667

[21] Dent J. Approaches to driving the evolving understanding of lower oesophageal sphincter mechanical function. *Journal of smooth muscle research = Nihon Heikatsukin Gakkai kikanshi*, 2007; 43(1):1–14. doi:10.1540/jsmr.43.1

[22] Dent J. A new technique for continuous sphincter pressure measurement. *Gastroenterology*, 1976; 71(2):263–267. doi:10.1016/S0016-5085(76)80199-0

[23] Clouse RE, Staiano a., & Alrakawi a. Development of a topographic analysis system for manometric studies in the gastrointestinal tract. *Gastrointestinal Endoscopy*, 1998; 48(4):395–401. doi:10.1016/S0016-5107(98)70010-0

[24] Bredenoord AJ, Fox M, Kahrilas PJ, Pandolfino JE, & Schwizer W. Chicago Classification Criteria of Esophageal Motility Disorders Defined in High Resolution Esophageal Pressure Topography (EPT). *Neurogastroenterology & Motility*, 2012; 24(S1):57–65. doi:10.1016/j.biotechadv.2011.08.021.Secreted

[25] McMahon BP, Jobe B a., Pandolfino JE, & Gregersen H. Do we really understand the role of the oesophagogastric junction in disease? *World Journal of Gastroenterology*, 2009; 15(2):144–150. doi:10.3748/wjg.15.144

[26] Dent J, Holloway RH, Toouli J, & Dodds WJ. Mechanisms of lower oesophageal sphincter incompetence in patients with symptomatic gastrooesophageal reflux. *Gut*, 1988; 29(8):1020–1028. doi:10.1136/gut.29.8.1020

[27] Shi G, Ergun G a., Manka M, & Kahrilas PJ. Lower esophageal sphincter relaxation characteristics using a sleeve sensor in clinical manometry. *American Journal of Gastroenterology*, 1998; 93(12):2373–2379. doi:10.1111/j.1572-0241.1998.00690.x

[28] Bodger K, & Trudgill N. Guidelines for oesophageal manometry and pH monitoring. *Water*, 2006; (November):1–12. doi:10.1046/j.1365-2982.1999.00151.x

[29] Clouse RE, Staiano A, Alrakawi A, & Haroian L. Application of topographical methods to clinical esophageal manometry. *American Journal of Gastroenterology*, 2000; 95(10):2720–2730. doi:10.1016/S0002-9270(00)01971-7

[30] Clouse RE, & Staiano A. Topography of the esophageal peristaltic pressure wave. *American Journal of Physiology - Gastrointestinal and Liver Physiology*, 1991; 261(4):G677–G684.

[31] Clouse RE, & Staiano A. Topography of normal and high-amplitude esophageal peristalsis. *American Journal of Physiology - Gastrointestinal and Liver Physiology*, 1993; 265(6):G1098–G1107.

[32] Gyawali CP. High resolution manometry: The Ray Clouse legacy. *Neurogastroenterology and Motility*, 2012; 24(SUPPL. 1):2–4. doi:10.1111/j.1365-2982.2011.01836.x

[33] O'Rourke A, Morgan LB, Coss-Adame E, Morrison M, Weinberger P, & Postma G. The Effect of Voluntary Pharyngeal Swallowing Maneuvers on Esophageal Swallowing Physiology. *Dysphagia*, 2014; 1–7. doi:10.1007/s00455-013-9505-6

[34] Salvador R, Dubecz A, Polomsky M, Gellerson O, Jones CE, Raymond DP, … Peters JH. A New Era in Esophageal Diagnostics: The Image-Based Paradigm of High-Resolution Manometry. *Journal of the American College of Surgeons*, 2009; 208(6):1035–1044. doi:10.1016/j.jamcollsurg.2009.02.049

[35] Pandolfino JE, El-Serag HB, Zhang Q, Shah N, Ghosh SK, & Kahrilas PJ. Obesity: A challenge to esophagogastric junction integrity. *Gastroenterology*, 2006; 130(3):639–649. doi:10.1053/j.gastro.2005.12.016

[36] Pandolfino JE, & Kahrilas PJ. AGA technical review on the clinical use of esophageal manometry. *Gastroenterology*, 2005; 128(1):209–224. doi:10.1053/j.gastro.2004.11.008

[37] Sifrim D, & Fornari F. Non-achalasic motor disorders of the oesophagus. *Best Practice and Research in Clinical Gastroenterology*, 2007; 21(4):575–593. doi:10.1016/j.bpg.2007.03.009

[38] Spechler SJ, & Castell DO. Classification of oesophageal motility abnormalities. *Gut*, 2001; 49(1):145–151. doi:10.1136/gut.49.1.145

[39] Diamant NE. Regulation and dysregulation of esophageal motor function. In *Progress in understanding and management of gastrointestinal motility disorders*, 1993; (Janssens J., pp. 85–103).

[40] Spechler SJ, Souza RF, Rosenberg SJ, Ruben R a, & Goyal RK. Heartburn in patients with achalasia. *Gut*, 1995; 37(3):305–308. doi:10.1136/gut.38.3.475-a

[41] Reynolds JC, & Parkman HP. Achalasia. *Gastroenterology Clinics of North America*, 1989; 18(2):223–255.

[42] Goldbum JR, Whyte RI, Orringer MB, & Appleman HD. Achalasia. A morphologic study of 42 resected specimens. *The American Journal of Surgical Pathology*, 1994; 18(4):327–

337.

[43] Holloway RH, Dodds WJ, & Helm JF. Integrity of cholinergic innervation to the lower esophageal sphincter in achalasia. *Gastroenterology*, 1986; 90:924–929.

[44] Singaram C, Koch J, & Gaumnitz EA. Nature of neuronal loss in human achalasia. *Gastroenterology*, 1996; 110:A259.

[45] Saha JK, Sengupta JN, & Goyal RK. Role of chloride ions in lower esophageal sphincter tone and relaxation. *American Journal of Physiology - Gastrointestinal and Liver Physiology*, 1992; 263(1):G115–G126.

[46] Yamato S, Spechler SJ, & Goyal RK. Role of nitric oxide in esophageal peristalsis in the opossum. *Gastroenterology*, 1992; 103:197–204.

[47] Goldenberg SP, Burrell M, & Fette GC. Classic and vigorous achalasia: a comparison of manometric, radiographic, and clinical findings. *Gastroenterology*, 1991; 101:743–748.

[48] Spechler SJ. AGA Technical Review on Treatment of Patients With Dysphagia Caused by Benign Disorders of the Distal Esophagus. *Gastroenterology*, 1999; 117:233–254. doi:10.1016/S0016-5085(99)70572-X

[49] Dudnick RS, Castell JA, & Castell DO. Abnormal upper esophageal sphincter function in achalasia. *American Journal of Gastroenterology*, 1992; 87:1712–1715.

[50] Zhang ZG, & Diamant NE. Repetitive Contractions of the Upper Esophageal Body and Sphincter in Achalasia. *Dysphagia*, 1994; 9:12–19.

[51] Massey BT, Hogan WJ, Dodds WJ, & Dantas RO. Alteration of the upper esophageal sphincter belch reflex in patients with achalasia. *Gastroenterology*, 1992; 103(5):1574–1579.

[52] Vantrappen G, Janssens J, Hellemans J, & Coremans G. Achalasia, diffuse esophageal spasm, and related motility disorders. *Gastroenterology*, 1979; 76(3):450–457.

[53] Goldblum JR, Rice TW, & Richter JE. Histopathologic features in esophagomyotomy specimens from patients with achalasia. *Gastroenterology*, 1996; 111(3):648–654.

[54] Katz PO, Richter JE, & Cowan R. Apparent complete lower esophageal sphincter relaxation in achalasia. *Gastroenterology*, 1986; 90:978–983.

[55] Champion J, Delisle N, & Hunt T. Myenteric plexus in spastic motility disorders. *Journal of Gastrointestinal Surgery*, 2001; 5(5):514–516.

[56] Dalton CB, Castell DO, & Richter JE. The changing faces of the nutcracker esophagus. *American Journal of Gastroenterology*, 1988; 83(6):623–628.

[57] Benjamin SB, Gerhardt DC, & Castell DO. High amplitude, peristaltic esophageal contractions associated with chest pain and/or dysphagia. *Gastroenterology*, 1979;

77(3):478–483.

[58] Achem SR, & Benjamin SB. Esophageal dysmotility (spastic dysmotility). *The esophagus, 2nd edn. Boston: Little, Brown and Company*, 1995; 247–268.

[59] Richter JE, Wu WC, Johns DN, Blackwell JN, Nelson JL 3rd, Castell JA, & Castell DO. Esophageal manometry in 95 healthy adult volunteers. Variability of pressures with age and frequency of "abnormal" contractions. *Digestive Diseases and Sciences*, 1987; 32(6):583–592.

[60] Achem SR, Kolts BE, & Burton L. Segmental versus diffuse nutcracker esophagus: an intermittent motility pattern. *American Journal of Gastroenterology*, 1993; 88(6):847–851.

[61] Freidin N, Mittal RK, Traube M, & McCallum RW. Segmental high amplitude peristaltic contractions in the distal esophagus. *American Journal of Gastroenterology*, 1989; 84(6):619–623.

[62] Tutuian R, & Castell DO. Esophageal motility disorders (distal esophageal spasm, nutcracker esophagus, and hypertensive lower esophageal sphincter): modern management. *Current treatment options in gastroenterology*, 2006; 9(4):283–94. doi:10.1007/s11938-006-0010-y

[63] Code CF, Schlegel JF, & Kelley ML. Hypertensive lower esophageal sphincter. *Proc Staff Mayo Clinic*, 1960; 35:391–399.

[64] Bassotti G, Alunni G, Cocchieri M, Pelli MA, & Morelli A. Isolated hypertensive lower esophageal sphincter: clinical and manometric aspects of an uncommon esophageal motor abnormality. *Journal of clinical gastroenterology*, 1992; 14(4):285–287.

[65] Katada N, Hinder R a, Hinder PR, Lund RJ, Perdikis G, Stalzer R a, & McGinn TR. The hypertensive lower esophageal sphincter. *American journal of surgery*, 1996; 172(5):439–442; discussion 442–443. doi:10.1016/S0002-9610(96)00219-X

[66] Katzka DA, Sidhu M, & Castell DO. Hypertensive lower esophageal sphincter pressures and gastroesophageal reflux: an apparent paradox that is not unusual. *American Journal of Gastroenterology* (n.d.).

[67] Waterman DC, Dalton CB, Ott DJ, Castell JA, Bradley LA, Castell DO, & Richter JE. Hypertensive lower esophageal sphincter: what does it mean? *Journal of clinical gastroenterology1*, 1989; 11(2):139–146.

[68] Freidin N, Traube M, Mittal RK, & McCallum RW. The hypertensive lower esophageal sphincter. Manometric and clinical aspects. *Digestive Diseases and Sciences*, 1989; 34(7):1063–1067.

[69] Bassotti G, Battaglia E, Debernardi V, Germani U, Quiriconi F, Dughera L, … Emanuelli G. Esophageal dysfunction in scleroderma. Relationship with disease subsets. *Arthritis & Rheumatism*, 1997; 40(12):2252–2259.

[70] Lock G, Holstege A, Lang B, & Schölmerich J. Gastrointestinal manifestations of progressive systemic sclerosis. *American Journal of Gastroenterology*, 1997; 92(5):763–771.

[71] Cohen S. The gastrointestinal manifestations of scleroderma: pathogenesis and management. *Gastroenterology*, 1980; 79(1):155–166.

[72] Cohen S. Motor Disorders of the Esophagus. *New England Journal of Medicine*, 1979; 301(4):184–192. doi:10.1056/NEJM197907263010404

[73] Yarze JC, Varga J, Stampfl D, Castell DO, & Jimenez SA. Esophageal function in systemic sclerosis: a prospective evaluation of motility and acid reflux in 36 patients. *American Journal of Gastroenterology*, 1993; 88(6):870–876.

[74] Richter JE, Blackwell JN, Wu WC, Johns DN, Cowan RJ, & Castell DO. Relationship of radionuclide liquid bolus transport and esophageal manometry. *Journal of Laboratory and Clinical Medicine*, 1987; 109(2):217–224.

[75] Turner R, Lipshutz W, Miller W, Rittenberg G, Schumacher HR, & Cohen S. Esophageal dysfunction in collagen disease. *The American Journal of the Medical Sciences*, 1973; 265(3):191–199.

[76] Zamost BJ, Hirschberg J, Ippoliti AF, Furst DE, Clements PJ, & Weinstein WM. Esophagitis in scleroderma. Prevalence and risk factors. *Gastroenterology*, 1987; 92(2):421–428.

[77] Leite LP, Johnston BT, Barrett J, Castell J a., & Castell DO. Ineffective esophageal motility (IEM): The primary finding in patients with nonspecific esophageal motility disorder. *Digestive Diseases and Sciences*, 1997; 42(9):1859–1865. doi:10.1023/A:1018802908358

[78] Zaninotto G, DeMeester TR, Schwizer W, Johansson KE, & Cheng SC. The lower esophageal sphincter in health and disease. *American journal of surgery*, 1988; .

[79] Kahrilas PJ, Ghosh SK, & Pandolfino JE. Esophageal motility disorders in terms of pressure topography: the Chicago Classification. *Journal of clinical gastroenterology*, 2008; 42(5):627–635. doi:10.1097/MCG.0b013e31815ea291

[80] Kahrilas PJ, Bredenoord a. J, Fox M, Gyawali CP, Roman S, Smout a. JPM, & Pandolfino JE. The Chicago Classification of esophageal motility disorders, v3.0. *Neurogastroenterology & Motility*, 2015; 27(2):160–174. doi:10.1111/nmo.12477

[81] Pandolfino JE, Leslie E, Luger D, Mitchell B, Kwiatek MA, & Kahrilas PJ. The contractile deceleration point: an important physiologic landmark on oesophageal pressure topography. *Neurogastroenterology & Motility*, 2010; 22(4):395–e90. doi:10.1016/j.biotechadv.2011.08.021.Secreted

[82] Pandolfino JE, Roman S, Carlson D, Luger D, Bidari K, Boris L, … Kahrilas PJ. Distal esophageal spasm in high-resolution esophageal pressure topography: defining clinical phenotypes. *Gastroenterology*, 2011; 141(2):469–475. doi:10.1038/nature11130.Reduced

[83] Shapiro AH, Jaffrin MY, & Weinberg SL. Peristaltic pumping with long wavelengths at low Reynolds number. *Journal of Fluid Mechanics*, 1969; 37:799–825. doi:10.1017/S0022112069000899

[84] Yin F, & Fung YC. Peristaltic Waves in Circular Cylindrical Tubes. *Journal of Applied Mechanics*, 1969; 36(3):579. doi:10.1115/1.3564720

[85] Brasseur JG, Corrsin S, & Lu NQ. The influence of a peripheral layer of different viscosity on peristaltic pumping with Newtonian fluids. *Journal of Fluid Mechanics*, 1987; 174:495–519. doi:10.1017/S0022112087000211

[86] Takabatake S, Ayukawa K, & Mori A. Peristaltic pumping in circular cylindrical tubes: a numerical study of fluid transport and its efficiency. *Journal of Fluid Mechanics*, 2006; 193:267. doi:10.1017/S0022112088002149

[87] Misra JC, & Pandey SK. Peristaltic transport of a particle-fluid suspension in a cylindrical tube. *Computers & Mathematics with Applications*, 1994; 28(4):131–145. doi:10.1016/0898-1221(94)00134-0

[88] Misra JC, & Pandey SK. Peristaltic transport in a tapered tube. *Mathematical and Computer Modelling*, 1995; 22(8):137–151. doi:10.1016/0895-7177(95)00162-U

[89] Kanaka Raju K, & Devanathan R. Peristaltic motion of a non-Newtonian fluid. *Rheologica Acta*, 1974; 13(6):944–948. doi:10.1007/BF01526678

[90] Bohme G, & Friedrich R. Peristaltic flow of viscoelastic liquids. *Journal of Fluid Mechanics*, 1983; 128:109–122. doi:10.1017/S0022112083000403

[91] Srivastava LM, & Srivastava VP. Peristaltic transport of blood: Casson model—II. *Journal of Biomechanics*, 1984; 17(11):821–829. doi:10.1016/0021-9290(84)90140-4

[92] Rao AR, & Usha S. Peristaltic transport of two immiscible viscous fluids in a circular tube. *Journal of Fluid Mechanics*, 2006; 298(-1):271. doi:10.1017/S0022112095003302

[93] Rath HJ. Peristalic flow through a lobe-shaped tube. *International Journal of Mechanical Sciences*, 1982; 24(6):359–367. doi:10.1016/0020-7403(82)90069-8

[94] Li M, & Brasseur JG. Non-steady peristaltic transport in finite-length tubes. *Journal of Fluid Mechanics*, 1993; 248(-1):129. doi:10.1017/S0022112093000710

[95] Misra JC, & Pandey SK. A mathematical model for oesophageal swallowing of a food-bolus. *Mathematical and Computer Modelling*, 2001; 33(8-9):997–1009. doi:10.1016/S0895-7177(00)00295-8

[96] Toklu E. A new mathematical model of peristaltic flow on esophageal bolus transport. *Scientific Research and Essays*, 2011; 6(31):6606–6614. doi:10.5897/SRE11.1502

[97] Ren J, Massey BT, Dodds WJ, Kern MK, Brasseur JG, Shaker R, … Arndorfer RC. Determinants of intrabolus pressure during esophageal peristaltic bolus transport. *The*

American journal of physiology, 1993; 264(3 Pt 1):G407–G413.

[98] Fan J, & Gijbels I. *Local polynomial modelling and its applications*. *Monographs on Statistics and Applied Probability*, 1996; (Vol. 66).

[99] Nagelkerke NJD. A note on a general definition of the coefficient of determination. *Biometrika*, 1991; 78(3):691–692. doi:10.1093/biomet/78.3.691

[100] Bulmer MG. *Principles of Statistics*. *British medical journal*, 1967; (Dover Publ.). New York. doi:10.1002/bimj.19710130208

[101] Richter JE, & Castell DO. *The Esophagus*, 2011; (5th ed.). Wiley-Blackwell.

[102] Pandolfino JE, Ghosh SK, Rice J, Clarke JO, Kwiatek M a, & Kahrilas PJ. Classifying esophageal motility by pressure topography characteristics: a study of 400 patients and 75 controls. *The American journal of gastroenterology*, 2008; 103(1):27–37. doi:10.1111/j.1572-0241.2007.01532.x

[103] Nayar DS, Khandwala F, Achkar E, Shay SS, Richter JE, Falk GW, … Vaezi MF. Esophageal manometry: assessment of interpreter consistency. *Clinical gastroenterology and hepatology : the official clinical practice journal of the American Gastroenterological Association*, 2005; 3(3):218–24. doi:10.1016/S1542-3565(04)00617-2

[104] Smithline A, Hawes R, & Lehman G. Sphincter of Oddi manometry: interobserver variability. *Gastrointestinal endoscopy*39(4):486–91.

[105] Brennan P, & Silman a. Statistical methods for assessing observer variability in clinical measures. *BMJ (Clinical research ed.)*, 1992; 304(6840):1491–1494. doi:10.1136/bmj.304.6840.1491

[106] Hastie TJ, & Tibshirani RJ. Generalized Additive Models. In *Monographs on statistics and Applied Probability*, 1990; (p. 352). doi:10.1016/j.csda.2010.05.004

[107] Hyvarinen A, Karhunen J, & Oja E. *Independent Component Analysis*, 2001; . John Wiley & Sons.

[108] Cho YK. How to Interpret Esophageal Impedance pH Monitoring. *Journal of neurogastroenterology and motility*, 2010; 16(3):327–30. doi:10.5056/jnm.2010.16.3.327

[109] Bredenoord a. J. Impedance-pH monitoring: New standard for measuring gastro-oesophageal reflux. *Neurogastroenterology and Motility*, 2008; 20:434–439. doi:10.1111/j.1365-2982.2008.01131.x

[110] Goyal RK, Biancani P, Phillips a., & Spiro HM. Mechanical properties of the esophageal wall. *Journal of Clinical Investigation*, 1971; 50(7):1456–1465. doi:10.1172/JCI106630

[111] Moré JJ, & Sorensen DC. Computing a Trust Region Step. *SIAM Journal on Scientific and Statistical Computing*, 1983; 4(3):553–572. doi:10.1137/0904038

[112] Equation Solving Algorithms (http://it.mathworks.com/help/optim/ug/equation-solving-algorithms.html).

APPENDIX A

A MULTISTEP PROCEDURE FOR THE BIOMECHANICAL CHARACTERIZATION OF HOLLOW ORGANS BY MEANS OF A COUPLED EXPERIMENTAL AND COMPUTATIONAL APPROACH

Pathologies, diseases and motor disorders may affect the biomechanical behavior of different biological structures, compromising their functionality and causing disabilities and pain, representing a relevant social health problem. Many of these pathologies can be diagnosed and treated with specific diagnostic and surgical tools, which must be designed accounting for an accurate evaluation of their mechanical interaction with the biological structures themselves. The mechanical interaction gains even more relevance during the design of tools for minimum invasive surgery or diagnosis techniques, which aim to reduce effects of the diagnostic process or treatment on the patient and possibly shorten the recovery time. Therefore, computational tools are needed to properly interpret the mechanical behavior of biological tissues and structures in order to evaluate their mechanical interaction with biomedical devices.

The magnitude and the distribution of the mechanical stress within structures can be evaluated analytically by means of the theory of continuum mechanics, but some problems still present complex geometries and/or non-linear constitutive laws. This kind of problems do not have an analytical solution, hence they can only be solved using numerical methods. Numerical methods are widely adopted in civil and industrial engineering fields, and the concept can be easily transferred to bioengineering. Additionally, numerical modeling activities in the bioengineering field gain further relevance due to the adaptation phenomena that characterize living tissues when mechanical stimuli are applied.

The development of numerical models requires the definition of virtual solid models, such as Finite Element Models (FEM), reproducing the exact morphology of the anatomical region of interest, constrained by appropriate boundary conditions, and characterized by constitutive models defined

on purpose. Constitutive models are mathematical relationships between stretch, strain and time that are capable to predict the mechanical behavior of materials. The definition of such models is not an easy task, since biological tissues, with particular regard to soft tissues, are often characterized by nonlinear responses. Nonlinearities can be classified in geometrical nonlinearities, due to the effect of large displacements on the configuration of the structure, and material nonlinearities, that are related to the material behavior that is nonlinear due to various physiological phenomena such as fibers uncrimping. Further aspects, as time-dependency, must be taken into account for the characterization of biological tissues. The high percentage of liquid component, recovery phenomena and fiber rearrangement phenomena that take place within biological materials are responsible for time-dependent response of the tissues, leading to visco-hyperelastic formulations. In addition, most of the biological tissues are also fiber-reinforced in order to guarantee the maximum efficiency of the entire structure and strongly anisotropic responses.

The mechanical characterization of a biological structure requires a strongly multidisciplinary approach, and can be performed according to a multistep procedure. The aim of the overall procedure pertains to define computational tools capable to interpret the mechanical behavior of biological materials and structures. In detail, according to this procedure, a histo-morphometrical analysis should be firstly performed in order to understand the micro- and macro-structural configuration of the anatomical site. Such analysis is mandatory for the evaluation of the orientation of the different families of fibers within the tissues, for the characterization of the actual morphology of the structures, for the definition of the geometry of virtual solid models, for the evaluation of the constitutive framework to be developed, and, finally, for the definition of the experimental tests to be performed at the tissue level. Such tests, as mono- or multi-axial tensile tests, must be performed on biological samples in order to assess the visco-hyperelasto-plastic anisotropic behavior of the tissues and to produce experimental data for the identification of the parameters of the constitutive models to be developed. In fact, constitutive models must be formulated to interpret results from experimental tests at the tissue level. With regard to the constitutive models, the optimum set of model parameters can be evaluated by minimizing the discrepancy between model results and experimental data by means of specific stochastic-deterministic iterative procedure. Further experimental tests should be performed at the structure level in order to overcome the limitations of the tensile tests. As a matter of fact, the cutting procedure of the experimental samples for the tensile tests interrupts the continuity of the families

of fibers, preventing them to express their mechanical function. For instance, with regard to tubular structures, inflation tests should be performed in order to collect experimental results at the structure level. Subsequently, physio-mechanical models should be developed in order to interpret the pressure-volume-time relationship characterizing the inflated structure. Once again, the parameters of the physio-mechanical models, can be identified by minimizing the discrepancy between model results and experimental data. Combining constitutive models, the corresponding identified parameters and results from the morphometrical analysis will lead to a comprehensive virtual model, as a Finite Element Model able to interpret the mechanical behavior of the overall structure. Such FEM must be applied to simulate the experimental conditions of inflation tests, and the corresponding numerical results must be compared with results from experimental testing at structure level to mutually validate the finite element model, the constitutive models and the corresponding parameters. At the end of the multistep procedure, the numerical model can be considered a reliable tool to evaluate the mechanical behavior of the specific anatomical site, also accounting for the interaction of the biological structures with biomedical devices. The procedure described above is summarized in the following figure.

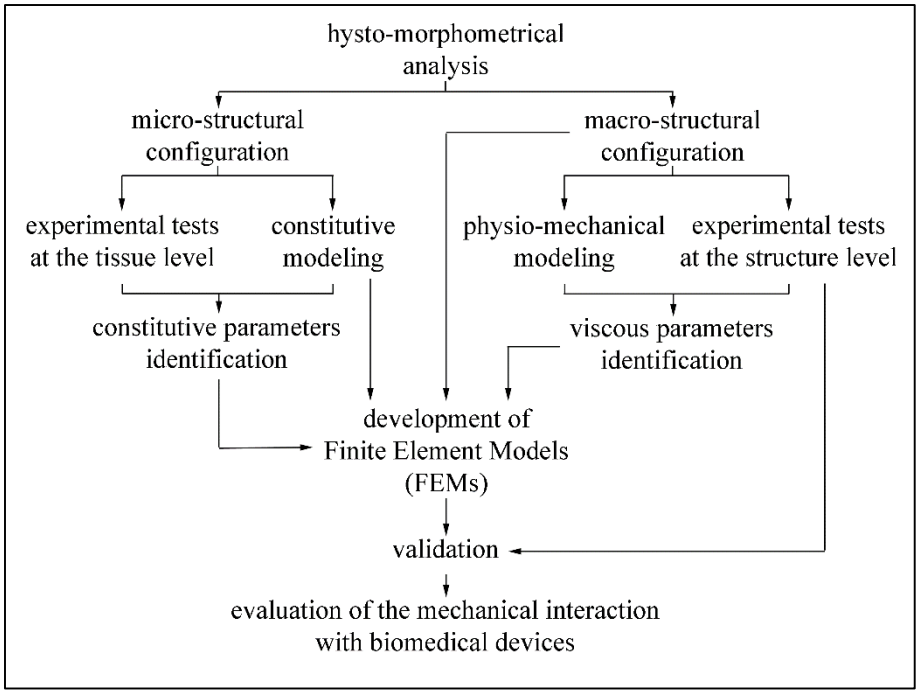

Schematic representation of the multistep procedure for the development of reliable models for the evaluation of the mechanical response of a biological structure.

APPENDIX B

FUTURE ADVANCEMENTS

Model tuning

The formulation of $\delta(x,t)$ within the physiological model definition in paragraph 3.2.1 contains two numerical constants: $\frac{5}{4}$ and $\frac{1}{4}$. These values were not chosen randomly, since their difference was set to be 1. This constraint was created, in order to satisfy the equation

$$\Delta(x) = 2 \cdot \left(\lim_{t \to +\infty} \delta(x,t) - \lim_{t \to -\infty} \delta(x,t) \right),$$

as $\Delta(x)$ was meant to be directly related to the pressure difference between after and before the bolus transit, and not to a fraction of it. The same constraint can be expressed more intuitively as: "the difference between the chosen numerical constants should be equal to 1". While, infinite couples of numbers can respect this constraint, the chosen couple $\left(\frac{5}{4}, \frac{1}{4}\right)$ maintains the maximum point of $p(x,t)$ equal to the maximum point of the function $s(x,t)$ without changing the "S-shaped" nature of $\delta(x,t)$. A more rational definition might be suggested in order to determine the optimal value of these constants, or, alternatively, another function may be proposed for the "S-shaped" function $\delta(x,t)$.

Double check of the traditional diagnosis

As observed by Dr. Joseph A. Murray (MD, Dept. of Gastroenterology and Hepatology – Mayo Clinic, Minnesota, US) during the presentation of this work at the OESO 13th World Conference in Monaco (Montecarlo), the traditional diagnosis, which was considered 100% reliable in testing the software, is affected by intra- and inter- observer variabilities instead. For this reason, the traditional diagnoses of the considered dataset should be re-evaluated by experts in this field, in light of the

corresponding autonomic diagnoses given by the software. Finally, the "first" diagnoses and the "double-checked" diagnosis should be statistically compared in order to assess whether the traditional diagnostic process can be (positively) biased by the autonomic diagnostic procedure.

Enlargement and sharing of the training set

The parameters distributions represent the basis for the autonomic diagnosis procedure, since the classification is performed by comparing patient-specific parameters to the parameters distributions of different groups of subjects of the dataset. The parameters distributions are assessed on the basis of the parameters identified for each subject of the dataset. Unfortunately, the extremely low incidence of some disorders – for example Achalasia pattern III – makes the corresponding parameters distribution unstable. In other words, the reliability of the statistical distributions depends on the dimension of the dataset, and so does the reliability of the entire procedure. A preliminary database was developed in this study, but it must be largely extended and continuously updated involving different research groups, in order to improve the reliability of the autonomic diagnosis procedure.

Accurate definition of regions of interest

The computation of the similarity index, which represents the affinity between the patient-specific parameters and the parameters distribution of a group of subjects accounts for the definition of regions of interest. Such regions are defined as continuous non-overlapping regions of the colored bands in Figure 4.1. Alternatively, we might statistically define such regions for each parameter of each group of subjects running the Student's t-test at each position x and considering "region of interest" the set of positions statistically different from the healthy dataset.

Extension of the algorithm to further pathologies

The above-mentioned algorithm was designed and tested considering a sub-set of the available pathologies. Some of the excluded groups of subjects were too small, while some others did not show significant differences in parameters distributions, making them indiscernible from the healthy dataset. Enlarging the training set would allow to increase the number of subjects of the small groups, to show differences in parameters distributions and, as a consequence, to include further pathologies within the autonomic diagnosis procedure.

Analysis of single deglutitions

As described in detail in paragraph 3.2.3, the diagnosis of healthy or pathologic conditions of a patient is performed on the basis of the pressure map regarding his or her "mean deglutition", which is obtained by overlapping the pressure maps of the ten deglutitions acquired during the HRM test, and considering the mean value of the corresponding pixels. The action is undertaken in order to reduce the influence of artifacts due to heartbeat and breathing movements, but prevents to detect symptoms that occur in a minor percentage of the deglutitions. The autonomic diagnosis procedure can be improved by considering the ten deglutitions of the patient separately. The reduction of the influence of artifacts from each one of the ten pressure maps can be performed during the pre-processing phase, by applying approximation [106] or independent component analysis (ICA) [107] techniques.

Data compression algorithms

Huge amounts of data are often involved in research, and efficient algorithms are necessary to manage and store them. When dealing with data from HRM, a large amount of memory is needed to store the pressure evolution over time recorded by the sensors of the probe. As mentioned in paragraph 3.2.4, after the model parameters identification procedure, model results carry the same clinical information as the corresponding raw data, but only require the storage of the evolution of the parameters position along the esophageal length. As a matter of example, signals recorded by the 36 equally-spaced sensors at a rate of 100 samples/sec for about 10 minutes requires to store 36*100*600=2160000 numbers. On the other hand, to store the model information of the corresponding median deglutition, as the evolution of 6 parameters on a higher-resolution grid of 100 positions along the esophagus and a time grid of 100 samples/sec for a timespan of about 20 seconds, only 6*100+100*20=2600 numbers are required, as less than a 830^{th} of the memory. This high compression rate suggests the applicability of the model as a reliable tool for the implementation of lossy compression algorithms for HRM data.

Analysis of considerable amount of data

Some applications in biomedicine involve the evaluation of the incidence of a specific pathology on large numbers of patients or the distribution of different pathologies within a population. Within the scope of esophageal motility disorders, if a database of thousands of HRM was at disposal, such

analyses could be done by considering the diagnosis made by the different experts who analyzed the different HRMs, but a huge inter-operator variability would affect the corresponding results. Alternatively, each HRM of the dataset could be re-analyzed by an assigned operator, but this task would be extremely time consuming and intra-operator variability would still be present. The application of autonomic diagnosis procedure would be able to address both the issues, since no working hours would be required and no inter- or intra-operator variabilities would be introduced.

Integration with other sources of information

With regard to the diagnosis of esophageal motility disorders, the final diagnosis often requires the evaluation of sources of information that are complementary to manometry. As a matter of example, the presence of obstructing tumors can be detected by means of imaging techniques, such as endoscopy, ultrasonography, x-ray scan or magnetic resonance. The different types of gastroesophageal reflux, their composition, proximal extent, duration and clearing are usually assessed by means of impedance monitoring, which is a clinical test that gives information about the conductivity of the surrounding tissues [108][109]. Finally, a proper biomechanical characterization of the esophageal structures remains a fundamental issue to determine the best biomaterial for replacement, when needed [110].

The developed procedure should be improved by making capable to diagnose the healthy or pathological condition of a patient accounting for further sources of information, as a wider overview of the same patient. Hopefully, the autonomic diagnosis made on the basis of different investigation techniques is even more reliable than the autonomic diagnosis described in Chapter 4.

New probe for the biomechanical and functional characterization of the esophagus

A larger number of clinical tests gives information about the health status of the patients and increases the probability to correctly diagnose its health condition, autonomously or traditionally. However, this kind of investigation implies non-negligible invasiveness for the patient, since all of the mentioned tests require the placement of an endoesophageal catheter, the ingestion of contrast media and/or exposition to ionizing radiations. Moreover, costs for instrumentation and required personnel would raise the overall expensiveness. Alternatively, information about conductivity, histology, morphometry, functionality and mechanical behavior can be collected in one single

clinical test, drastically reducing costs and invasiveness. A similar test would require the development of an innovative diagnostic tool able to gather all of the information by means of a single placement of a transnasal probe. Such a tool is already under development in cooperation with Scuola Superiore Sant'Anna of Pisa (Italy).

APPENDIX C

TRUST-REGION REFLECTIVE ALGORITHM

Optimization methods based on the Trust-Region Reflective algorithm aim to minimize a function $f(\boldsymbol{x}): \mathrm{R}^n \to \mathrm{R}$, given a starting point $\boldsymbol{x}_0$. The minimum point of $f(\boldsymbol{x})$ is found iteratively: the aim of each step of the procedure is to find a value of $f(\boldsymbol{x})$ that is lower than the one obtained at the previous step. The idea is to approximate $f(\boldsymbol{x})$ with a simpler function $q(\boldsymbol{x})$, which "reasonably" reflects the behavior of $f(\boldsymbol{x})$ in a neighborhood N – the trust region – of $\boldsymbol{x}_0$. A trial step is computed by minimizing over N, as the trust region subproblem:

$$\min_{\boldsymbol{s}} \{q(\boldsymbol{s}), \boldsymbol{s} \in \mathrm{N}\}.$$

$\boldsymbol{x}_0$ is updated to $\boldsymbol{x}_1 = \boldsymbol{x}_0 + \boldsymbol{s}$ only if $f(\boldsymbol{x}_0 + \boldsymbol{s}) < f(\boldsymbol{x}_0)$. Otherwise, $\boldsymbol{x}_1 = \boldsymbol{x}_0$ and the region of trust is shrunk before repeating the trial step computation.

In the unconstrained Trust-Region method [111], $q(\boldsymbol{x})$ is defined with the first two terms of the Taylor approximation of $f(\boldsymbol{x})$ and N is usually spherical or ellipsoidal, so that the subproblem becomes:

$$\min_{\boldsymbol{s}} \left\{ \frac{1}{2} \boldsymbol{s}^T \boldsymbol{H} \boldsymbol{s} + \boldsymbol{s}^T \boldsymbol{g} : \|\boldsymbol{D}\boldsymbol{s}\| \le \Delta \right\},$$

where $\boldsymbol{g}$ is the gradient of $f(\boldsymbol{x})$ at $\boldsymbol{x}_0$, $\boldsymbol{H}$ is the Hessian matrix, $\boldsymbol{D}$ is a diagonal scaling matrix and Δ is a positive scalar. The adopted Matlab™ (The MathWorks Inc., Natick, MA) routines restrict the trust-region subproblem to a two-dimensional subspace S, which is determined by means of the preconditioned conjugate gradient process. S is the linear space spanned by $\boldsymbol{s}_1$ and $\boldsymbol{s}_2$, where $\boldsymbol{s}_1$ is in the direction of $\boldsymbol{g}$ and $\boldsymbol{s}_2$ is either a solution to $\boldsymbol{H} \cdot \boldsymbol{s}_2 = -\boldsymbol{g}$ or a direction of

negative curvature $\boldsymbol{s}_2^T \cdot \boldsymbol{H} \cdot \boldsymbol{s}_2 < 0$. The flow chart of the unconstrained minimization using trust-region ideas can be summarized as follows:

1) formulate the two-dimensional subproblem
2) solve of the subproblem to determine the trial step $\boldsymbol{s}$
3) if $f\left(\boldsymbol{x}_i + \boldsymbol{s}\right) < f\left(\boldsymbol{x}_i\right)$, then $\boldsymbol{x}_{i+1} = \boldsymbol{x}_i + \boldsymbol{s}$
4) decrease Δ if $f\left(\boldsymbol{x}_i + \boldsymbol{s}\right) \geq f\left(\boldsymbol{x}_i\right)$.

These steps are iterated until convergence [112].